Impact of MIMO Transmission on CAF-based Geolocation

Jacob I. Overfield

Thesis submitted to the Faculty of the
Virginia Polytechnic Institute and State University
in partial fulfillment of the requirements for the degree of

Master of Science
in
Electrical Engineering

R. Michael Buehrer, Chair
Jeffrey H. Reed
J. Michael Ruohoniemi

May 16, 2013
Blacksburg, Virginia

Keywords: MIMO, SISO, CAF, Cross Ambiguity Function, Complex Ambiguity Function, Geolocation, TDOA, Differential Delay, FDOA, Differential Doppler, Position, Location

Impact of MIMO Transmission on CAF-based Geolocation

Jacob I. Overfield

ABSTRACT

The Cross Ambiguity Function (CAF) is often used for passive geolocation of an emitter based on the time difference of arrival (TDOA) and frequency difference of arrival (FDOA) of the received signals. CAF performance has been thoroughly investigated in regards to traditional single-input single-output (SISO) signals. Little is known about how the CAF will respond to signals from multiple-input multiple-output (MIMO) systems which utilize multiple antennas. This thesis focuses on characterizing the CAF's magnitude distribution in order to determine the probability of correctly determining the correct TDOA/FDOA bin, and the resulting impact on geolocation. The received signals are studied in the presence of additive white Gaussian noise (AWGN) as well as multi-channel propagation effects such as phase ambiguities and offsets due to multi-antenna transmission.

Two and four transmit antennas using either a form of spatial multiplexing or space-time block coding are the focus of this work because they are mostly commonly found in currently deployed communication systems. The effects of these transmit schemes are studied with respect to TDOA/FDOA error and the resulting position error. The analysis is performed using a detection theory framework as opposed to estimation theory in order to emphasize the impact of MIMO transmission on determining the correct TDOA/FDOA bin. A simple method using the CAF magnitude as a decision statistic is also presented so that TDOA/FDOA errors can be detected and filtered in an attempt to improve positioning estimates.

Acknowledgments

First and foremost I would like to acknowledge my parents for all of their support especially throughout my college career. I give many thanks to my mentor and teacher Dr. Michael Buehrer who has taught me so much over the years. I would also like to thank the outstanding professors at Virginia Tech, in particular Dr. Michael Ruohoniemi who I have been lucky enough to enjoy several classes with during my undergraduate years. Thanks also to Dr. Claudio Da Silva and Dr. Jeffery Reed who encouraged and introduced me to graduate school and Wireless @ VT. I would also like to acknowledge the Hume Center with Dr. Robert McGwier and Dr. Charles Clancy for the amazing research and scholarship opportunities.

Contents

List of Figures

Chapter 1

Introduction

Geolocation has become an important aspect of our daily lives as we rely on GPS and other assistive technologies to pinpoint our location on Earth. Applications for geolocation technology exist in both the military and civilian sectors; such as locating an enemy transponder or a cell phone during a 911 call. Just as the reliance on geolocation services is growing, there has also been an increase in the use of communication systems with multiple antennas. These multi-antenna technologies are typically described as multiple-input multiple-output (MIMO) communication systems. Compared to single-input single-output (SISO) systems with single antennas at the transmitter and receiver, MIMO systems are gaining popularity (such as in LTE and WiFi) because they promise an increase in throughput without the need for additional bandwidth. MIMO techniques exploit the properties of multipath to create multiple independent parallel channels which they can utilize for either faster or more reliable communications. Many questions arise regarding how MIMO transmission affects traditional geolocation techniques. This report studies the effects of MIMO signals on one particular signal processing approach to geolocation which relies on the Cross-Ambiguity-Function (CAF).

Using a pair of received signals from two separate receivers, the CAF is able to simultaneously calculate TDOA and FDOA. CAF processing is similar to using a matched filter on the received signal, except in this case the filter is another received signal. By correlating two signals in time and frequency the CAF searches a grid of time and frequency differentials to find those that cause peak values. With SISO signals this cross correlation is more deterministic and a general peak is typically easy to find; MIMO signals produce more complex results.

Typically a MIMO system involves transmit-receive nodes utilizing two or more antennas on each side of the link which take advantage of multiple spatial channels to increase capacity and robustness. Two major forms of MIMO include spatial multiplexing (SMUX) and space-time block coding (STBC). Spatial multiplexing parallelizes a transmitted signal across spatially separated antennas in order to increase throughput at the receiver. STBC uses orthogonal coding in space and time to decrease the bit error rate due to multipath fading. Until now CAF research has been restricted to a SISO signal assumption where there is only one channel between each transmit-receive pair.

The primary paper on the CAF is presented by Stein in [23] where he derives the Cramér-Rao lower bound (CRLB) for TDOA/FDOA estimation as well as discussing efficient CAF calculation methods. In another paper [24], Stein also derives the maximum likelihood (ML) estimator for TDOA/FDOA for unknown signals. Wax also discusses the ML and CRLB of the combined estimation of TDOA/FDOA and phase [26]. In regards to discrete CAF calculation, Auslander and Tolimieri discuss efficient computation methods in [3]. Fowler is well versed in CAF processing and TDOA/FDOA positioning with several papers on topics such as signal models with TDOA/FDOA [9] and their data compression for sharing information between collectors [4]. In another recent paper, [19], Pourhomayoun and Fowler develop a single step location technique that they claim outperforms that first proposed by

Weiss in [27] called the Direct Position Determination method (DPD). There are also several theses on the subject of the CAF and TDOA/FDOA positioning that are worth mentioning [12, 28]. Yet all of these works focus on traditional CAF processing with SISO signals; there are no references in the literature that examine the effects of MIMO transmission on CAF positioning.

In regards to positioning, Torrieri in [25] provides a good reference for TDOA/FDOA geolocation as well as describing geometric dilution of precision and circular error probable. In another paper [5], Chestnut provides a novel method for combining TDOA/FDOA and platform measurement variances and converting them to position covariances for error ellipse calculations. In the textbooks [17] and [18] both by Poisel, gradient descent methods are discussed for iterative position determination from TDOA/FDOA among other observables. Another reference for geolocation and positioning in general is the handbook by Zekavat and Buehrer [29]. An algebraic solution developed by Ho in [10] constrains the TDOA/FDOA problem to a situation where the emitter has a known altitude. Then in [16], Pattison extends Ho's work by adding a sensitivity analysis to TDOA/FDOA and other parameters.

This thesis will first provide a background on the CAF and derive the probability of detection error based on the distribution of the CAF magnitude in Chapter 1.2. The framework for this approach is to treat the TDOA/FDOA estimation problem as that of detecting the discrete TDOA/FDOA bin that corresponds to the true values. To form a basis for comparison the distribution of the CAF magnitude for SISO signals in AWGN is derived along with the full probability of detection error expression in Chapter 2. Next the distribution and probability of error for MIMO signals using SMUX and Alamouti STBC (ASTBC) for a transmitter with two antennas is derived in Chapter 3, and is extended to four transmit antennas in Chapter 4 with simulation results following in Chapter 5. Then in Chapter 6, detection theory is once again applied to find and remove CAF errors in an attempt to improve geolocation at the

expense of discarding data. Finally in Chapter 7 TDOA/FDOA geolocation is introduced and the impact of TDOA/FDOA errors are realized when they are translated to position estimation.

1.1 SISO and MIMO Systems

It is well known in the field of information theory founded by Shannon that there are theoretical channel capacity limits. In classical single-input single-output systems there is only one channel between the transmitter and receiver. The capacity of this channel is limited by many factors such as the available bandwidth and the signal-to-noise-ratio (SNR). In an attempt to increase capacity, multiple-input multiple-output systems use the existence of multiple channels in space. By utilizing multiple antennas MIMO systems can use multipath propagation properties due to a rich scattering environment to exploit independent spatial channels. Assuming sufficient antenna spacing and a rich scattering environment there will be a maximum of $min\ (N_t, N_r)$ independent channels between the transmitter and receiver where N_t and N_r are the number of transmit and receive antennas respectively. The signal model below is used to represent the received signals of a 2x2 MIMO system where there are two transmit and receive antennas:

$$\bar{\mathbf{r}} = \mathbf{H}\bar{\mathbf{s}} + \bar{\mathbf{n}} \tag{1.1}$$

$$\begin{bmatrix} \mathbf{r_1} \\ \mathbf{r_2} \end{bmatrix} = \begin{bmatrix} h_{1,1} & h_{1,2} \\ h_{2,1} & h_{2,2} \end{bmatrix} \begin{bmatrix} \mathbf{s_1} \\ \mathbf{s_2} \end{bmatrix} + \begin{bmatrix} \mathbf{n_1} \\ \mathbf{n_2} \end{bmatrix} \tag{1.2}$$

where $\mathbf{r}_r$ is the received signal, $\mathbf{s}_l$ is the transmitted signal, $\mathbf{n}_r$ is additive white Gaussian noise (AWGN), and $h_{r,l}$ is the channel between the rth receive and lth transmit antenna and is typically modeled as $h_{r,l} = \alpha_{r,l}\, e^{j\theta_{r,l}}$ where $\alpha_{r,l}$ is some attenuation coefficient due to fading and $\theta_{r,l}$ is a random phase shift. If we assume that the receiver is airborne then we

can also assume that there is a heavy line of sight component in the received signal and that there won't be any noticeable multipath fading so that the attenuation coefficient can be set to one. The resulting channel matrix under this assumption is now:

$$\mathbf{H} = \begin{bmatrix} e^{j\theta_{1,1}} & e^{j\theta_{1,2}} \\ e^{j\theta_{2,1}} & e^{j\theta_{2,2}} \end{bmatrix}. \tag{1.3}$$

A typical 2x2 MIMO system configuration is shown in Figure 1.1 illustrating the existence of multiple channels and the random phases between the transmitter and receiver.

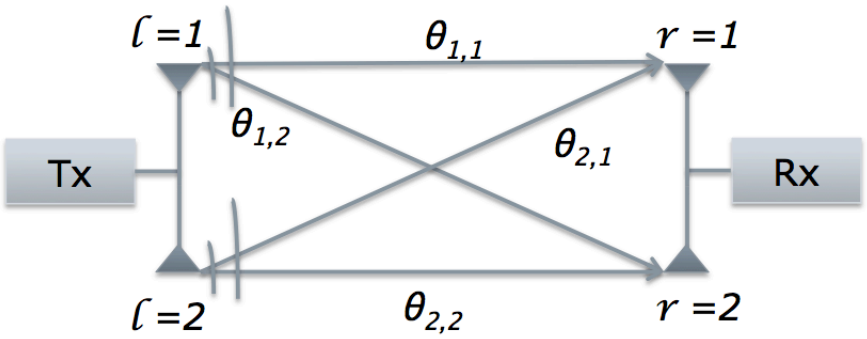

Figure 1.1: Classical MIMO System Configuration. A 2x2 system where each transmitter and receiver has two antennas. Assuming the receiver is airborne there will only be random phase shifts from the transmit to receive antennas.

For the purposes of this thesis, there will be one transmitter (SISO or MIMO) and two receivers each with one antenna. Therefore the overall system is considered SISO when the transmitter has a single antenna as shown in Figure 1.2, and MIMO when it has multiple antennas as shown in Figure 1.3. This is not a classical definition of MIMO, but because the assumption is that our receivers are listening passively to the communications of a MIMO system (where the transmitters and receivers have multiple antennas), we therefore call the general scenario MIMO despite the fact that geolocation receivers do not have multiple antennas.

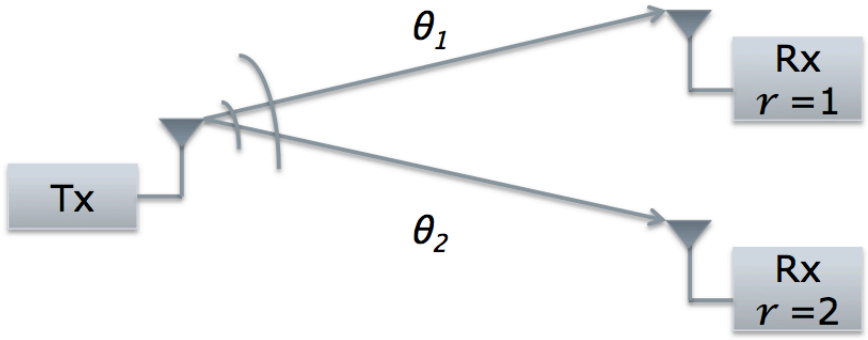

Figure 1.2: SISO System Configuration. There is one emitter with a single transmit antenna and two collectors, each has one receive antenna.

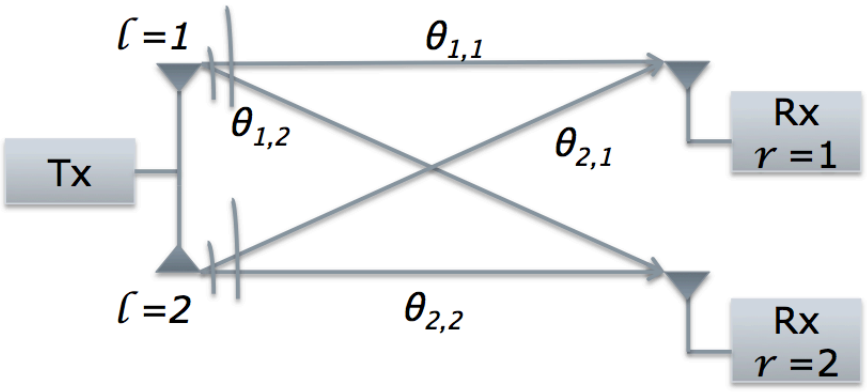

Figure 1.3: MIMO System Configuration. Although by definition not truly MIMO, the receivers each have one antenna but the transmitter has two antennas (although not shown here the number of transmit antennas could be more than two). There will still be random phase shifts due to the channel as one would expect in a true MIMO scenario.

The two types of MIMO transmission that will be discussed in this thesis are spatial multiplexing (SMUX) and space-time block coding (STBC). Typically spatial multiplexing is used to provide a capacity gain because two (or more) independent symbol streams can be transmitted simultaneously; in general allowing for faster bit-rates. STBC provides a diversity gain which improves the robustness of the transmission and can reduce the bit-error-rate. A diagram illustrating the transmission of SMUX (or also sometimes abbreviated SM or SMX

in the literature) is shown in Figure 1.4. With SMUX there are two symbol streams, $\hat{\mathbf{b}}_1$ and $\hat{\mathbf{b}}_2$ as shown in the figure, which can be assumed independent (after encoding and interleaving) and are transmitted simultaneously on antennas separated in space. The antenna distance depends on many factors such as the environment and the frequency or wavelength of the signal. In general the antennas need to be separated enough to provide low spatial correlation, in many cases half wavelength spacing can be used. STBC uses an orthogonal block code to multiplex one symbol stream into several which can then be transmitted in parallel across space as depicted in Figure 1.5. One such block code for two transmit antennas was first introduced by Alamouti [2] and is given by:

$$\mathbf{C} = \begin{bmatrix} b^{(1)} & -b^{(2)*} \\ b^{(2)} & b^{(1)*} \end{bmatrix} \tag{1.4}$$

where the rows represent the symbol transmitted on each antenna and the columns represent the transmission period. The Alamouti code is unique in that it is full rate, meaning that the symbol rate before and after the code is the same. For more than two antennas there are no known codes that are both full rate and orthogonal for complex signals, but there are less than full rate codes and codes that are quasi-orthogonal.

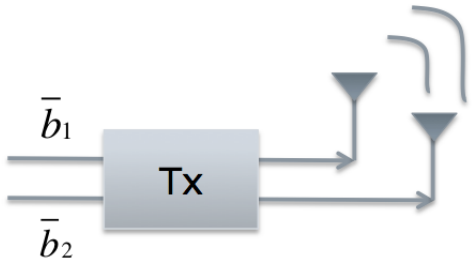

Figure 1.4: SMUX System Configuration. Each antenna transmits an independent symbol stream.

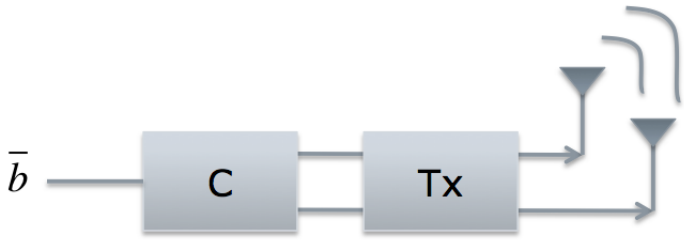

Figure 1.5: ASTBC System Configuration. A single symbol stream is parallelized onto multiple antennas through the coding matrix **C**.

The main difference between SMUX and STBC assumed by this thesis, is how the symbols look between each transmit antenna. For SMUX we assume that at any given symbol period the transmitted symbols on any given antenna are independent from those of any other antenna. This assumption is not valid for STBC techniques due to the nature of the coding. As we will see the STBC transmitted signals contrast with those of SMUX in that they can correlate in time and space.

1.2 System Model

The underlying geolocation scenario is the classical attempt to passively determine the position of a transmitter by using the received signals from multiple mobile receivers. For simplicity the transmitter, sometimes referred to as the emitter, is assumed to be stationary. The receivers, also called collectors, are assumed airborne so that there will be a heavy line-of-sight component and multipath can be considered negligible. In both the SISO and MIMO cases the collectors will each only have one antenna. The focus is on the most basic situation where there are only two collectors, since the CAF operates only on two received signals at a time. The assumption is made that the collectors are time and frequency synchronized with each other (although not synchronized in any way with the transmitter), allowing the

focus to be on the effects of other aspects of the received signals. We start the analysis by defining the observables of interest, TDOA and FDOA:

$$\text{TDOA} = \Delta\tau = t_1 - t_2 = (\tau_1 - t_e) - (\tau_2 - t_e) = \tau_1 - \tau_2 \tag{1.5}$$

$$\text{FDOA} = \Delta f = f_1 - f_2 = (f_c + f_{d1}) - (f_c + f_{d2}) = f_{d1} - f_{d2} \tag{1.6}$$

where t_e is some arbitrary time of signal transmission, t_r is the time of arrival of the signal for each receiver r, f_r is the frequency of arrival, $f_d r$ is the Doppler shift of the signal observed at the receiver r, and f_c is the transmitted carrier frequency. We define the following list of parameters important to the received signal model:

r =1, 2, ... Receiver index
l =1, 2, ..., N_t Transmitting antenna index
N_t =1, 2, ... Number of transmitting antennas, number of simultaneously transmitted signals
$b_l(t)$ = Signal envelope, randomly modulated symbols from transmit antenna l
τ_r = Delay due to signal propagation and range from transmitter to rth receiver
f_{dr} = Doppler due to relative velocity of rth receiver
$\theta_{r,l}$ = Random phase offset due to the channel from the rth receiver to the lth transmitter, assumed to be uniformly distributed over $[0, 2\pi]$
P_r = Signal power at the rth receiver

If we assume the collectors are time and frequency synchronized, after down-converting the complex baseband received signals will be:

$$\tilde{r}_r(t) = \sum_{l=1}^{N_t} \sqrt{P_r/N_t}\; b_l(t - \tau_r) e^{j(2\pi f_{dr} t + \theta_{r,l})}. \tag{1.7}$$

Note that this can be used to model both SISO and MIMO signals. Since we have two collectors during any given signal collection period there will be two received signals from which we can perform the CAF to calculate TDOA/FDOA simultaneously. The CAF is defined as:

$$\Lambda(\Delta\hat{\tau}, \Delta\hat{f}) = \int_0^T \tilde{r}_1(t)\tilde{r}_2^*(t - \Delta\hat{\tau}) e^{-j2\pi\Delta\hat{f}t} dt \tag{1.8}$$

where $\Delta\hat{t}$ and $\Delta\hat{f}$ are differential delays and Dopplers corresponding to TDOA and FDOA estimates, respectively. The $(*)$ operator denotes the complex conjugate.

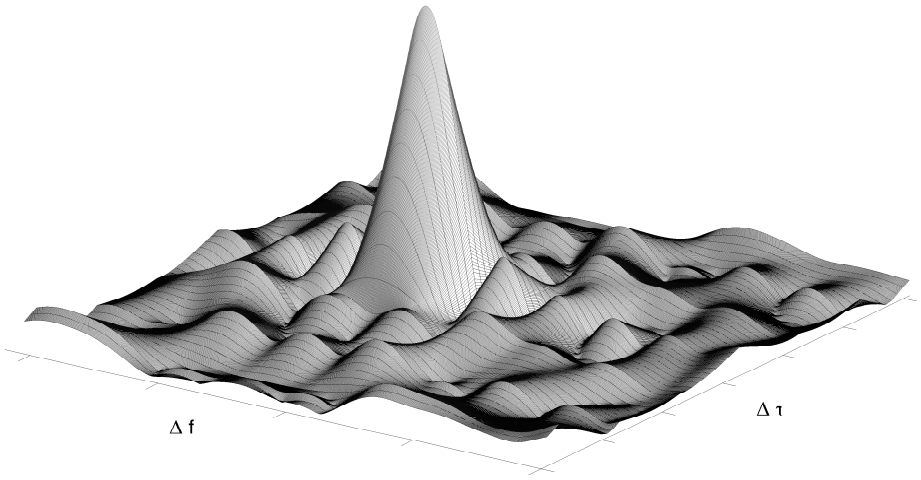

Figure 1.6: CAF Magnitude Surface. Example of the magnitude surface created by the CAF in time and frequency.

Thus the CAF searches over a grid of TDOA/FDOA values $(\Delta\hat{\tau}, \Delta\hat{f})$ whilst correlating the received signals in time and frequency. With traditional SISO signals in the absence of noise, the $\Delta\hat{\tau}$ and $\Delta\hat{f}$ that correspond to the actual TDOA and FDOA yield the maximum of the CAF magnitude:

$$\Delta\tau, \Delta f = \underset{\Delta\hat{\tau}, \Delta\hat{f}}{\arg\max} |\Lambda(\Delta\hat{\tau}, \Delta\hat{f})|. \tag{1.9}$$

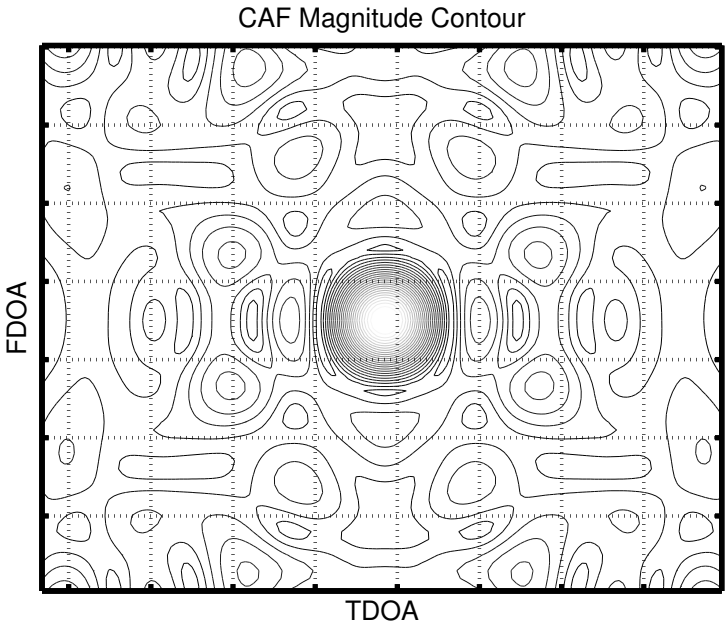

Figure 1.7: CAF Grid. Top down view of the CAF showing the TDOA/FDOA search grid.

As shown in Figures 1.6 and 1.7 the CAF has a main lobe which corresponds to the correct TDOA/FDOA location. It has been shown by Stein that the main lobe width is proportional to the CRLB for TDOA/FDOA and is given by [23]:

$$\sigma_{\Delta\tau} = \frac{1}{\mathcal{B}} \frac{1}{\sqrt{BT\gamma}} \tag{1.10}$$

$$\sigma_{\Delta f} = \frac{1}{T_e} \frac{1}{\sqrt{BT\gamma}} \tag{1.11}$$

where:

B= noise bandwidth at the receiver input, assumed the same for both receivers
$\mathcal{B}$= "rms radian frequency" in the received signal spectrum
T_e= "rms integration time"
γ= effective input SNR

and $\mathcal{B}$ and T_e are defined as:

$$\mathcal{B} = 2\pi \left[\frac{\int_{-\infty}^{\infty} f^2 W_s(f) df}{\int_{-\infty}^{\infty} W_s(f) df} \right]^{1/2} \tag{1.12}$$

$$T_e = 2\pi \left[\frac{\int_{-\infty}^{\infty} t^2 |w(t)|^2 dt}{\int_{-\infty}^{\infty} |w(t)|^2 dt} \right]^{1/2} \tag{1.13}$$

where $W_s(f)$ is the power spectral density of the transmit signal $w(t)$. The effective input SNR, γ, is defined as:

$$\frac{1}{\gamma} = \frac{1}{2} \left[\frac{1}{\gamma_1} + \frac{1}{\gamma_2} + \frac{1}{\gamma_1 \gamma_2} \right] \tag{1.14}$$

where γ_1 and γ_2 are the individual channel SNR's at each receiver. In general, TDOA accuracy improves for larger signal bandwidths and FDOA accuracy improves for larger integration periods. In the discrete domain TDOA and FDOA resolution is inversely proportional to the sampling frequency and number of samples respectively. Assuming the received signals are sampled so that there is one sample per symbol, then there will be one time-frequency bin which corresponds to the CAF peak and the correct TDOA/FDOA value. The focus is now on finding which bin corresponds to the main lobe, for once the main lobe is found further processing can be performed to obtain higher resolution estimates of TDOA/FDOA. An example of the CAF surface when there is one sample per symbol is shown in Figure 1.8, where there is one main lobe peak and all other bins can be considered some form of noise.

Using this approach if there are M TDOA bins and N FDOA bins the CAF surface grid has a total of MN bins, one of which corresponds to the main lobe and the correct TDOA/FDOA bin and has the magnitude value C_p. Then there will be $MN - 1$ bins left which are designated the noise bins, which are modeled as complex Gaussian noise, and given the label

n_k where $k = 1, 2, ..., MN - 1$. Therefore the CAF magnitude is described as:

$$|\Lambda(\Delta\hat{\tau}, \Delta\hat{f})| = \begin{cases} C_p & \Delta\hat{\tau} = \Delta\tau, \Delta\hat{f} = \Delta f \\ |n_k| & \text{otherwise.} \end{cases} \tag{1.15}$$

Using this detection theory framework the probability of error can be defined as:

$$\mathcal{P}[\text{Error}] = 1 - \mathcal{P}[\Delta\hat{\tau} = \Delta\tau, \Delta\hat{f} = \Delta f] \tag{1.16}$$

where it is emphasized that the true and correct TDOA/FDOA bin will be denoted by $\Delta\tau$ and Δf. Now we can find the probability of error using these terms:

$$\mathcal{P}[\text{Error}] = 1 - \mathcal{P}[C_p > |n_k| \ \forall k] = \mathcal{P}[C_p < \hat{n}, \hat{n} = \max_k\{|n_k|\}] \tag{1.17}$$

where C_p has a probability density function (PDF) $f_{C_p}(c)$ depending on the signal type, and $\hat{n}$ is the max absolute value of all $MN - 1$ noise terms with the cumulative density function $F_{\hat{n}}(\gamma)$. From order statistics the cumulative density function (CDF) of the largest noise value can be written as [7]:

$$F_{\hat{n}}(\gamma) = \mathcal{P}[n_1, n_2, ..., n_{MN-1} \leq \gamma] = F_n^{MN-1}(\gamma) \tag{1.18}$$

where $F_n(\gamma)$ is the CDF of $|n_k|$. The PDF of the max noise term is the derivative of the CDF, $f_{\hat{n}}(\gamma) = \frac{d}{d\gamma}F_{\hat{n}}(\gamma)$. The probability of error is then:

$$\begin{aligned} \mathcal{P}[C_p < \hat{n}] &= \int_0^\infty \int_0^\gamma f_{\hat{n}}(\gamma) f_{C_p}(c) dc d\gamma. \\ &= \int_0^\infty f_{\hat{n}}(\gamma) F_{C_p}(\gamma) d\gamma. \end{aligned} \tag{1.19}$$

The distributions of the noise bins and correct TDOA/FDOA bin, which depends on the signal type (i.e. SISO, spatial multiplexing, STBC), are needed to find the probability of error. In the following sections we show the derivation of these distributions for SISO and MIMO signals and complete the probability of error analysis. Note that n_k is not strictly noise, and therefore neither is $\hat{n}$, but they will be modeled as complex Gaussian noise which

is a good approximation as we will show in the following chapters.

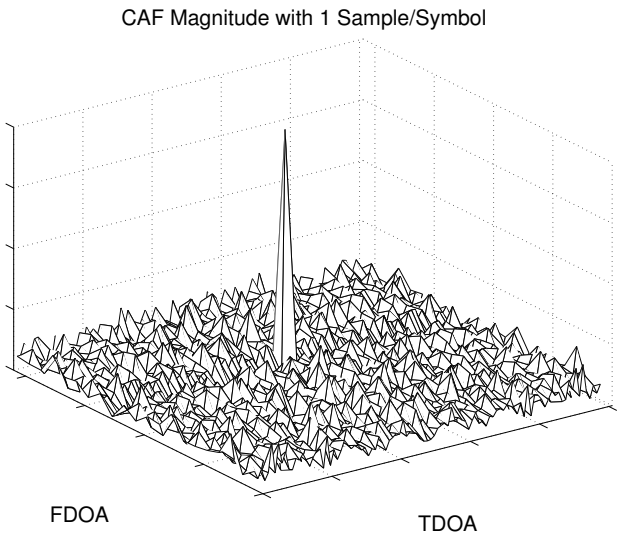

Figure 1.8: CAF Magnitude Surface with Minimum Sampling. The received symbols have been sampled at the symbol peak with 1 Sample/Symbol. Therefore there is only one bin that corresponds to the CAF main lobe and therefore the correct TDOA/FDOA bin.

Chapter 2

The CAF Applied to SISO Signals

To discuss how MIMO signals affect the CAF it is important to first understand CAF processing with SISO signals. This section will therefore provide a theoretical analysis which represents how the CAF is typically calculated on SISO signals. Our goal in this section is to find the value of the CAF main lobe without noise, which means we are looking for the CAF magnitude at $\Delta\tau, \Delta f$. Assuming we have one transmitter and two receivers then the two received signals will have $r = 1, 2$, $l = 1$, so we can drop the subscript for l reducing the summation in (1.7) to:

$$\tilde{r}_r(t) = \sqrt{P_r} b(t - \tau_r) e^{j(2\pi f_{dr} t + \theta_r)} \tag{2.1}$$

Now using the CAF on the two received signals:

$$\begin{aligned} \Lambda(\Delta\hat{t}, \Delta\hat{f}) &= \int_0^T \tilde{r}_1(t) \tilde{r}_2^*(t - \Delta\hat{\tau}) e^{-j2\pi\Delta\hat{f}t} dt \\ &= \sqrt{P_1 P_2} \int_0^T b(t - \tau_1) b(t - \tau_2 - \Delta\hat{\tau}) e^{j(2\pi(f_{d1} - f_{d2})t - 2\pi\Delta\hat{f}t + \theta_1 - \theta_2)} dt \end{aligned} \tag{2.2}$$

The maximum magnitude will occur at $\Delta\hat{\tau} = \Delta\tau = \tau_1 - \tau_2$ and $\Delta\hat{f} = \Delta f = f_{d1} - f_{d2}$:

$$\begin{aligned}\Lambda_{max} &= \Lambda(\tau_1 - \tau_2, f_{d1} - f_{d2}) \\ &= \sqrt{P_1 P_2}\int_0^T b^2(t-\tau_1)e^{j(\theta_1-\theta_2)}dt \\ &= \sqrt{P_1 P_2}e^{j(\theta_1-\theta_2)}\int_0^T 1dt = T\sqrt{P_1 P_2}e^{j(\theta_1-\theta_2)}\end{aligned}$$

which makes the assumption that when the signal envelope is squared it is equal to one ($b^2(t) = 1$). Then taking the magnitude we finally have:

$$|\Lambda(\Delta\tau, \Delta\tau)| = T\sqrt{P_1 P_2} \tag{2.3}$$

Thus at the correct TDOA/FDOA bin the CAF magnitude for SISO is a constant proportional to the two received signal amplitudes and integration period, in the absence of noise.

2.1 Noise Analysis

We have shown the CAF magnitude at the correct TDOA/FDOA without noise. Now we include additive white Gaussian noise (AWGN) in the analysis in order to show its CAF magnitude distribution. Using the same signal model as before but with the extra complex noise term:

$$\tilde{r}_r(t) = \sqrt{P_r}b(t-\tau_r)e^{j(2\pi f_{dr}t+\theta_r)} + \tilde{n}_r(t)$$

where $\tilde{n}_r(t)$ is a complex Gaussian random process with the underlying distribution given by $\mathcal{N}_c\left(0, \frac{\sigma_{n,r}^2}{2}\right)$ (where the c denotes complex) with noise power $\sigma_{n,r}^2$ split equally in the real and imaginary parts. The notation $\mathcal{N}_c(\mu, \sigma^2)$ is used to represent the complex normal distribution with mean μ and variance σ^2 in each dimension. As before, the two received

signals are put into the CAF:

$$\Lambda(\Delta\hat{\tau},\Delta\hat{f}) = \int_0^T \left(\sqrt{P_1}b(t-\tau_1)e^{j(2\pi f_{d1}t+\theta_1)} + \tilde{n}_1(t)\right) \\ * \left(\sqrt{P_2}b^*(t-\tau_2-\Delta\hat{\tau})e^{-j(2\pi f_{d2}t+\theta_2)} + \tilde{n}_2^*(t)\right) e^{-j(2\pi\Delta\hat{f})t}dt$$

$$\begin{aligned}\Lambda(\Delta\hat{\tau},\Delta\hat{f}) = \int_0^T & \left(\sqrt{P_1}b(t-\tau_1)e^{j(2\pi f_{d1}t+\theta_1)}\sqrt{P_2}b^*(t-\tau_2-\Delta\hat{\tau})e^{-j(2\pi f_{d2}t+\theta_2)}\right) e^{-j(2\pi\Delta\hat{f})t} \\ & + \left(\sqrt{P_1}b(t-\tau_1)e^{j(2\pi f_{d1}t+\theta_1)}\right)\tilde{n}_2(t)e^{-j(2\pi\Delta\hat{f})t} \\ & + \left(\sqrt{P_2}b^*(t-\tau_2-\Delta\hat{\tau})e^{j(2\pi f_{d2}t+\theta_2)}\right)\tilde{n}_1(t)e^{-j(2\pi\Delta\hat{f})t} \\ & + \tilde{n}_1(t)\tilde{n}_2(t)e^{-j(2\pi\Delta\hat{f})t}dt\end{aligned}$$

We therefore have the desired signal term (the first term in the integral), and three noise terms. We can rewrite this as:

$$\Lambda(\Delta\hat{\tau},\Delta\hat{f}) = \int_0^T \left(d(t) + N_1(t) + N_2(t) + N_3(t)\right) dt$$

where $d(t)$ is our desired signal term and the noise terms are $N_{1-3}(t)$.

2.1.1 SISO CAF Magnitude Distribution at the Correct TDOA/FDOA Bin in Noise

Focusing on the CAF magnitude at $\Delta\hat{\tau} = \Delta\tau$ and $\Delta\hat{f} = \Delta f$ the desired term reduces to $T\sqrt{P_1P_2}$, the result from equation (2.3). The first and second noise terms ($N_1(t)$ and $N_2(t)$) can be approximated as complex Gaussian (stationary) random processes and thus the integration over T will yield:

$$\int_0^T N_1(t)dt + \int_0^T N_2(t)dt \sim \mathcal{N}_c\left(0, \frac{TP_1\sigma_{n,2}^2}{2}\right) + \mathcal{N}_c\left(0, \frac{TP_2\sigma_{n,1}^2}{2}\right) \tag{2.4}$$

since each term is the integration of complex Gaussian random processes. The third noise term is more complicated but we can start by finding the variance:

$$\begin{aligned} Var[N_3(t)] =& \mathrm{E}\left[\int_0^T \int_0^T \left(N_3(t)\right)\left(N_3^*(s)\right) dtds\right] \\ =& \int_0^T \int_0^T \mathrm{E}\left[\left(\tilde{n}_1(t)\tilde{n}_1^*(s)\right)\left(\tilde{n}_2^*(t)\tilde{n}_2^*(s)\right)\right] dtds \end{aligned} \tag{2.5}$$

where $\mathrm{E}[\cdot]$ denotes the expectation operator. Because the noise processes are assumed white each sample in time is uncorrelated with any other sample therefore the products $\tilde{n}(t)\tilde{n}^*(s)$ will be zero unless $t = s$, thus:

$$Var[N_3(t)] = \int_0^T \mathrm{E}\left[\tilde{n}_1(t)\tilde{n}_1^*(t)\right]\mathrm{E}\left[\tilde{n}_2^*(t)\tilde{n}_2^*(t)\right] dt.$$

Breaking the noise terms into real and imaginary parts:

$$\begin{aligned} Var[N_3(t)] &= \int_0^T \left(\mathrm{E}[n_{1,re}^2(t)] + \mathrm{E}[n_{1,im}^2(t)]\right)\left(\mathrm{E}[n_{2,re}^2(t)] + \mathrm{E}[n_{2,im}^2(t)]\right) dt \\ &= \int_0^T \left(\frac{\sigma_{n,1}^2}{2} + \frac{\sigma_{n,1}^2}{2}\right)\left(\frac{\sigma_{n,2}^2}{2} + \frac{\sigma_{n,2}^2}{2}\right) dt \end{aligned}$$

and finally:

$$Var[N_3(t)] = T\sigma_{n,1}^2\sigma_{n,2}^2.$$

Using the Central Limit Theorem (CLT) and assuming there are a sufficient number of samples (large enough T) the third term can be approximated as a complex Gaussian:

$$\int_0^T N_3(t)dt \sim \mathcal{N}_c\left(0, \frac{T\sigma_{n,1}^2\sigma_{n,2}^2}{2}\right).$$

Using the normal distribution notation we can put all the terms back together:

$$\begin{aligned} |\Lambda(\Delta\tau, \Delta f)| \sim & \left| T\sqrt{P_1P_2}e^{j(\theta_1-\theta_2)} + \mathcal{N}_c\left(0, \frac{TP_1\sigma_{n,2}^2}{2}\right)e^{j\theta_1}\right. \\ & \left. + \mathcal{N}_c\left(0, \frac{TP_2\sigma_{n,1}^2}{2}\right)e^{j\theta_2} + \mathcal{N}_c\left(0, \frac{T\sigma_{n,1}^2\sigma_{n,2}^2}{2}\right)\right| \\ \sim & \left|\mathcal{N}_c\left(T\sqrt{P_1P_2}, \frac{T}{2}(P_1\sigma_{n,2}^2 + P_2\sigma_{n,1}^2 + \sigma_{n,1}^2\sigma_{n,2}^2)\right)\right|. \end{aligned}$$

The magnitude of a complex Gaussian is obviously Rician so the CDF of the CAF magnitude of the main lobe (correct TDOA/FDOA bin) for SISO is:

$$F_{C_p}(c) = 1 - \mathcal{Q}_1\left(\frac{v}{\sigma_c}, \frac{c}{\sigma_c}\right) \tag{2.6}$$

where the location parameter $v = \frac{T\sqrt{P_1 P_2}}{2}$ and with scale parameter $\sigma_c^2 = \frac{T}{2}(P_1\sigma_{n,2}^2 + P_2\sigma_{n,1}^2 + \sigma_{n,1}^2\sigma_{n,2}^2)$. For reference purposes $\mathcal{Q}_M(a,b)$ is the Marcum Q-function which is given by:

$$\mathcal{Q}_M(a,b) = \int_b^\infty x\left(\frac{x}{a}\right)^{M-1} e^{\left(-\frac{x^2+a^2}{2}\right)}\mathcal{I}_{M-1}(ax)dx$$

and $\mathcal{I}_\alpha$ is the modified Bessel function of order α where $\mathcal{I}_\alpha(x) = j^{-\alpha}\mathcal{J}_\alpha(jx)$ and $\mathcal{J}_\alpha$ is the Bessel function of the first kind and $j = \sqrt{-1}$ the imaginary unit.

2.1.2 SISO CAF Distribution of the Noise Bins

The CAF magnitude at any of the incorrect bins will have a similar result as before except for the desired term. The symbols in the received signals no longer correlate in time or frequency so the desired term can be modeled as:

$$d(t) = \sqrt{P_1 P_2}\int_0^T B(t)e^{j2\pi ft}dt \tag{2.7}$$

where $B(t)$ represents the product of the transmitted symbols at different delays, and f is a uniform random frequency over the search range of the CAF. If we at first assume that BPSK modulation is used then $B(t)$ is a series of signed pulses and can be modeled as:

$$B(t) = \sum_{k=0}^{N_{sym}} S_k P(t + kT_{sym})$$

where P is the pulse shape, T_{sym} is the symbol period, N_{sym} is the number of symbols, and S_k is defined as:

$$S_k = \begin{cases} +1 & p = 0.5 \\ -1 & p = 0.5 \end{cases}$$

where p is the probability of a ± 1 being transmitted which is assumed equal. The CAF integration is therefore a sum of binary random variables and is equal to the transformation of a binomial random variable $B_v \sim \mathcal{B}(N_{sym}, p = 0.5)$ where the number of trials is N_{sym} and the probability of success is $p = 0.5$. This new random variable is designated β:

$$\beta = \sum_{k=0}^{N_{sym}} S_k = (2 * B_v - N_{sym}). \tag{2.8}$$

And β has the following probability density function:

$$P_\beta(b) = \sum_{n=0}^{N_{sym}} \binom{N_{sym}}{n} \frac{1}{2^{N_{sym}}} \delta \left[n - \frac{N_{sym} + b}{2} \right] \tag{2.9}$$

for even values of $b \in [-N_{sym}, N_{sym}]$, and where $\binom{n}{k} = \frac{n!}{k!(n-k)!}$ denotes the combination operator. This result can vary based on the pulse shape of the signal, but assuming we are sampling at the peak of the pulse and have one sample per symbol this result will still apply. If the number of symbols is large enough then we can approximate β with a Gaussian distribution, $\mathcal{N}(0, N_{sym})$, by the CLT. If there is oversampling then we need to multiply β by the oversampling factor (or by T_{sym} the symbol period in the continuous domain).

Because of the complex exponential in equation (2.7), β becomes a complex Gaussian random variable with the variance split equally in the real and imaginary parts. Therefore going back to the continuous domain $\beta \sim \mathcal{N}_c\left(0, \sigma_\beta^2\right)$, where for BPSK modulation $\sigma_\beta^2 = \frac{T}{2} P_1 P_2$. For higher order modulation schemes β can still be modeled as a complex Gaussian random variable, but the variance is specific to each modulation scheme. In general, as the modulation order increases, the variance of β decreases since it is less likely that the symbols will combine coherently. Therefore even in the absence of AWGN in the received signal, there will still be $MN - 1$ "noise bins" due to the randomness of the signal and how the received signals correlate. This realization will prove to be of much more importance when dealing with MIMO signals.

Using the Gaussian approximation of β the CAF magnitude when $\Delta\hat{\tau} \neq \Delta\tau$ and $\Delta\hat{f} \neq \Delta f$ is:

$$\Lambda(\Delta\hat{\tau} \neq \Delta\tau, \Delta\hat{f} \neq \Delta f) \sim \left|\mathcal{N}_c\left(0, \sigma_c^2 + \sigma_\beta^2\right)\right|$$

which results in a Rayleigh random variable with the following CDF:

$$F_n(\gamma) = 1 - e^{\frac{-\gamma^2}{2\sigma^2}} \tag{2.10}$$

where $\sigma^2 = \sigma_c^2 + \sigma_\beta^2$ and $\sigma_c^2 = \frac{T}{2}(P_1\sigma_{n,2}^2 + P_2\sigma_{n,1}^2 + \sigma_{n,1}^2\sigma_{n,2}^2)$, as derived previously, and σ_β varies depending on the modulation of the received signals.

The CAF magnitude of the main lobe (correct TDOA/FDOA bin) and the noise bins is plotted in Figure 2.1 from simulated CAF data (as described later in Chapter 5) and compared to the theoretical distributions derived in this section. The results confirm that the CAF magnitude at the correct TDOA/FDOA bin follows a Rice distribution and that of the noise bins follows a Rayleigh distribution.

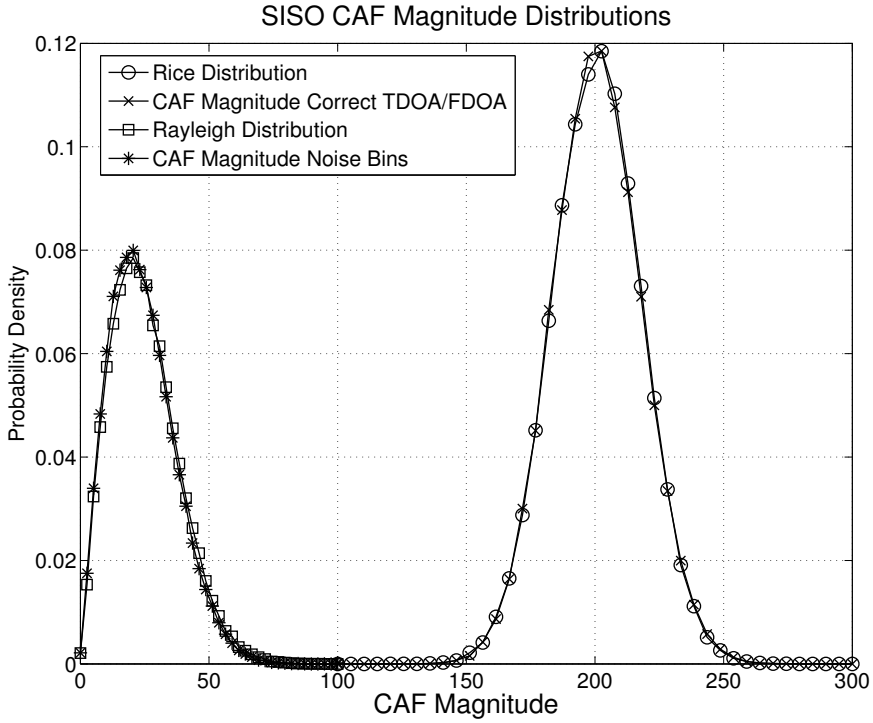

Figure 2.1: SISO CAF Magnitude Distributions with Noise. The distributions are compared to the Rice and Rayleigh distributions with $P_1 = P_2 = 1$, $T = 200$, and $\sigma_n^2 = 1$ (0 dB SNR) showing the closeness of fit.

2.2 SISO Probability of Error

Now that the distributions of the CAF peak and noise are determined we can express the probability of error. Since the distribution of the noise is Rayleigh, then from equation (1.18) and (2.10) the distribution of the max noise bin is:

$$F_{\hat{n}}(\gamma) = \left(1 - e^{\frac{-\gamma^2}{2\sigma^2}}\right)^{MN-1} \tag{2.11}$$

and the PDF is:

$$f_{\hat{n}}(\gamma) = (MN-1)\frac{\gamma}{\sigma^2}\left(1 - e^{\frac{-\gamma^2}{2\sigma^2}}\right)^{MN-2} e^{\frac{-\gamma^2}{2\sigma^2}}. \tag{2.12}$$

which is shown in Figure 2.3 along with the distribution of the noise and the CAF main lobe. The probability of error is the amount of overlap of the max noise distribution and that of the CAF main lobe. Written out using the Rician CDF of the CAF peak the probability of error is:

$$\mathcal{P}[C_p < \hat{n}] = \int_0^\infty f_{\hat{n}}(\gamma) F_{C_p}(\gamma) d\gamma$$

$$\mathcal{P}[\text{SISO Error}] = \int_0^\infty (MN-1)\frac{\gamma}{\sigma^2}\left(1 - e^{\frac{-\gamma^2}{2\sigma^2}}\right)^{MN-2} e^{\frac{-\gamma^2}{2\sigma^2}} \left(1 - \mathcal{Q}_1\left(\frac{v}{\sigma_c}, \frac{\gamma}{\sigma_c}\right)\right) d\gamma \quad (2.13)$$

where again $\sigma^2 = \sigma_c^2 + \sigma_\beta^2$ and $\sigma_c^2 = \frac{T}{2}(P_1\sigma_{n,2}^2 + P_2\sigma_{n,1}^2 + \sigma_{n,1}^2\sigma_{n,2}^2)$. For most of this thesis it is assumed that the signal power and noise power of the received signals is the same at the two collectors so that $P_1 = P_2$ and $\sigma_n = \sigma_{n,1} = \sigma_{n,2}$ therefore $\sigma_c^2 = \frac{T\sigma_n^2}{2}(P_1 + P_2 + \sigma_n^2)$.

An example of the SISO CAF probability of error is shown in Figure 2.2 illustrating a BPSK result where $\sigma_\beta = \frac{T}{2}P_1P_2$.

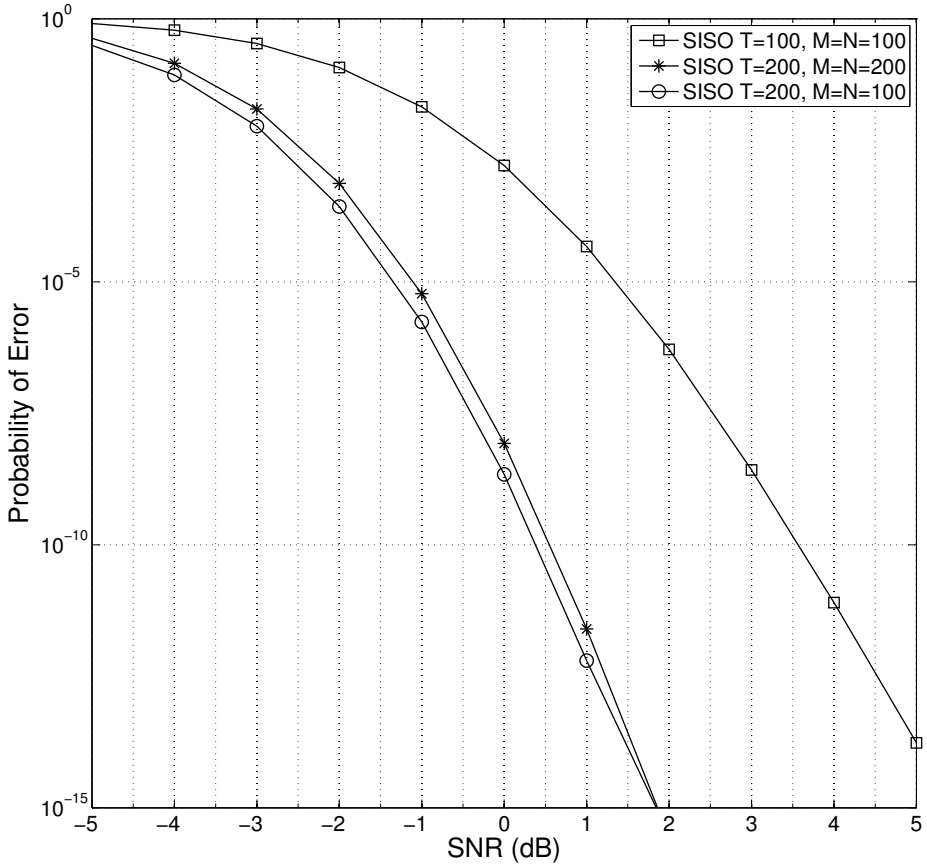

Figure 2.2: SISO Probability of Error. Evaluated from equation (2.13) using numerical integration with $P_1 = P_2 = 1$ and $\sigma_n^2 = 1/\text{SNR}$ for different integration periods (T) and search grid size (M, N).

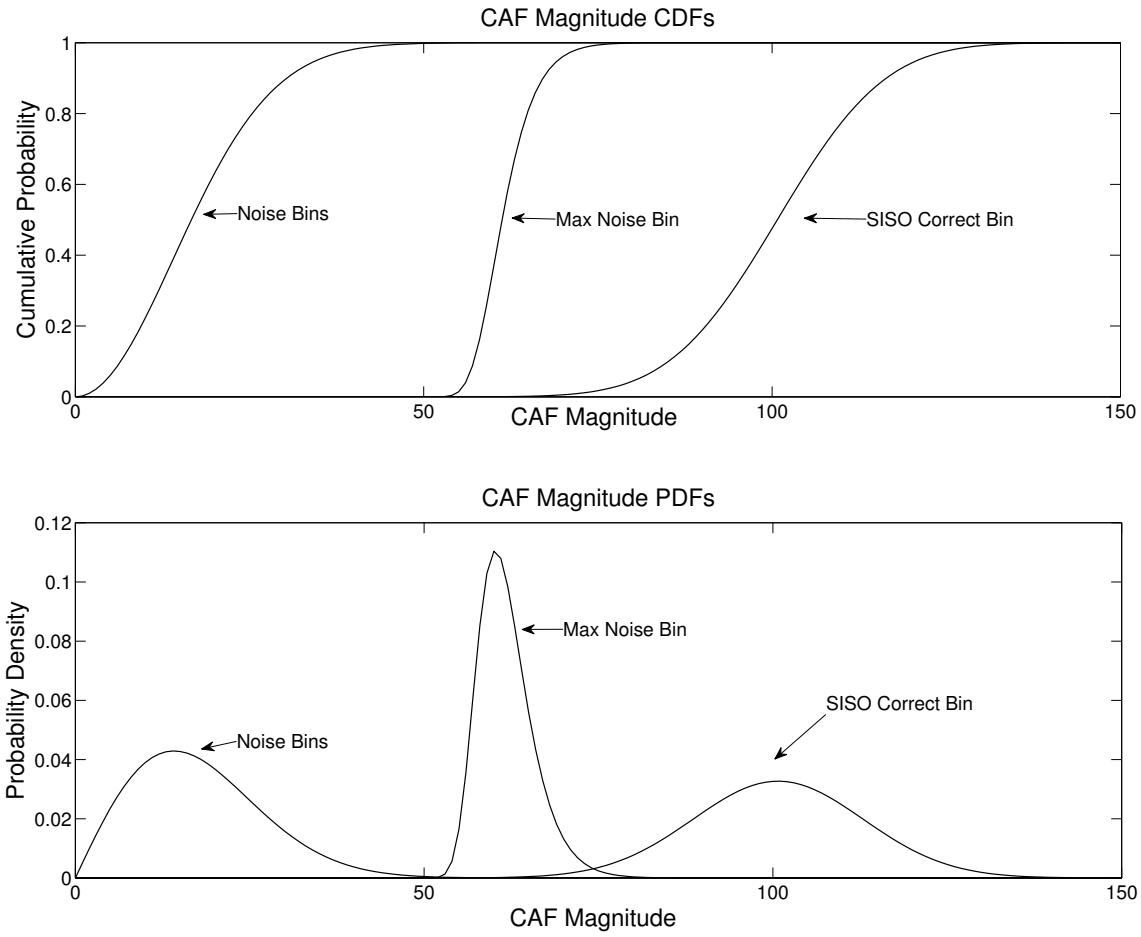

Figure 2.3: SISO and Noise Distributions. Distributions of the main lobe CAF magnitude and that of the noise bins and max noise bin for $P_1 = P_2 = 1$, $T = 100$, and $\sigma_n^2 = 1$.

Chapter 3

The CAF Applied to MIMO Signals: Two Transmit Antennas

In this thesis we are interested in the impact that MIMO transmission has on standard CAF processing. Thus, we repeat the analysis in Chapter 2 in order to find the PDF of the CAF main lobe for the case where the transmitter is MIMO with two antennas. Therefore once again we are looking for the CAF magnitude at the correct TDOA/FDOA bin. Using the signal model from (1.7) and ignoring noise for now, the received signal for the first receiver ($r = 1$) will be:

$$\tilde{r}_1(t) = \sqrt{P_1/2}\, b_1(t-\tau_1)e^{j(2\pi f_{d1}t+\theta_{1,1})} + \sqrt{P_2/2}\, b_2(t-\tau_1)e^{j(2\pi f_{d1}t+\theta_{1,2})} \tag{3.1}$$

where the two terms represent the signals received from the two transmit antennas, and again $\theta_{r,l}$ is the phase of the signal from transmitter l to receiver r. Calculating the CAF on these signals using (1.8) and we have:

$$\Lambda(\Delta\hat{\tau}, \Delta\hat{f}) = \sqrt{\frac{P_1P_2}{4}} \int_0^T e^{j2\pi f_{d1}t} e^{-j2\pi f_{d2}t} e^{-j2\pi\Delta f t} e^{-j2\pi\psi}$$

$$(e^{j\theta_{1,1}} b_1(t-\tau_1) + e^{j\theta_{1,2}} b_2(t-\tau_1))(e^{j\theta_{2,1}} b_1^*(t-\tau_2-\Delta\tau) + e^{j\theta_{2,2}} b_2^*(t-\tau_2-\Delta\tau))dt$$

The main CAF lobe is located at bins $\Delta\hat{\tau} = \tau_1 - \tau_2$ and $\Delta\hat{f} = f_{d1} - f_{d2}$:

$$\Lambda(\tau_1 - \tau_2, f_{d1} - f_{d2}) = \sqrt{\frac{P_1 P_2}{4}} \int_0^T e^{-j2\pi\psi}(e^{j(\theta_{1,1}+\theta_{2,1})} b_1^2(t-\tau_1)$$

$$+e^{j(\theta_{1,1}+\theta_{2,2})} b_1(t-\tau_1) b_2^*(t-\tau_1) + e^{j(\theta_{1,2}+\theta_{2,1})} b_2(t-\tau_1) b_1^*(t-\tau_1) + e^{j(\theta_{1,2}+\theta_{2,2})} b_2^2(t-\tau_1))dt$$

where ψ is a phase offset due to $\Delta\tau$. Combining the random phases so that θ_A to θ_D are uniform independent random phases from $0 - 2\pi$ and assuming we take one of the phases as our reference then:

$$\Lambda(\Delta\hat{\tau}, \Delta\hat{f}) = \sqrt{\frac{P_1 P_2}{4}} e^{j\theta_A} \int_0^T (b_1^2(t-\tau_1) + e^{j\theta_B} b_1(t-\tau_1) b_2^*(t-\tau_1) \tag{3.2}$$

$$+ e^{j\theta_C} b_1^*(t-\tau_1) b_2(t-\tau_1) + e^{j\theta_D} b_2^2(t-\tau_1))dt.$$

The integration of the signal cross terms $b_1(t-\tau_1)b_2(t-\tau_1)$ can be modeled as a random variable β as shown in Chapter 2.1.2. Thus the result from equation (3.2) can be represented as the following function of random variables:

$$\Lambda(\Delta\tau, \Delta f) = \sqrt{\frac{P_1 P_2}{4}} e^{j\theta_A} \left[T + Te^{j\theta_D} + \beta\left(e^{j\theta_B} + e^{j\theta_C}\right)\right]. \tag{3.3}$$

Finally the CAF magnitude of the main lobe is the random variable C_p:

$$C_p = |\Lambda(\Delta\tau, \Delta f)| \tag{3.4}$$

$$C_p = \frac{\sqrt{P_1 P_2}}{2} \left|T + Te^{j\theta_D} + \beta(e^{j\theta_B} + e^{j\theta_C})\right| \tag{3.5}$$

In general the MIMO CAF maximum, even in the absence of noise, is a randomly distributed value due to both the channel phases and symbol combining. This means the received signals could add incoherently, effectively reducing the SNR. Thus, even in very high SNR environments, the peak of the CAF may not correspond to the true TDOA/FDOA. The next sections will focus on different MIMO transmission schemes, and how the CAF magnitude is affected.

When noise is present the derivation is similar to that of Chapter 2.1.1 and so we will generalize that the CAF magnitude becomes:

$$C_p = \left| \frac{\sqrt{P_1 P_2}}{2} \left(T + T e^{j\theta_D} + \beta(e^{j\theta_B} + e^{j\theta_C}) \right) + \tilde{n} \right| \tag{3.6}$$

where $\tilde{n} \sim \mathcal{N}_c \left(0, \sigma_c^2 = \frac{T\sigma_n^2}{2}(P_1 + P_2 + \sigma_n^2) \right)$ once again assuming that the noise power at both receivers is the same and equal to σ_n^2.

3.1 Alamouti Space Time Block Coding (ASTBC)

For ASTBC transmission, CAF magnitude equation (3.4) can be simplified further given the nature of space-time-block-coding. Due to the orthogonality of the STBCs when the received signals from each antenna are cross correlated, the β that is produced is approximately zero. We can show this more specifically if we generate the following symbol stream in discrete time prior to space-time encoding:

$$\bar{\mathbf{b}} = \left[b^{(1)},\ b^{(2)},\ b^{(3)},\ b^{(4)},\ b^{(5)},\ b^{(6)},\ \ldots\ ,\ b^{(N_{sym})} \right] \tag{3.7}$$

and then applying the Alamouti coding matrix from equation (1.4) reproduced below:

$$\mathbf{C} = \begin{bmatrix} b^{(1)} & -b^{(2)*} \\ b^{(2)} & b^{(1)*} \end{bmatrix}$$

then the signals from the two transmit antennas will now look like:

$$\begin{aligned} \bar{\mathbf{b}}_1 &= [\ \ b^{(1)},\ \ -b^{(2)*},\ \ b^{(3)},\ \ -b^{(4)*},\ \ b^{(5)},\ \ -b^{(6)*},\ \ldots\ ,\ -b^{(N_{sym})*}] \\ \bar{\mathbf{b}}_2 &= [\ \ b^{(2)},\ \ \ \ b^{(1)*},\ \ b^{(4)},\ \ \ \ b^{(3)*},\ \ b^{(6)},\ \ \ \ b^{(5)*},\ \ldots\ ,\ b^{(N_{sym}-1)*}] \end{aligned} \tag{3.8}$$

where $\bar{\mathbf{b}}_1$ is the the symbol stream transmitted from antenna 1, and $\bar{\mathbf{b}}_2$ is the symbol stream transmitted from antenna 2. So now the cross product of the $b_1(t)$ and $b_2^*(t)$ (ignoring the

time delay offset τ_1) during integration in discrete time will appear as:

$$\bar{\mathbf{b}}_1\bar{\mathbf{b}}_2^{\dagger} = b^{(1)}b^{(2)*} - b^{(1)}b^{(2)*} + b^{(3)}b^{(4)*} - b^{(3)}b^{(4)*} + \ \ldots\ - b^{(N_{sym})*}b^{(N_{sym}-1)} \tag{3.9}$$

where the "†" indicates the Hermitian transpose operator. Every other term in the summation is followed by its negation. Therefore when we integrate, the terms add to zero (again this is only when $\Delta\tau = \tau_1 - \tau_2$). We therefore consider β negligible and can ignore it, leaving the CAF random variable C_P as follows:

$$C_p = \frac{\sqrt{P_1P_2}}{2}T|1 + e^{j\theta}|. \tag{3.10}$$

First we point out that the random variable $|1 + e^{j\theta}|^2$ has been widely studied such as in [22]. When we add the scale factor P so that the random variable is $\zeta = |P + Pe^{j\theta}|$ then by following [22] the PDF can be shown to be:

$$f_{C_p}(c) = \frac{c}{\pi P^2\sqrt{1 - \left(\frac{c^2-2P^2}{2P^2}\right)^2}} \qquad 0 \le c < 2P \tag{3.11}$$

where $P = \frac{\sqrt{P_1P_2}}{2}T$ in this case. When we add noise the CAF magnitude random variable becomes:

$$C_p = \left|\frac{\sqrt{P_1P_2}}{2}T\left(1 + e^{j\theta}\right) + \tilde{n}\right|. \tag{3.12}$$

This random variable has also been studied extensively such as in [1, 6, 8] and one of the most well known versions of the CDF is from [21]:

$$F_{c_p}(c) = \int_0^{\infty} c\mathcal{J}_0(Pz)^{N_t}\mathcal{J}_1(cz)e^{\frac{z^2\sigma_{c_p}^2}{2}}dz \tag{3.13}$$

where $N_t = 2$ for the case of two transmit antennas, $\mathcal{J}_\alpha(x)$ is the Bessel function of the first kind with order α, and $\sigma_{c_p}^2 = \frac{T\sigma_n^2}{2}(P_1 + P_2 + \sigma_n^2)$ the noise variance as derived from Section 2.1.1. This integral has been expressed and evaluated using a number of mathematical techniques. There are nearly a hundred references that are outlined in [1] that cover many aspects, applications, and extensions to the problem of evaluating this integral. However with

today's computing capability this integral can easily be solved using numerical methods, and so for our purposes we will rely on numerical integration. Typically this integral cannot be evaluated for low values of $\sigma^2_{c_p}$, but in that case the PDF in (3.11) can be used. It should be noted that this version of the CDF assumes that the coefficients of the phase vectors (P) are all deterministic and equal. This is appropriate for this application but there are other applications where a different form of the CDF is needed which doesn't assume all coefficients are equal [1, 21].

The CDF and PDF of the main lobe of the CAF for ASTBC transmission are shown in Figure 3.1 where there is a noticeable peak near the number of transmitted symbols but also a heavy tail in the distribution covering lower magnitudes. With higher probabilities of a lower CAF magnitude comes the greater probability of error as we will see later in Section 3.3.

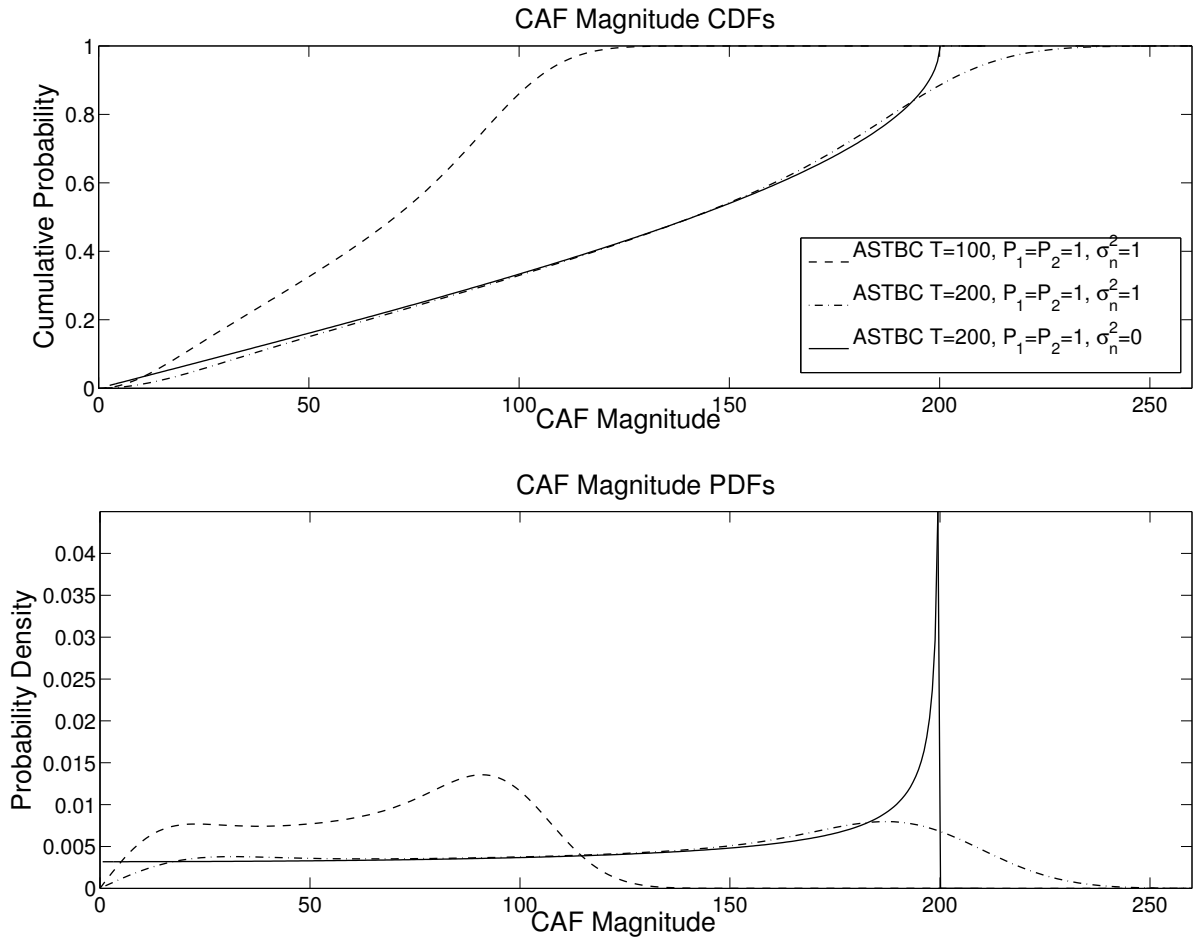

Figure 3.1: ASTBC Magnitude Distributions. Theoretical CAF magnitude distributions at the correct TDOA/FDOA bin from equation (3.13) using numerical integration.

3.1.1 Correlation Sidelobes

Due to the coding matrix of ASTBC the CAF surface will not only have one main peak at $\Delta\hat{\tau} = \tau_1 - \tau_1$ and $\Delta\hat{f} = f_{d1} - f_{d2}$ but also two correlation side lobes at $\Delta\hat{\tau} = \tau_1 - \tau_2 \pm T_{sym}$. Given the fading induced on the main lobe by the random phases, it is possible that these sidelobes could have a magnitude greater than the main lobe and therefore cause an error in TDOA on the order of $\pm T_{sym}$. To illustrate this effect we will derive the expression for the

CAF magnitude at these sidelobes.

Referring back to equation (3.2) but now focusing on the CAF bin where $\Delta\hat{\tau} = \tau_1 - \tau_2 \pm T_{sym}$ and $\Delta\hat{f} = \Delta f$ yields:

$$\Lambda(\Delta\tau \pm T_{sym}, \Delta f) = \sqrt{\frac{P_1 P_2}{4}} \int_0^T e^{-j2\pi\psi} * \tag{3.14}$$
$$\big[b_1(t-\tau_1)b_1^*(t-\tau_1 \pm T_{sym})e^{j\theta_A} + b_1(t-\tau_1)b_2^*(t-\tau_1 \pm T_{sym})e^{j\theta_B}$$
$$+b_2(t-\tau_1)b_1^*(t-\tau_1 \pm T_{sym})e^{j\theta_C} + b_2(t-\tau_1)b_2^*(t-\tau_1 \pm T_{sym})e^{j\theta_D}\big]\, dt$$

We can examine the data signals to determine what happens when we multiply and sum these signals. Although there will be two side lobes at $\pm T_{sym}$ we will focus on $-T_{sym}$ for this analysis. The data streams can be written as follows:

$$\bar{\mathbf{b}}_1 = [\ b^{(1)},\ -b^{(2)*},\ b^{(3)},\ -b^{(4)*},\ b^{(5)},\ -b^{(6)*},\ \ldots,\ -b^{(N_{sym})*}]$$
$$z^{-1}\bar{\mathbf{b}}_1 = [\ 0,\ b^{(1)},\ -b^{(2)*},\ b^{(3)},\ -b^{(4)*},\ b^{(5)},\ \ldots,\ b^{(N_{sym}-1)}]$$

where z^{-1} is the delay operator indicating a delay of one symbol period. Then we can find all the cross correlation terms in the discrete domain:

$$\begin{aligned}
\bar{\mathbf{b}}_1 \odot z^{-1}\bar{\mathbf{b}}_1^* &= [\ 0,\ -b^{(1)*}b^{(2)*},\ -b^{(2)}b^{(3)},\ -b^{(3)*}b^{(4)*},\ -b^{(4)}b^{(5)},\ -b^{(5)*}b^{(6)*},\ \ldots]\\
\bar{\mathbf{b}}_2 \odot z^{-1}\bar{\mathbf{b}}_2^* &= [\ 0,\ b^{(1)*}b^{(2)*},\ b^{(1)}b^{(4)},\ b^{(3)*}b^{(4)*},\ b^{(3)}b^{(6)},\ b^{(5)*}b^{(6)*},\ \ldots]\\
\bar{\mathbf{b}}_1 \odot z^{-1}\bar{\mathbf{b}}_2^* &= [\ 0,\ -(b^{(2)*})^2,\ b^{(1)}b^{(3)},\ -(b^{(4)*})^2,\ b^{(3)}b^{(5)},\ -(b^{(6)*})^2,\ \ldots]\\
\bar{\mathbf{b}}_2 \odot z^{-1}\bar{\mathbf{b}}_1^* &= [\ 0,\ (b^{(1)*})^2,\ -b^{(2)}b^{(4)},\ (b^{(3)*})^2,\ -b^{(4)}b^{(6)},\ (b^{(5)*})^2,\ \ldots]
\end{aligned}$$

where "$\odot$" signifies the multiplication is element by element. Ignoring the zero of the first symbol and including the random phases from our original expression in equation (3.14), the result is periodic and follows this general pattern with two repeating periods:

$$-b^{(1)*}b^{(2)*}e^{j\theta_A} + b^{(1)*}b^{(2)*}e^{j\theta_B} + (b^{(1)*})^2e^{j\theta_C} - (b^{(2)*})^2e^{j\theta_D},$$
$$-b^{(2)}b^{(3)}e^{j\theta_A} + b^{(1)}b^{(4)}e^{j\theta_B} + b^{(1)}b^{(3)}e^{j\theta_C} - b^{(2)}b^{(4)}e^{j\theta_D}, \ldots$$

Therefore due to the correlation and auto-correlation between the signals and their delayed

versions, the integration during the CAF will not have a zero mean. We can generalize the CAF magnitude at the sidelobes to be:

$$\Lambda(\Delta\tau \pm T_{sym}, \Delta f) = \sqrt{\frac{P_1 P_2}{4}} \left| \left(\frac{T}{2} + \beta_1\right) + (\beta_2 + \beta_3)e^{j\theta_A} + (\beta_2 + \beta_4)e^{j\theta_B} + \left(\frac{T}{2} + \beta_5\right) e^{j\theta_D} \right| \tag{3.15}$$

where each β_k is independent and identically distributed, and using the Gaussian approximation $\beta_k \sim \mathcal{N}(0, \frac{\sigma_\beta^2}{2})$, where σ_β^2 is defined for β as from Chapter 2.1.2. The variance is halved because there are two repeating periods during the cross correlation and thus each period occurs half as many times during the integration interval.

Thus, at the delays $\Delta\tau \pm T_{sym}$ there will be two secondary peaks that will have a magnitude approximately one half that of the CAF at the correct TDOA/FDOA. Thus there is a probability that either of these sidelobes could be mistaken for the CAF peak, a probability that is much larger than in the spatial multiplexing scenario. The PDF of the sidelobes is plotted in Figure 3.2 where it is obvious that the PDF is not that of noise. As predicted by equation 3.15 the PDF of the CAF magnitude at the sidelobes peaks at about half that of the PDF of the main lobe. An illustration of the actual CAF surface when the sidelobes are larger than the main lobe is shown in Figure 3.3.

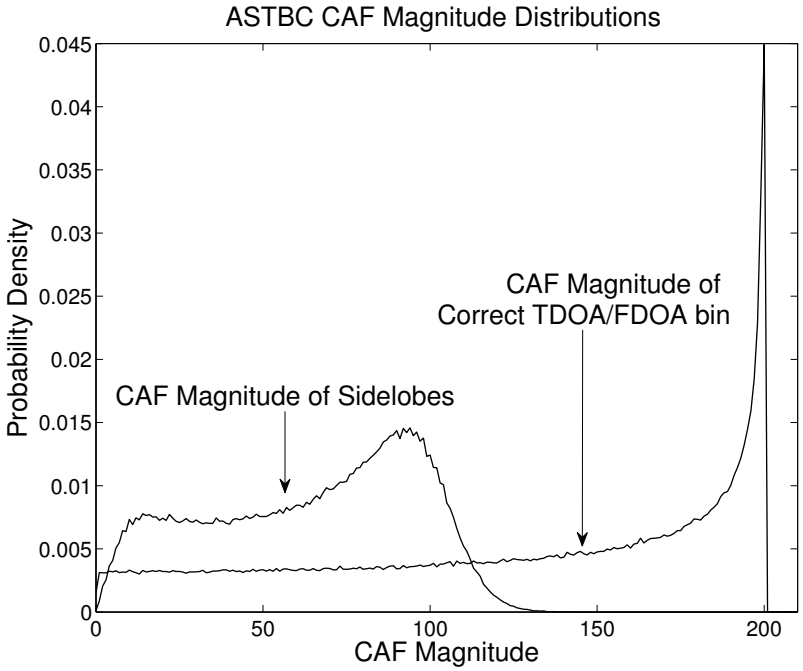

Figure 3.2: ASTBC Sidelobes Magnitude PDF. CAF Magnitude distributions of ASTBC at the correct TDOA/FDOA peak and that of the sidelobes. Notice how the sidelobe distribution is focused around a magnitude that is half that of the correct TDOA/FDOA magnitude. There is no noise present in this example.

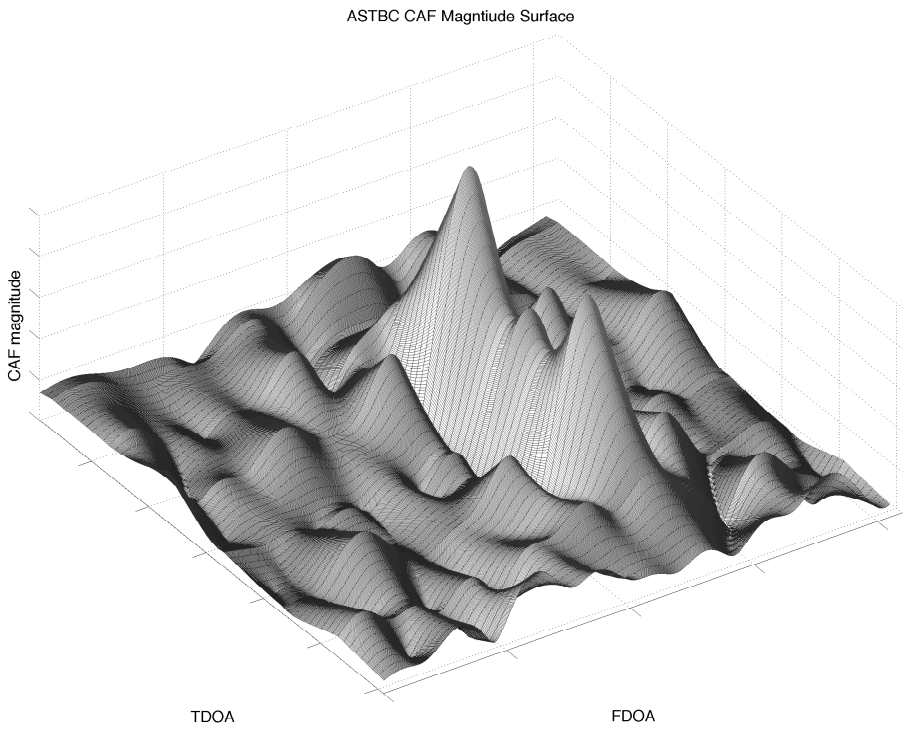

Figure 3.3: ASTBC CAF Magnitude Surface with Sidelobes. The surface shows three peaks: one main lobe (center) and two sidelobes (left and right of center). In this case the main lobe has a lower magnitude than either of the sidelobes so a TDOA/FDOA error will occur on the order of $\pm T_{sym}$.

3.2 Spatial Multiplexing

Spatial multiplexing MIMO transmits two independent signals on each antenna, thus the symbols from the two antennas have no correlation. In fact, each antenna could use a different modulation scheme. Thus we must find the CDF of the random variable from (3.4) while accounting for β. In Chapter 2.1.2 we have shown how β can be approximated as a zero-mean Gaussian random variable when we are not focusing on the CAF magnitude at the correct TDOA/FDOA bin. Now for spatial multiplexing, β is multiplied by two random

phase vectors, which results in a new distribution. Instead of attempting to find this new distribution we can simply make the assumption that we can approximate $\beta(e^{j\theta_B} + e^{j\theta_C})$ by a zero mean complex Gaussian random variable. Another reason for making this assumption is the fact that as the modulation order increases the variance on β decreases and thus can be ignored just as with ASTBC. The worst case scenario (in the sense that the Gaussian approximation fits the least) then would be that SMUX is used in conjunction with BPSK modulation, and would result in:

$$\tilde{n}_\beta \triangleq \beta(e^{j\theta_B} + e^{j\theta_C}) \sim \mathcal{N}_c\left(0, \frac{TP_1P_2}{2}\right)$$

Our CAF magnitude random variable is now the sum of random vectors in noise:

$$C_p = \left|P + Pe^{j\theta_D} + \tilde{n}_\beta + \tilde{n}\right| \tag{3.16}$$

where again the scale factor $P = \frac{\sqrt{P_1P_2}}{2}T$ and $\tilde{n} \sim \mathcal{N}_c\left(0, \sigma_c^2 = \frac{T\sigma_n^2}{2}(P_1 + P_2 + \sigma_n^2)\right)$ is the noise as derived in Chapter 2.1.1. Then the CDF of the CAF magnitude at the correct TDOA/FDOA bin will follow (3.13) where $\sigma_{c_p}^2 = \sigma_c^2 + \sigma_\beta^2$ and again σ_β^2 depends on the modulation and pulse shape but for BPSK $\sigma_\beta^2 = \frac{T}{2}P_1P_2$.

Admittedly, the Gaussian assumption of $\beta(e^{j\theta_B} + e^{j\theta_C})$ is weak as shown in Figure 3.4 which compares the exact distribution to the Gaussian approximation assuming BPSK and QPSK modulation. However this approximation will only slightly affect the resulting probability of error as we will show later in Chapter 5. Also, as the modulation order increases, the variance of β decreases, so at sufficiently high modulation orders β approaches zero and can be considered negligible altogether. This is because β represents the cross correlation of the transmitted symbols from each antenna, and as the modulation order increases, the likelihood that two symbols will add coherently decreases.

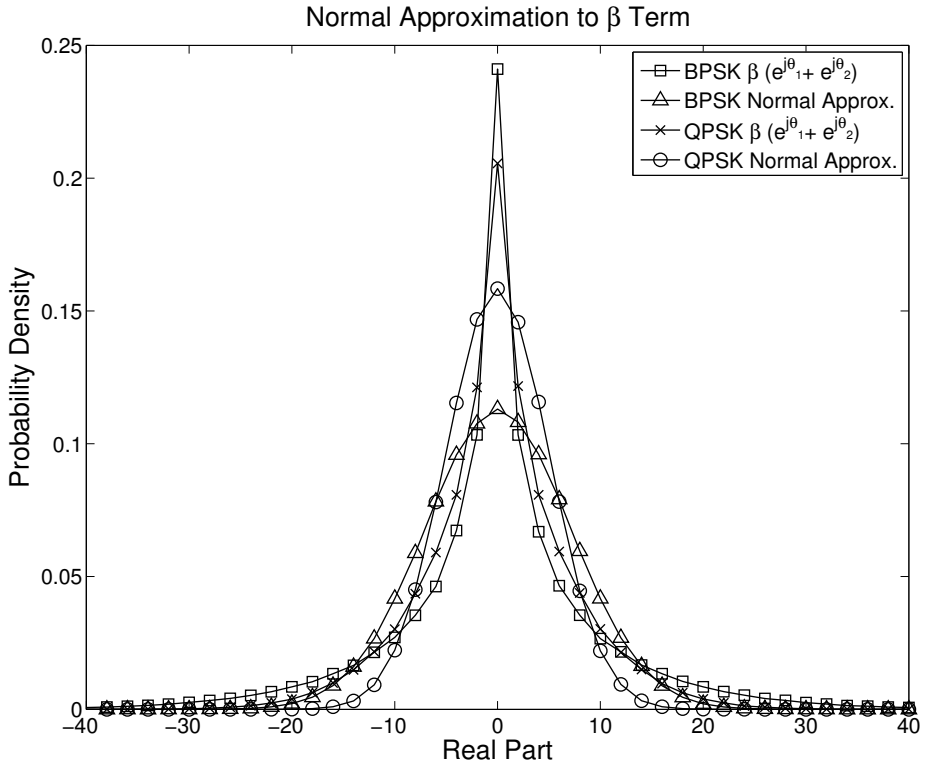

Figure 3.4: Distribution of β. Comparison showing the actual distribution of the real part of the term $\beta(e^{j\theta_B} + e^{j\theta_C})$ and the normal approximation for BPSK with variance equal to $\frac{TP_1P_2}{2}$ and QPSK with variance equal to $\frac{TP_1P_2}{4}$, where $T = 100$ and $P_1 = P_2 = 1$.

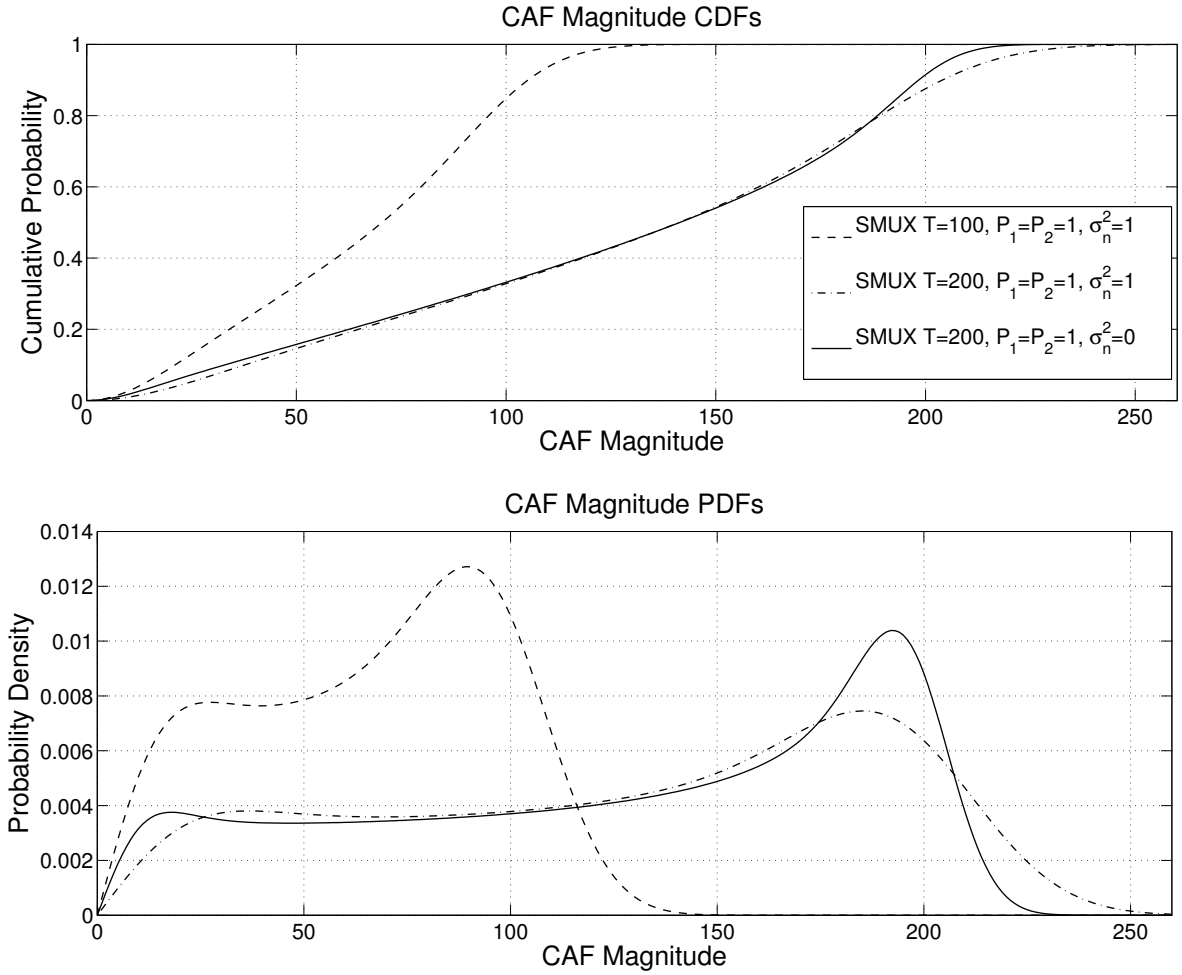

Figure 3.5: SMUX Magnitude Distributions. Distributions at the correct TDOA/FDOA bin using equation (3.13) and numerical integration.

3.3 MIMO Probability of Error

Now that we have derived the CAF magnitude CDF at the correct TDOA/FDOA bin for ASTBC and SMUX MIMO, we can use equation (1.19) to find the probability of error. Again the PDF of every other noise bin in the CAF surface is Rayleigh, and the max of all $MN - 1$ noise bins has the PDF given by (2.11). Therefore the probability of error for

MIMO with two transmit antennas is:

$$\mathcal{P}[\text{ MIMO Error }] = \int_0^\infty (MN-1)\frac{\gamma}{\sigma^2}\left(1-e^{\frac{-\gamma^2}{2\sigma^2}}\right)^{MN-2} e^{\frac{-\gamma^2}{2\sigma^2}} \int_0^\infty \gamma \mathcal{J}_0(Pz)^2 \mathcal{J}_1(\gamma z) e^{\frac{z^2\sigma_{c_p}^2}{2}} dz d\gamma \tag{3.17}$$

where again $\sigma^2 = \sigma_c^2 + \sigma_\beta^2$ (for the PDF of the max noise bin) and for ASTBC $\sigma_{c_p}^2 = \sigma_c^2$ but for SMUX $\sigma_{c_p}^2 = \sigma^2 = \sigma_c^2 + \sigma_\beta^2$. This analysis however ignores the presence of the correlation sidelobes that will arise for MIMO transmitters using STBC. This will affect the probability of error, but we leave that analysis for future work. Figure 3.6 shows several curves for ASTBC and SMUX as a function of the noise power and for several different values of the integration period and TDOA/FDOA search range (M and N respectively). In general both MIMO schemes have much higher probabilities of error compared to SISO with little noticeable difference between ASTBC and SMUX. Also, as the integration period increases the probability of error decreases, and as the number of TDOA/FDOA search bins (M and N) decreases so does the probability of error.

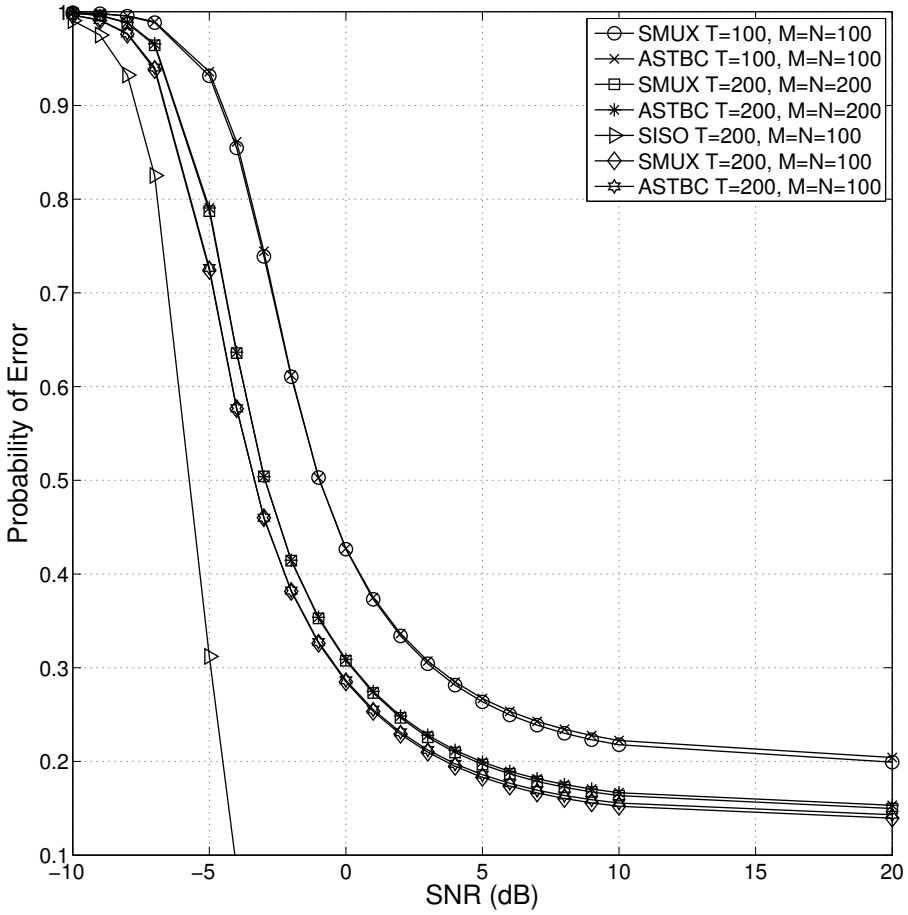

Figure 3.6: Two Transmit Antenna MIMO Probability of Error. Here $\sigma_n^2 = 1/\text{SNR}$ and several integration periods (T) and TDOA and FDOA search ranges (M and N respectively) are shown. The powers are kept constant so that $P_1 = P_2 = 1$ and $\sigma_\beta^2 = \frac{TP_1P_2}{2}$ for BPSK.

Chapter 4

The CAF Applied to MIMO Signals: Four Transmit Antennas

The two dominant modes of MIMO in existing communication systems have either two or four transmit antennas. We will now focus on extending the results from two antennas to four or more. Because this process is essentially the same as in the two antenna case, we can simply extend the equations to apply to the situation with four transmit antennas. Therefore by expanding equation (3.2) for the four antenna case where we have replaced $b_l(t-\tau_1)$ with the shorthand notation b_l where l is the numbered symbol stream from a corresponding antenna as defined previously then the CAF will appear as:

$$\begin{aligned}\Lambda(\Delta\tau,\Delta f) =& \frac{\sqrt{P_1P_2}}{4}e^{-j2\pi\psi}\int_0^T \left\{b_1^2e^{j\theta_A}+b_2^2e^{j\theta_B}+b_3^2e^{j\theta_C}+b_4^2e^{j\theta_D}\right. \\ &+ b_1b_2\left(e^{j\theta_E}+e^{j\theta_F}\right)+b_1b_3\left(e^{j\theta_G}+e^{j\theta_H}\right)+b_1b_4\left(e^{j\theta_I}+e^{j\theta_J}\right) \\ &\left.+ b_2b_3\left(e^{j\theta_K}+e^{j\theta_L}\right)+b_2b_4\left(e^{j\theta_M}+e^{j\theta_N}\right)+b_3b_4\left(e^{j\theta_O}+e^{j\theta_P}\right)\right\}dt.\end{aligned} \tag{4.1}$$

Simplifying as before:

$$\Lambda(\Delta\tau, \Delta f) = \frac{\sqrt{P_1 P_2}}{4} e^{j\psi} \left[T \sum_{i=1}^{4} e^{j\theta_i} + \sum_{k=1}^{6} \beta_k \left(e^{j\theta_{1,k}} + e^{j\theta_{2,k}} \right) \right] \tag{4.2}$$

where ψ is a phase offset due to $\Delta\tau$, the random phases due to the channel are θ_i and $\theta_{j,k}$, and the binomial random variable from the symbol combining is β_k. After taking the magnitude of the CAF we have the random variable:

$$C_p = \frac{\sqrt{P_1 P_2}}{4} \left| T + T \sum_{i=1}^{3} e^{j\theta_i} + \sum_{k=1}^{6} \beta_k \left(e^{j\theta_{1,k}} + e^{j\theta_{2,k}} \right) \right| \tag{4.3}$$

which will apply directly to spatial multiplexing MIMO with four transmitting antennas. For STBC MIMO once again β reduces to approximately zero due to the orthogonality of the STBCs. Thus the STBC CAF main lobe magnitude random variable with AWGN present for N_t transmit antennas becomes:

$$C_p = \left| P + P \sum_{i=1}^{N_t - 1} e^{j\theta_i} + \tilde{n} \right| \tag{4.4}$$

where $P = \frac{T\sqrt{P_1 P_2}}{N_t}$ and $\tilde{n} \sim \mathcal{N}_c \left(0, \sigma_c^2 = \frac{T\sigma_n^2}{2}(P_1 + P_2 + \sigma_n^2) \right)$ for BPSK modulation. Once again secondary (and even tertiary or higher order peaks depending on the block code) can arise due to the correlation of the block coding. For spatial multiplexing with four transmit antennas (SMUX4) the β terms can be approximated with a complex Gaussian distribution so that the random variable is now:

$$C_p = \frac{\sqrt{P_1 P_2}}{4} \left| T + T \sum_{i=1}^{3} e^{j\theta_i} + \sum_{k=1}^{6} \tilde{n}_{\beta,k} \right| \tag{4.5}$$

where each $\tilde{n}_{\beta,k}$ is distributed according to $\mathcal{N}_c \left(0, \frac{TP_1P_2}{N_t^2} \right)$ assuming BPSK modulation. Then the spatial multiplexing CAF magnitude random variable can be extended to N_t antennas and with AWGN present:

$$C_p = \left| P + P \sum_{i=1}^{N_t - 1} e^{j\theta_i} + \tilde{\nu}_{\beta,N_t} + \tilde{n} \right| \tag{4.6}$$

where $P = \frac{T\sqrt{P_1 P_2}}{N_t}$ and $\tilde{\nu}_{\beta,N_t} \sim \mathcal{N}_c\left(0, \frac{TP_1P_2}{N_t^2}\left(\frac{N_t^2-N_t}{2}\right)\right)$. Once again the CAF magnitude random variables are the sum of random phase vectors in Gaussian Noise and so the CDF will follow equation (3.13). The CDFs and PDFs are plotted in 4.1 for both STBC4 and SMUX4 where both distributions are very closely related. The distributions are so similar because as the number of antennas increases the number of phase terms increases by N_t but the variance on the β terms only increases by $\frac{N_t-1}{2}$, therefore the phase terms begin to dominate the distribution as N_t grows. The PDFs of the CAF main lobe magnitude are centered around values that are much lower when compared to SISO or even two antenna MIMO. This indicates that the probability of error for four antennas (and higher orders) will be higher.

Finally by using the CDF for the CAF magnitude of the main lobe the probability of error for MIMO signals with N_t transmit antennas is:

$$\mathcal{P}[\text{ MIMO Error }] = \int_0^\infty (MN-1)\frac{\gamma}{\sigma^2}\left(1-e^{\frac{-\gamma^2}{2\sigma^2}}\right)^{MN-2} e^{\frac{-\gamma^2}{2\sigma^2}} \int_0^\infty \gamma \mathcal{J}_0(Pz)^{N_t}\mathcal{J}_1(\gamma z)e^{\frac{z^2\sigma_{c_p}^2}{2}}dzd\gamma \tag{4.7}$$

where again $\sigma^2 = \sigma_c^2 + \sigma_\beta^2$ with $\sigma_c^2 = \frac{T\sigma_n^2}{2}(P_1+P_2+\sigma_n^2)$ and assuming BPSK $\sigma_\beta^2 = \frac{T}{2}P_1P_2$. For STBC MIMO $\sigma_{c_p}^2 = \sigma_c^2$ and for SMUX $\sigma_{c_p}^2 = \sigma_c^2 + \frac{TP_1P_2}{N_t^2}\left(\frac{N_t^2-N_t}{2}\right)$ (again assuming BPSK).

A few examples of the probability of error for four antenna MIMO are shown in Figure 4.2. Compared to SISO the probability of error is much higher for MIMO but there is little difference between SMUX4 and STBC4. It is possible that with four or more antennas SMUX can be approximated as STBC in regards to the distribution of the CAF main lobe magnitude and probability of error. It should be noted that once again the sidelobes for STBC4 have not been taken into account and will affect the actual probability of error.

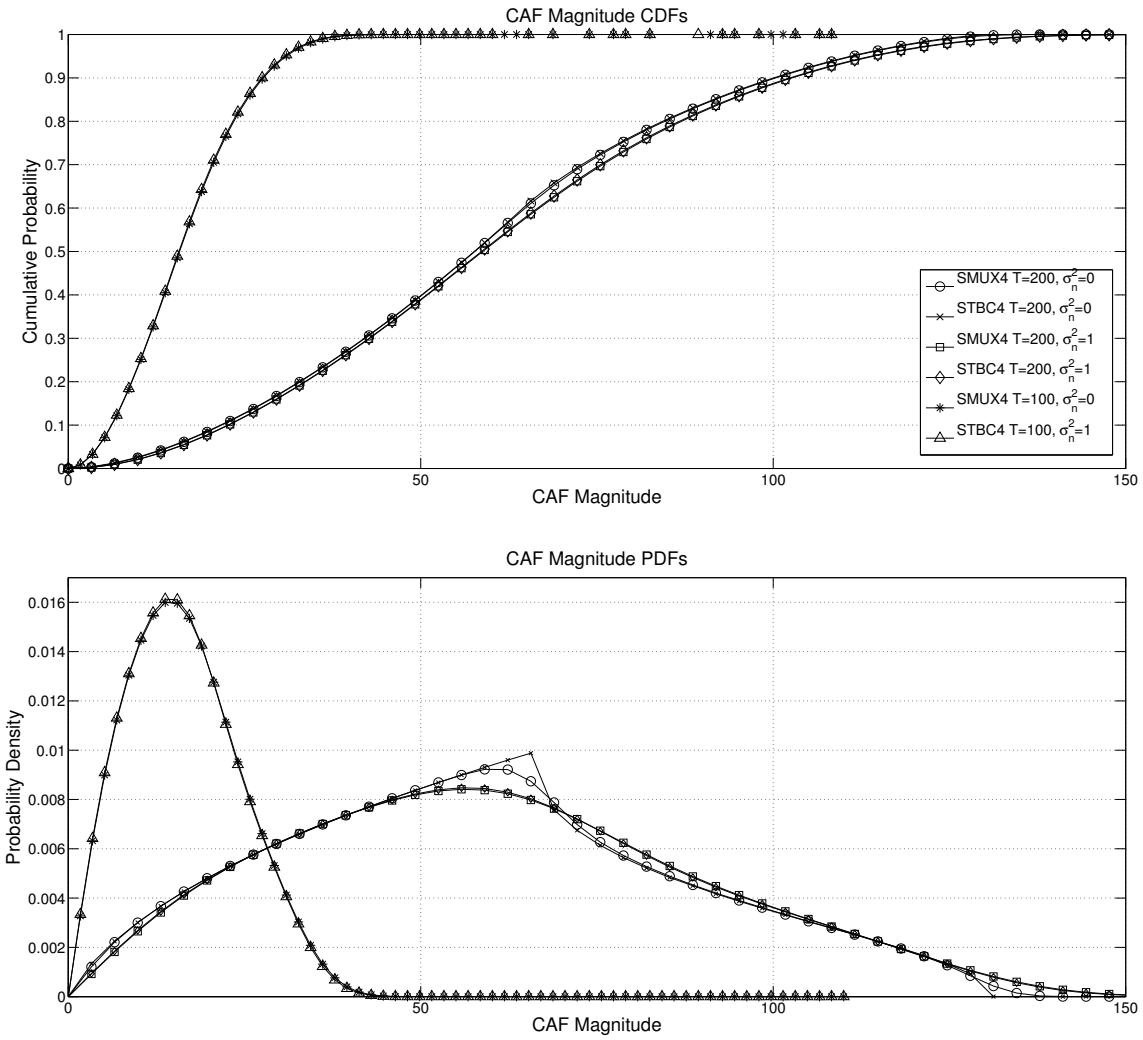

Figure 4.1: Four Transmit Antennas Magnitude Distributions. Theoretical CAF magnitude distributions at the correct TDOA/FDOA bin using equation (3.13) and numerical integration with $P_1 = P_2 = 1$ for several integration periods (T) and TDOA and FDOA search ranges (M and N respectively). The distributions for both SMUX4 and STBC4 are very close because as the number of antennas increases phase terms dominate the distribution.

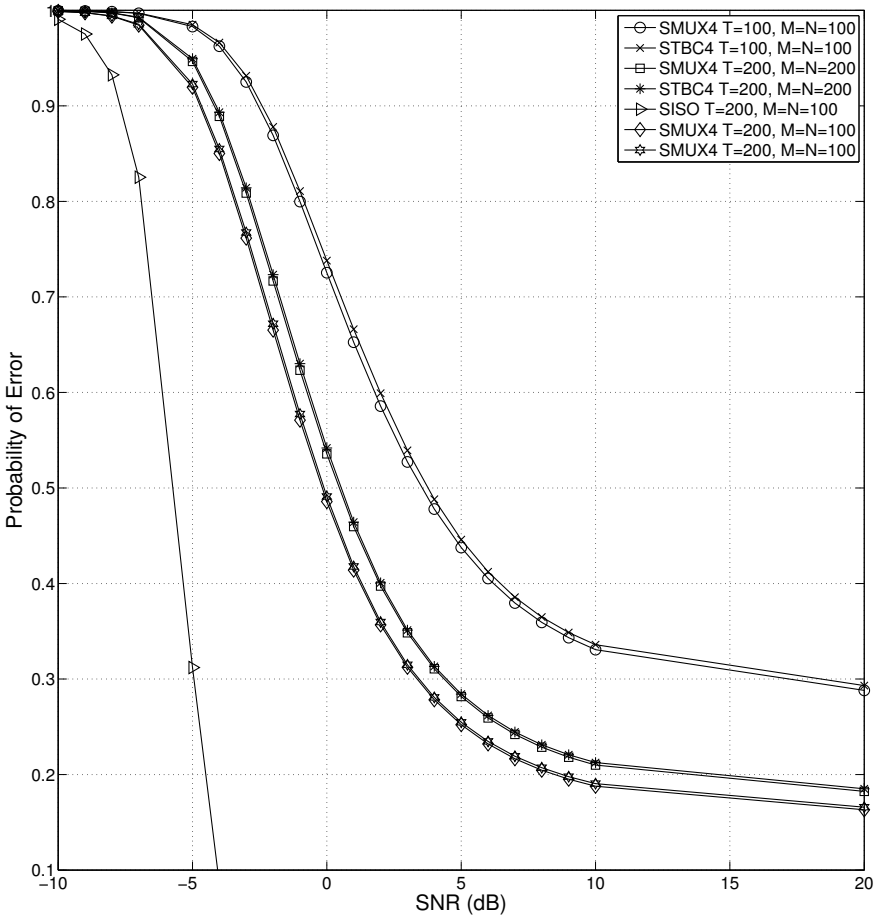

Figure 4.2: Four Transmit Antennas Probability of Error. From equation (4.7) evaluated by numerical integration with $P_1 = P_2 = 1$, $\sigma_n^2 = 1/\text{SNR}$ and several integration periods (T) and TDOA and FDOA search ranges (M and N respectively).

Chapter 5

CAF Simulation and Results

We can simulate the CAF with SISO and MIMO signals to confirm our theoretical hypothesis and gain more insight into CAF performance and functionality. For simulation purposes the CAF can be represented in the discrete time domain as:

$$\Lambda(q,k) = \sum_{n=1}^{N} \tilde{r}_1[n]\tilde{r}_2^*[n-q]e^{-j2\pi\frac{k}{N}n} \tag{5.1}$$

where q represents TDOA bins in number of samples and $\frac{k}{N}$ is the FDOA as a fraction of the sampling frequency and N is the number of samples in time [12]. The pair of q and k that cause $|\Lambda(q,k)|$ to be maximized corresponds to the estimated TDOA and FDOA. The CAF must therefore be computed over the entire range of q and k of interest. CAF processing therefore creates a three-dimensional surface iterating through independent variables q and k yielding the dependent variable $|\Lambda(q,k)|$. Using the sampling period t_s and frequency f_s we can find the TDOA and FDOA estimates in seconds and Hertz respectively:

$$\Delta\hat{\tau} = q * t_s \tag{5.2}$$

$$\Delta\hat{f} = k/N * f_s \tag{5.3}$$

In order to simplify the computational complexity, the CAF can be computed much more efficiently by using a Fast-Fourier-Transform (FFT). Using the notation for the FFT, $\mathcal{F}\{\cdot\}$, the CAF can now be represented as:

$$\Lambda(q, \mathbf{k}) = \mathcal{F}\left[\tilde{r}_1[\mathbf{n}] \odot \tilde{r}_2^*[\mathbf{n} - q]\right] \tag{5.4}$$

where $\mathbf{k}$ is a vector of N frequency values representing values in the range $\left[\frac{-f_s}{2}, \frac{f_s}{2}\right]$, $\mathbf{n}$ is a vector of sample times. Using this method the CAF was simulated with SISO and MIMO signals using BPSK modulation for various SNR values. The overall received signal power at each collector was normalized to one and the SNR of both received signals was kept the same between collectors.

The simulated results show the CAF magnitude PDFs and CDFs at the correct TDOA/FDOA bin in Figure 5.1 and match the theoretical analysis with Quantile-Quantile plots (Q-Q plots) showing the goodness of fit in Figure 5.3. As SNR decreases the CAF magnitude at the correct TDOA/FDOA bin is shown in Figure 5.2 to approach a Rayleigh distribution as we would expect given the Gaussian nature of the noise. The probability of error from simulated data also matches the theoretical analysis with slight deviations. There is likely some error due to numerical integration and this would explain why the SISO curves show a slight offset. The STBC simulated curves show more deviation from the theoretical curves likely due to the presence of the correlation sidelobes described earlier but not taken into account in the probability of error equations.

Also shown in the simulated results but not derived theoretically is the distribution of the CAF maximum value in Figure 5.5. This is the distribution of the simulated CAF surface's maximum absolute value, and thus corresponds to the estimated TDOA/FDOA bin as it would be calculated in a traditional geolocation scenario. Therefore this distribution shows the effects of all the properties that have been studied thus far. While the distributions

show the general shape of that of the main lobe (correct TDOA/FDOA bin as derived theoretically), the effects of the noise can also be seen as a spike in the distributions around lower CAF magnitudes. The STBC correlation sidelobes also cause spikes around half the magnitude of the main lobe.

In general the overall result is that SISO signals provide better TDOA/FDOA estimates as shown in the probability of error and in the TDOA/FDOA root-mean-square-error (RMSE) curves in Figures 5.4 and 5.6, respectively. Signals using MIMO transmission can incoherently combine at the receiver making it difficult for the signals to correlate and create a main lobe corresponding to the correct TDOA/FDOA. If there is no main lobe then TDOA/FDOA errors can be very far from the true value, which is not what one would expect if only noise were present. Even in the absence of noise the CAF magnitude is a random variable, and the scatter plots in Figures 5.7 and 5.8 show the difference between SISO and MIMO TDOA/FDOA calculation. These results show that more antennas degrade TDOA/FDOA estimation performance and that spatial multiplexing is preferable to STBC for geolocation.

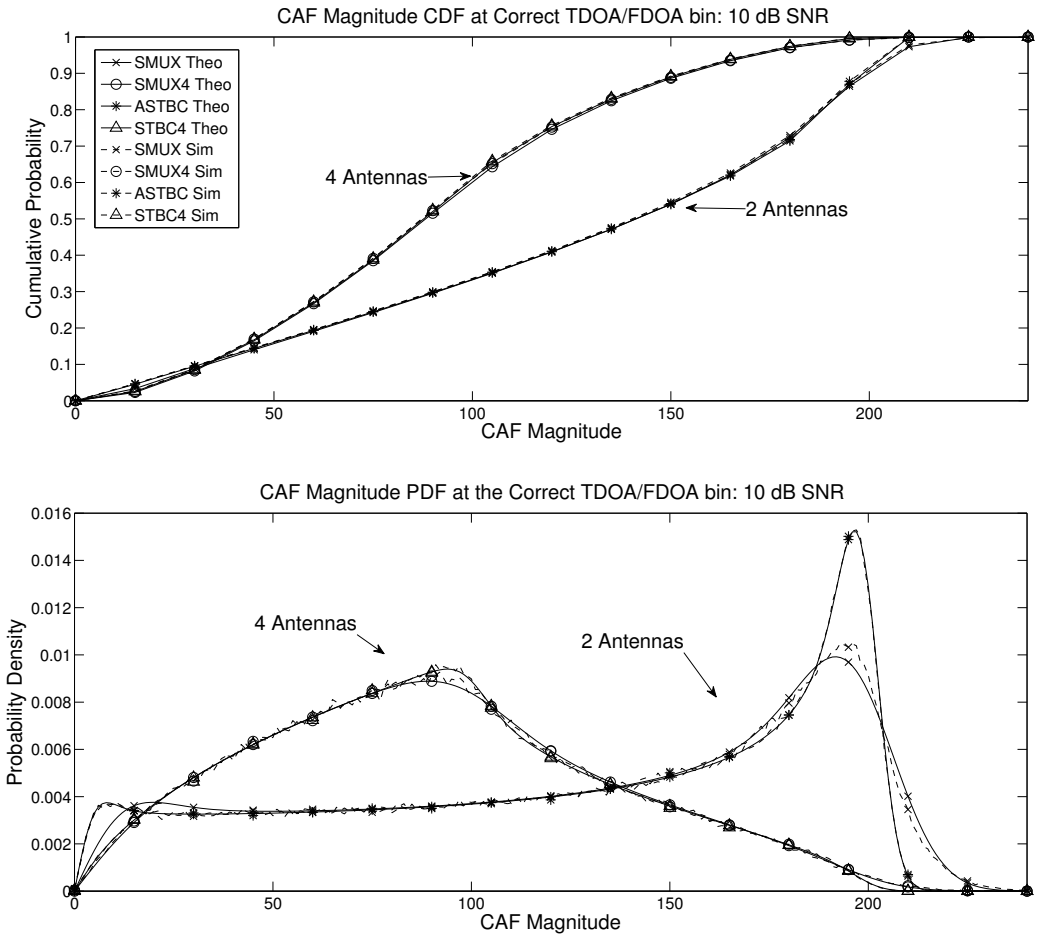

Figure 5.1: Simulated CAF CDFs and PDFs. Distributions of the CAF magnitude at the correct TDOA/FDOA bin for MIMO transmitter at 10 dB SNR. Notice that for a transmitter with four antennas the curves for both spatial multiplexing and STBC are close enough that we can approximate spatial multiplexing as STBC. Plots show both the theoretical result ("Theo") and the simulated CAF results ("Sim").

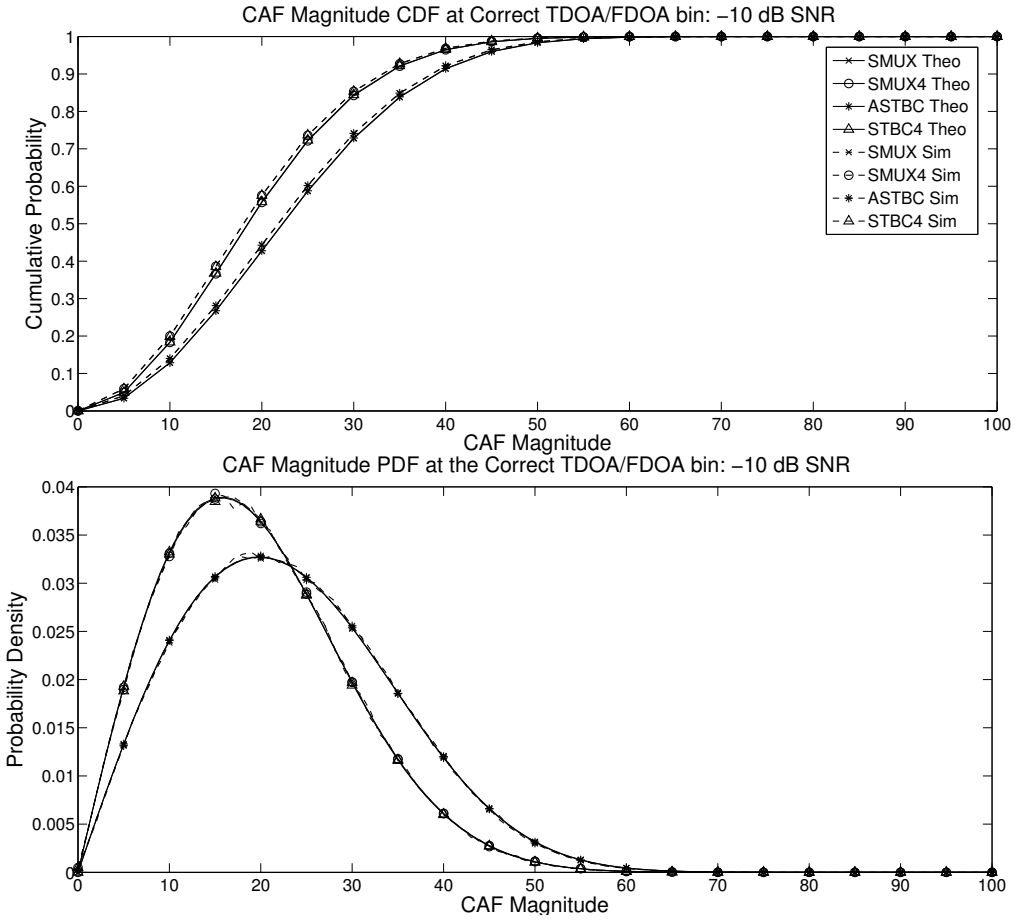

Figure 5.2: Simulated CAF PDFs and CDFs Low SNR. Distributions of the CAF magnitude at the correct TDOA/FDOA bin for MIMO transmitter for -10 dB SNR. At this low SNR the noise dominates the distributions and so they appear Rayleigh. Plots show both the theoretical result ("Theo") and the simulated CAF results ("Sim").

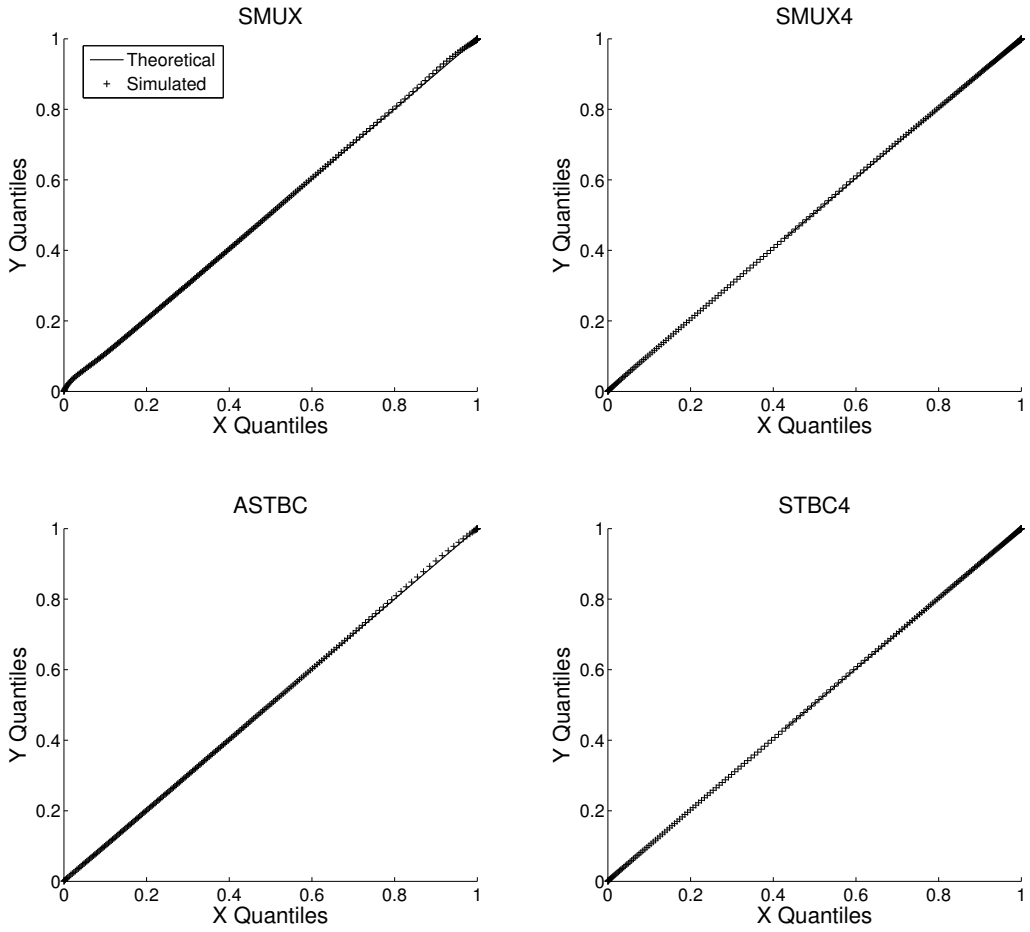

Figure 5.3: CAF CDF Q-Q Plots. Comparison between simulated and theoretical CAF CDFs for a noise level of 10 dB SNR. For SMUX there is a slight deviation in the tails due to the Gaussian approximation of β. The theoretical distributions fit the simulated data very well despite the approximation of the distribution of β for SMUX.

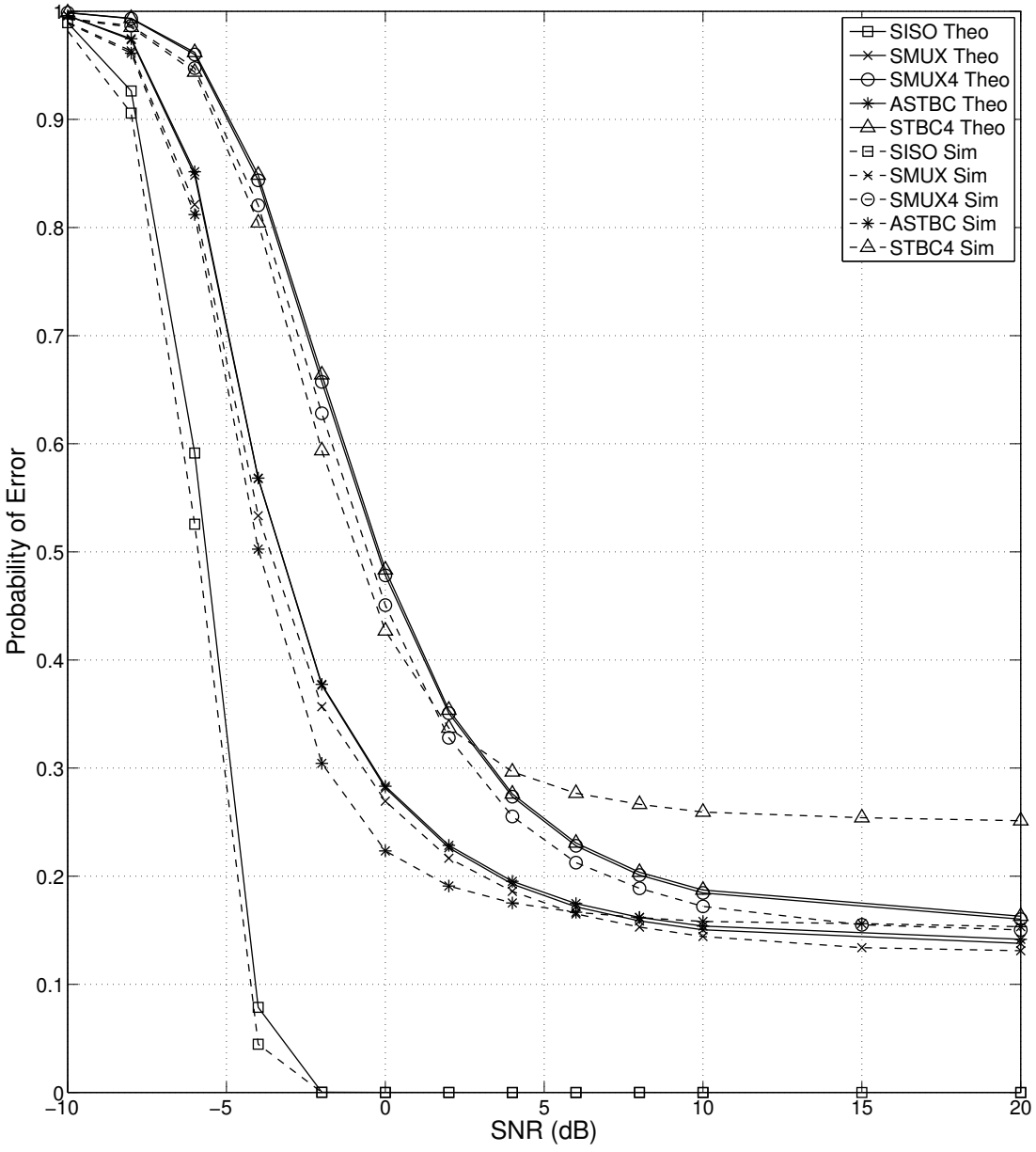

Figure 5.4: SISO and MIMO Probability of Error Curves. Probability of error, as in the probability that the wrong TDOA/FDOA bin is chosen. Plots show both the theoretical result ("Theo") and the simulated CAF results ("Sim"). For the STBC curves there is a noticeable discrepancy (particularly in the way the curves level off) likely due to the effects of the sidelobes which weren't accounted for in the theoretical probabilities of error. Also there will be some error due to the approximation of β that will affect the distribution of the noise for all the results.

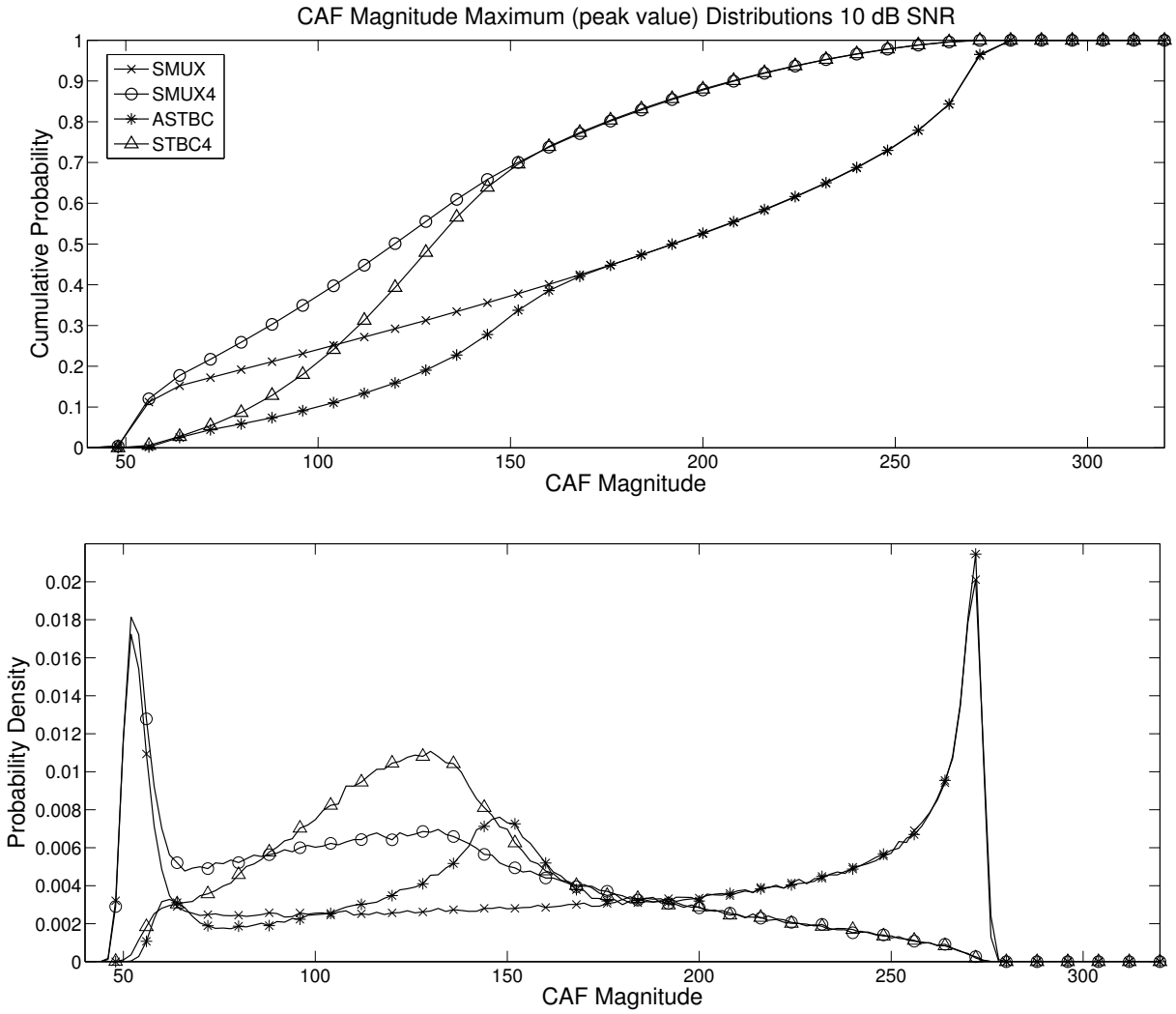

Figure 5.5: CAF Peak Distribution. Distributions of the CAF's maximum value, the value corresponding to the estimated (but not necessarily correct) TDOA/FDOA bin. This magnitude includes the effects of noise and the sidelobes because it is chosen as the maximum of the CAF surface. Each PDF has an extra peak at low CAF values, this is most likely due to noise, since it seems to follow the Rayleigh distribution. Also, although not as apparent in the 4 antenna STBC distribution, there is a noticeable peak in the Alamouti magnitude distribution at 150. This peak is due to the sidelobes and is approximately half the magnitude of the CAF at where the true TDOA/FDOA should be (about 300).

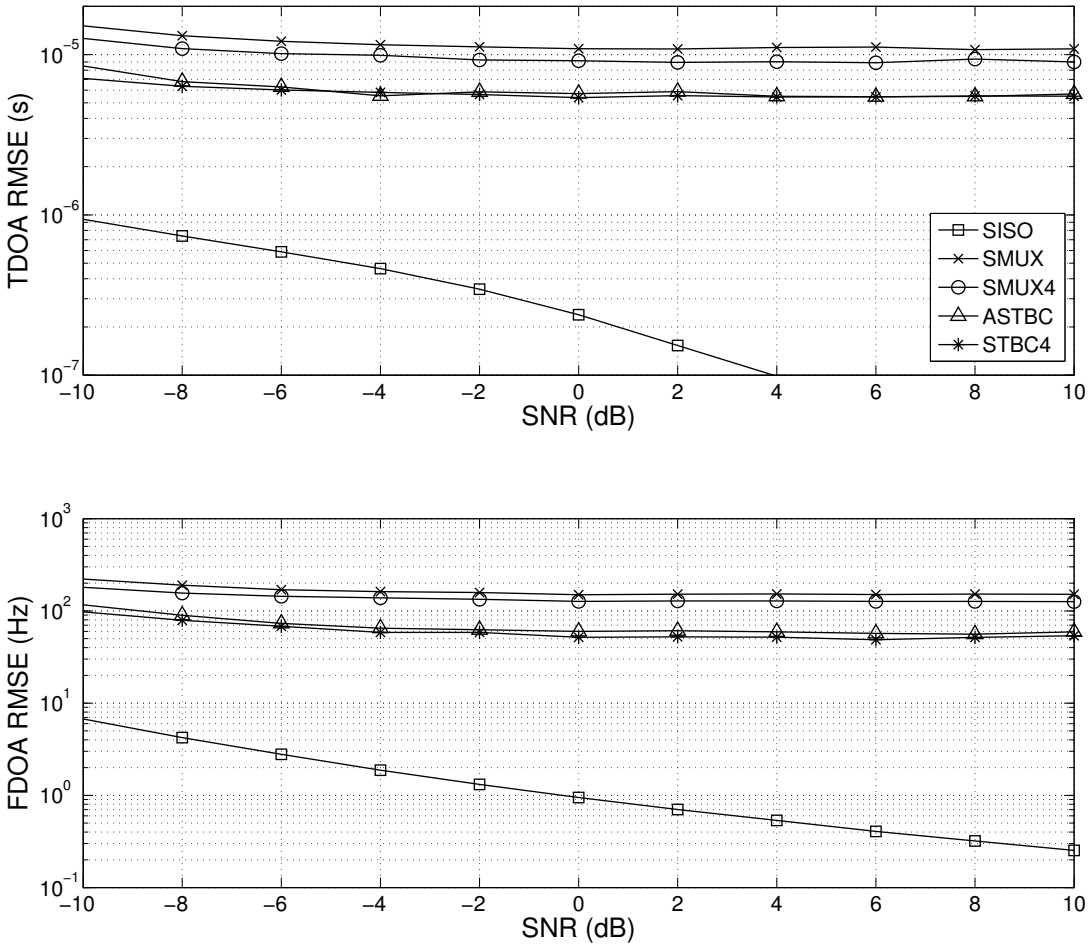

Figure 5.6: TDOA/FDOA RMSE. Root-mean-square-error curves are as function of SNR. In general because MIMO errors in TDOA/FDOA are large when the main lobe cannot be found, the average error is much larger than SISO. SISO errors tend to be due to minor fluctuations on the main lobe therefore producing minor TDOA/FDOA errors.

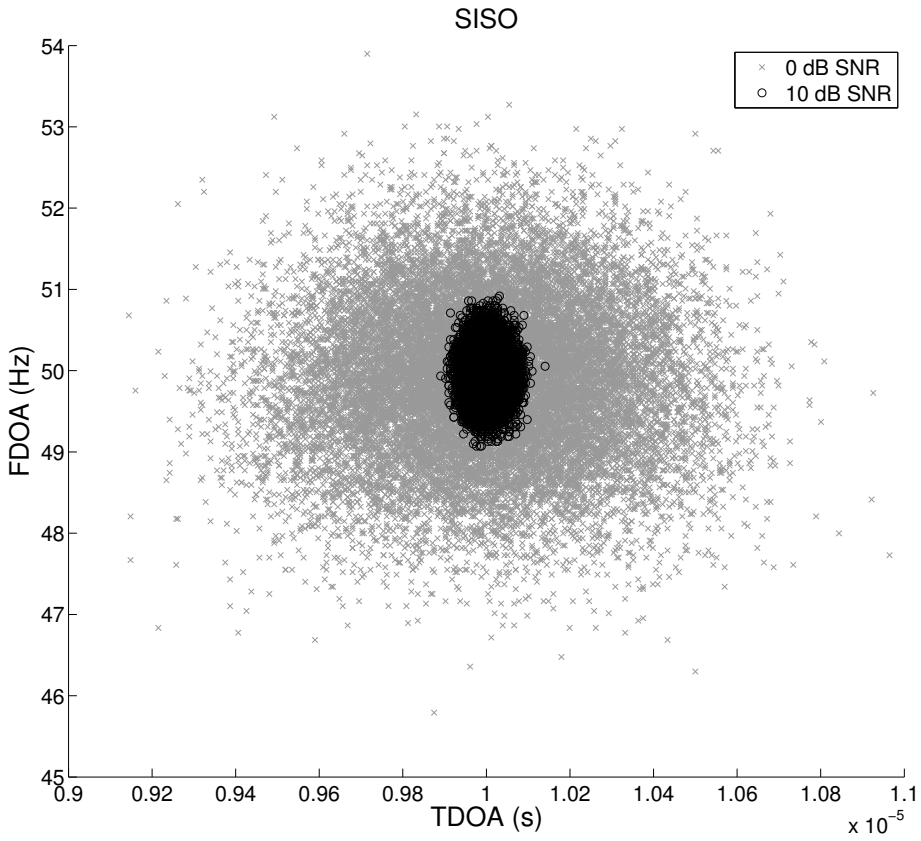

Figure 5.7: SISO TDOA/FDOA Scatter. Plot of TDOA vs. FDOA simulated estimates using SISO transmission and a higher resolution CAF. The correct FDOA is 50 Hz and TDOA is 10 μs. Notice a very Gaussian shape to the scattering, this is due to minor fluctuations of the main lobe caused by the noise. In general the errors are tightly bound within some ellipse proportional to the noise standard deviation, signal bandwidth, and integration period.

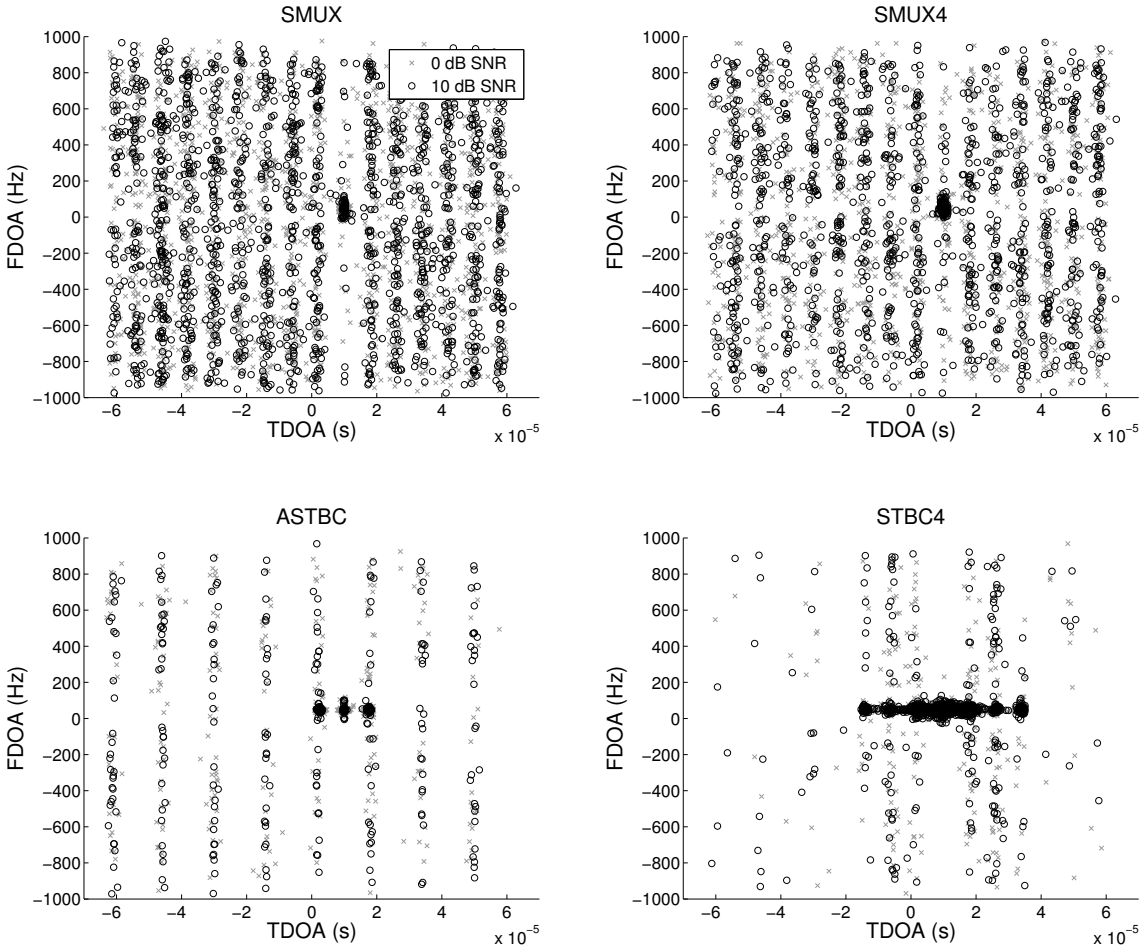

Figure 5.8: MIMO TDOA/FDOA Scatter. Plot of TDOA vs. FDOA simulated estimates for each MIMO type at 0 and 10 dB SNRs. Notice a central scattering ellipse for all MIMO cases but in general the scattering isn't concentrated within that ellipse. For SMUX there is a central ellipse but also wide scattering appearing almost uniformly distributed in TDOA/FDOA with a slight correlation on the order of the symbol period in the time domain. The STBC MIMO results show less widespread scattering in TDOA/FDOA but much more concentration on the sidelobes. For ASTBC there are two main sidelobes but for STBC4 there are three pairs of noticeable sidelobes where the number of sidelobes can depend on the coding matrix used.

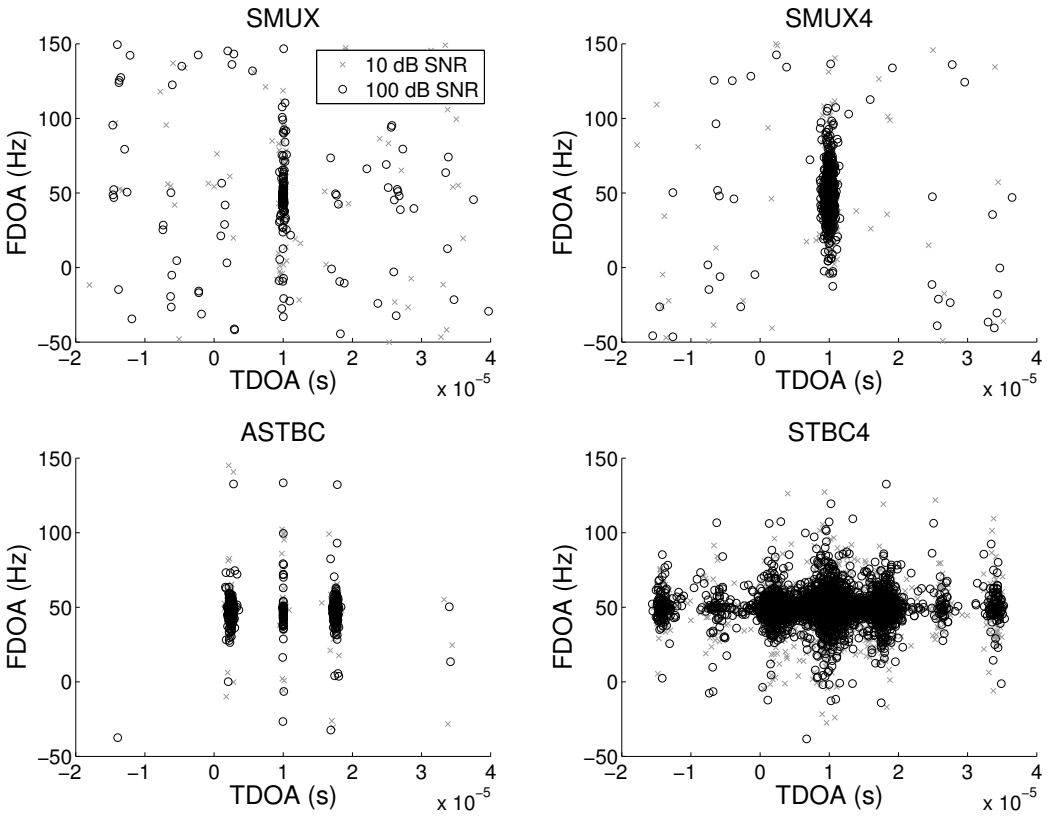

Figure 5.9: MIMO TDOA/FDOA Scatter Zoomed. Plot of TDOA vs. FDOA for each MIMO type at 10 and 100 dB SNRs showing how even when AWGN isn't present there is still scattering in TDOA/FDOA. Zoomed in on the main error ellipse one is able to better see the effects of the sidelobes.

Chapter 6

Detecting CAF Errors

As we have shown, the CAF magnitude is a random variable (even in the absence of noise), and thus causes errors in the estimate of TDOA/FDOA. However we can attempt to detect these errors when they occur by studying the level of maximum CAF magnitude. By comparing the measured CAF magnitude to some threshold which is defined by signal properties, we can detect if an error occurs. Using the following definitions from before and applying detection theory we demonstrate how CAF errors can be detected:

C_p = CAF magnitude at the correct TDOA/FDOA bin
$\hat{n}$ = max CAF magnitude at anywhere but the correct TDOA/FDOA (i.e. max of all noise bins, this could also include sidelobes for STBC from section 3.1.1)

The estimated TDOA/FDOA bin is the one that corresponds to the maximum CAF magnitude which we define as Z where:

$$Z = max\left[C_p, \hat{n}\right] \tag{6.1}$$

by definition. If we then choose a threshold value Υ, where any measured CAF magnitude less than the threshold is considered an error, we can therefore define classical detection theory probabilities:

$$\mathcal{P}[\text{Correct Detection}] = \mathcal{P}[Z > \Upsilon, \Delta\hat{\tau} = \Delta\tau \cap \Delta\hat{f} = \Delta f] = \mathcal{P}[C_p > \Upsilon]\mathcal{P}[C_p > \hat{n}]$$

$$\mathcal{P}[\text{Missed Detection}] = \mathcal{P}[Z < \Upsilon, \Delta\hat{\tau} = \Delta\tau \cap \Delta\hat{f} = \Delta f] = \mathcal{P}[C_p < \Upsilon]\mathcal{P}[C_p > \hat{n}]$$

$$\mathcal{P}[\text{False Alarm}] = \mathcal{P}[Z > \Upsilon, \Delta\hat{\tau} \neq \Delta\tau \cup \Delta\hat{f} \neq \Delta f] = \mathcal{P}[\hat{n} > \Upsilon]\mathcal{P}[C_p < \hat{n}].$$

Therefore the new probability of TDOA/FDOA error after filtering is identical to the probability of false alarm. It is difficult to find the optimal threshold value because there is no closed form solution of the MIMO CAF magnitude distributions. Instead the threshold can be determined based on plotting these probabilities, and then from the plots choosing a threshold that meets system specifications. We have plotted as an example several of these probabilities at different SNR values to compare the theoretical results to simulations. Obviously as the threshold increases we should expect the probability of error to decrease, but at the same time the probability of missed detection will also increase.

In order to detect and filter errors some *a priori* knowledge is needed about the received signals in order to determine an appropriate threshold level. For instance, in the absence of noise and for SISO signals, if there are 300 received symbols with received powers $P_1 = P_2 = 1$ then we can expect the CAF magnitude to be approximately $T\sqrt{P_1 P_2} = 300$ as derived in Chapter 2 (assuming one sample per symbol and sampling at the peak of each symbol). Since MIMO will perform at best as well as SISO, then the CAF magnitude when the received signals combine coherently will also be around the same as SISO. Thus we should choose some threshold less than 300 for this scenario.

Using the simulated CAF data for SISO and MIMO signals (with 300 symbols) the proba-

bility of error is plotted in Figure 6.1 where in general it decreases for increasing threshold levels except for STBC signals. The probability of error for STBC signals decreases for lower SNR's as the threshold increases but remains unchanged for higher SNR's, yet another indication of the presence of the correlation sidelobes and their affects on TDOA/FDOA error. The correlation sidelobes were shown to follow a similar distribution to that of the main lobe (Chapter 3.1.1) except approximately half the magnitude. Therefore the filtering threshold needs to be large enough compensate for the sidelobes in order to remove them. If the threshold was shown to increase even further it would eventually result in a zero probability of error for all SISO and MIMO signals.

Then the probability of missed detection shown in Figure 6.3 illustrates what percentage of correct TDOA/FDOA data is thrown away as the threshold increases. Therefore a balance needs to be obtained between the desired probability of error and the number of TDOA/FDOA samples that can be filtered. The general conclusion shown by the simulation results is that this method of filtering is proven to detect and remove TDOA/FDOA errors.

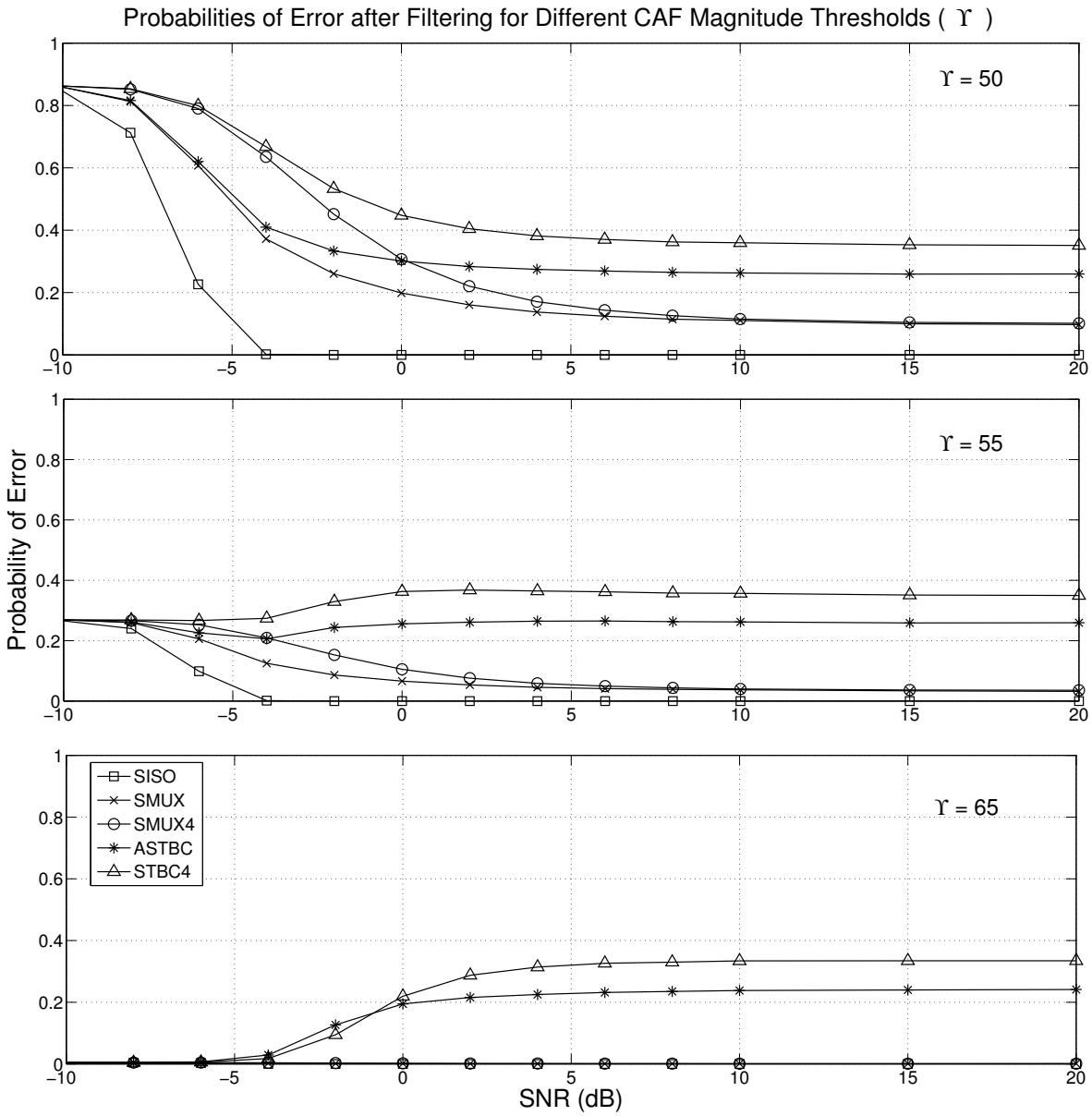

Figure 6.1: Probability of Error after Filtering. As the filtering threshold is increased the probability of error decreases. However, for STBC MIMO the filtering threshold needs to be high enough to filter out the sidelobes whose magnitude is a function of the received signal power. Because the overall received signal plus noise power is kept constant for simulation purposes as the SNR increases the received signal power increases and the noise power decreases. Therefore for higher SNRs the sidelobes CAF magnitudes are higher and a larger filtering threshold is needed to filter them out. Although not shown here, if the threshold is increased the probability of error for STBC will eventually converge to 0 for all SNRs.

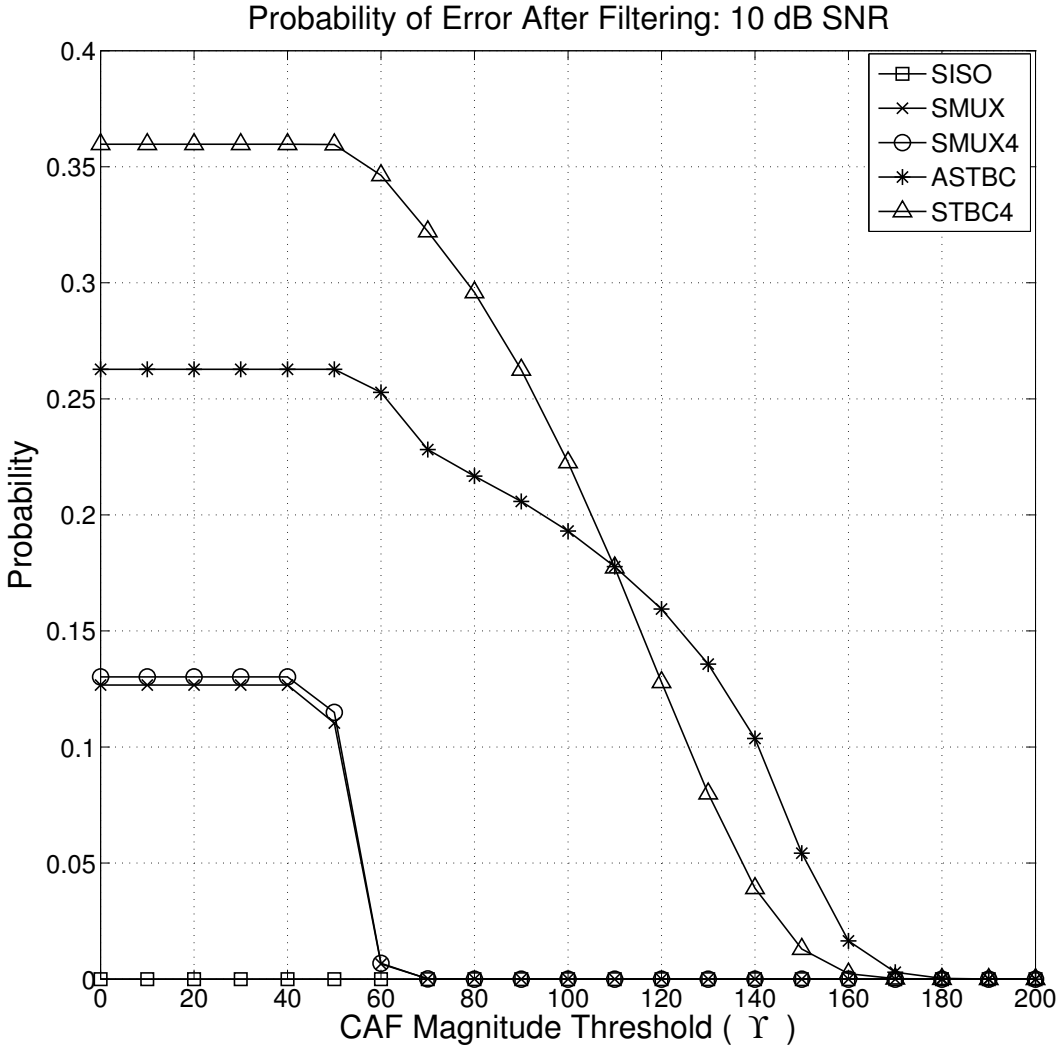

Figure 6.2: Probability of Error as a Function of Filtering Threshold. If the SNR is kept constant as the filtering threshold increases the probability of error decreases for all SISO and MIMO cases. It takes a much higher threshold to decrease the probability of error to zero for STBC because the sidelobes are more likely to have higher CAF magnitudes.

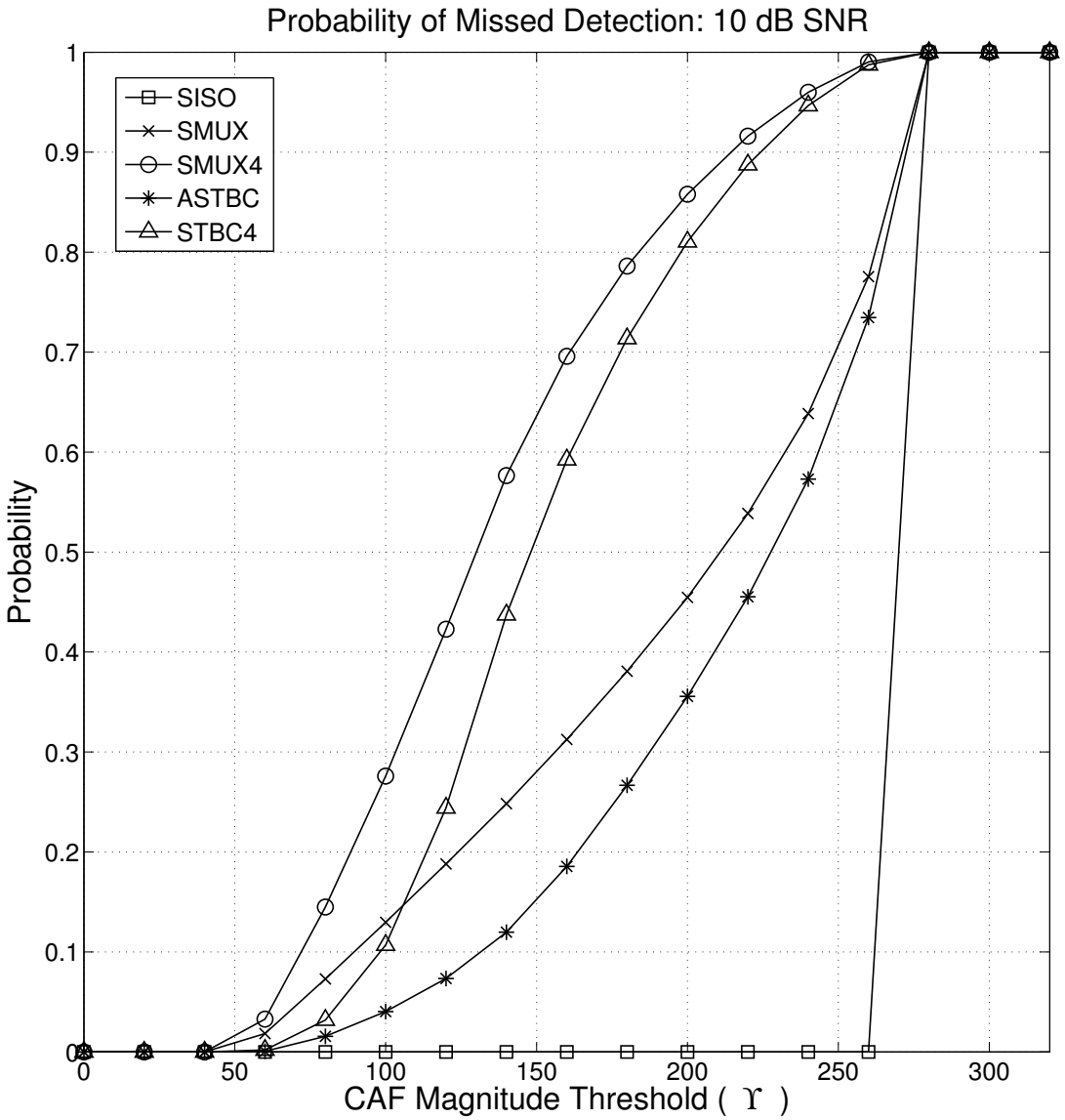

Figure 6.3: Probability of Missed Detection. In general as the filtering threshold increases the likelihood of filtering out a correct TDOA/FDOA increases. Therefore a balance must be found between reducing the probability of error and increasing the probability of a miss determined by the threshold.

Chapter 7

Geolocation using TDOA/FDOA

In order to understand the importance of TDOA/FDOA estimation it is necessary to discuss how they relate to positioning. Also it is important to understand how errors in TDOA/FDOA estimate translate to position estimation to better characterize and compare SISO and MIMO performance. Geolocation using TDOA/FDOA requires at least two collectors with some nonzero relative velocity to the transmitter. For our purposes the transmitter is assumed stationary, and the collectors are assumed airborne with some known position and velocity. TDOA and FDOA are related to position in Cartesian coordinates by:

$$\text{TDOA} = \frac{(R_1 - R_2)}{c} \tag{7.1}$$

$$\text{FDOA} = \frac{f_c}{c}\frac{d}{dt}(R_1 - R_2) \tag{7.2}$$

where the range between collector r and the emitter is R_r:

$$R_r = \sqrt{(x_r - x_e)^2 + (y_r - y_e)^2 + (z_r - z_e)^2}$$

and the emitter and collectors' coordinates are given by $[x_e, y_e, z_e]$ and $[x_r, y_r, z_r]$ respectively. By taking the time derivative FDOA is then:

$$\text{FDOA} = \left(\frac{f_c}{c}\right)\left(\mathbf{v}_1^T\mathbf{u}_1 - \mathbf{v}_2^T\mathbf{u}_2\right) \tag{7.3}$$

where $\mathbf{u}_r$ is the unit vector from collector r in the direction of the emitter, and $\mathbf{v}_r$ is the velocity vector of the collector, and so:

$$\mathbf{v}_r = [v_{x,r},\ v_{y,r},\ v_{z,r}]$$

$$\mathbf{u}_r = \frac{[(x_r - x_e),\ (y_r - y_e),\ (z_r - z_e)]}{\sqrt{(x_r - x_e)^2 + (y_r - y_e)^2 + (z_r - z_e)^2}}. \tag{7.4}$$

$$\mathbf{v}_r^T\mathbf{u}_r = \frac{v_{x,r}(x_r - x_e) + v_{y,r}(y_r - y_e) + v_{z,r}(z_r - z_e)}{\sqrt{(x_r - x_e)^2 + (y_r - y_e)^2 + (z_r - z_e)^2}}. \tag{7.5}$$

TDOA and FDOA are therefore scaled versions of the differential range and range-rate and yield a set of hyperbolic and complex quadratic curves, respectively [17]. The emitter's position can be found by determining the intersection of the lines of constant TDOA and FDOA [18]. An example of the constant TDOA/FDOA curves can be seen in Figure 7.1, along with the basic emitter-collector geometry scenario used for geolocation simulations later.

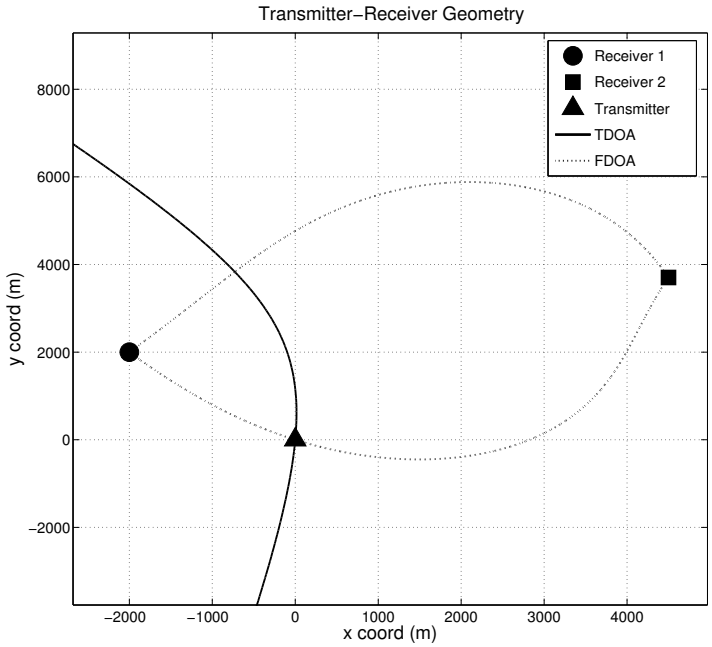

Figure 7.1: Geolocation Geometry. The location of the transmitter and receivers are shown along with the corresponding lines of constant TDOA/FDOA. At the intersection of the TDOA/FDOA curves lies the transmitter.

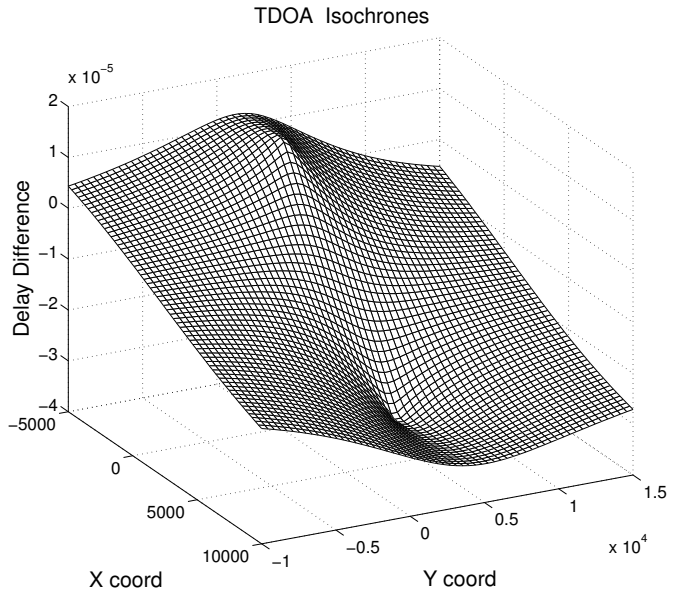

Figure 7.2: TDOA Isochrones. TDOA (in seconds) as a function of the emitter's position. The Z-plane intersects with lines of constant TDOA yielding the hyperbolic TDOA curves in Figure 7.1.

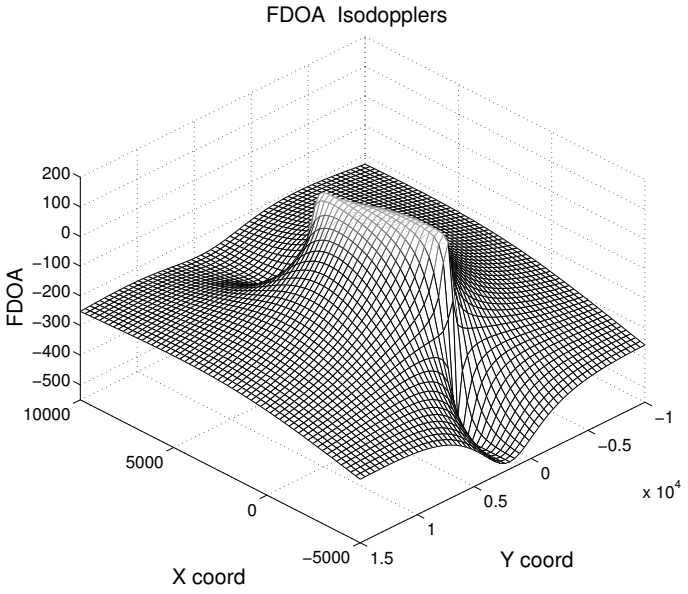

Figure 7.3: FDOA Isodopplers. FDOA (in Hz) as a function of the emitter's position. The Z-plane intersects with lines of constant FDOA yielding the complex quadratic curves in Figure 7.1.

Solving for the emitter's coordinates is nontrivial due to the nonlinear nature of the equations. This problem has been widely studied and there have been many techniques developed. Gradient descent techniques such as the Newton-Raphson and Gauss-Newton methods linearize the problem and iteratively solve for position [18]. Other methods constrain the problem by assuming some knowledge of the emitter's position such as its altitude as in [10].

For the purposes of this thesis a simple solution is needed in order to show how CAF errors in TDOA/FDOA affect the position estimate. Thus we can constrain the geolocation problem to two dimensions in order to simplify the equations without any loss of generality. In only two dimensions we now have:

$$\text{TDOA} = f_\tau(x_e, y_e) = \frac{1}{c}\left(\sqrt{(x_1 - x_e)^2 + (y_1 - y_e)^2} - \sqrt{(x_2 - x_e)^2 + (y_2 - y_e)^2}\right) \tag{7.6}$$

$$\text{FDOA} = f_f(x_e, y_e) = \frac{f_c}{c}\left(\frac{v_{x,1}(x_1 - x_e) + v_{y,1}(y_1 - y_e)}{\sqrt{(x_1 - x_e)^2 + (y_1 - y_e)^2}} - \frac{v_{x,2}(x_2 - x_e) + v_{y,2}(y_2 - y_e)}{\sqrt{(x_2 - x_e)^2 + (y_2 - y_e)^2}}\right) \tag{7.7}$$

which if we assume the carrier frequency can be accurately estimated and is therefore known, we now have two equations and two unknowns. This is still a nontrivial system of equations to solve due to the non-linearity. In fact it is difficult to solve for the emitter's coordinates explicitly in terms of the collectors' and TDOA/FDOA partly because multiple solutions arise due to the polynomial nature of the equations. This can be seen in Figure 7.1 where there is an ambiguity because there are multiple intersections of the TDOA/FDOA curves. Thus for this situation at least two solutions are possible with the potential for further imaginary solutions to arise as well. Using another set of TDOA/FDOA measurements can resolve the ambiguity, or by combining TDOA/FDOA with other positioning observables, such as angle-of-arrival (AOA) or received signal strength (RSS) to name a few. It is possible that ambiguities can be resolved based on general knowledge of the system geometry and what solutions are therefore feasible.

While there are numerical solvers available that can solve this system of equations, we will utilize a Newton-Raphson approach for simulation purposes. Gradient descent techniques can provide fast and accurate results but are not guaranteed to converge and require an initial guess of the emitter's position.

The general procedure for gradient descent methods start with an initial guess of the emitter's position. The initial guess should be chosen to help convergence which is dependent on a number of factors including the geometry of the emitter and collectors. In practical geolocation applications the window from which a random initial guess is chosen should be constrained to plausible results. For instance it is unlikely an emitter would be located at the center of the earth, or anywhere below ground assuming the collectors are airborne. General knowledge of the collectors, received signal strength, and antenna beam patterns can help to constrain the initial guess to within a reasonable search window. For the scenario we are considering the initial guess is chosen randomly within the search window as shown in Figure 7.4. This region was chosen because it guarantees convergence for perfect TDOA/FDOA and even for SISO signals at 0 dB SNR. Convergence does not necessarily mean the correct solution is obtained, merely that the stopping criteria was met and the solution did not diverge.

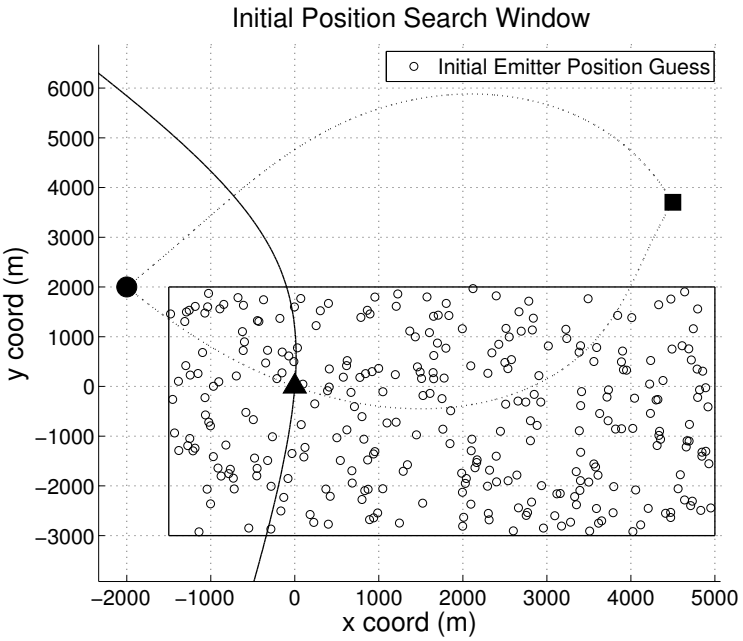

Figure 7.4: Initial Position Window. Choosing a random initial guess within this window guarantees convergence to the correct emitter location given perfect TDOA/FDOA measurements.

Once an initial guess has been chosen the general procedure is to update that guess by finding the error between the measured and calculated TDOA/FDOA by using the gradients as defined in the following process:

$$z_{i+1} = z_i + \frac{f_m - f(z_i)}{f'(z_i)} \tag{7.8}$$

where z_i is the estimate of the parameter of interest from the function $f(z_i)$ and its derivative $f'(z_i)$, f_m is the measured value, and i is the iteration index. Therefore for our purposes z_i would be the position of the emitter with the TDOA/FDOA functions $f(z_i)$ given by (1.5) and (1.6) and f_m would be the measured value of TDOA/FDOA from the CAF respectively. Therefore put into these terms the estimate of the emitter's position is given by:

$$p_{i+1} = p_i + \Delta p_i \tag{7.9}$$

$$p_i = [x_{e,i} \quad y_{e,i}]^T$$

where p_i is the estimate of the emitter's position with Cartesian coordinates $x_{e,i}$ and $y_{e,i}$ at the ith iteration index. Δp_i is the change in each position estimate given by $\Delta p_i = A^{-1}\delta_m$ where:

$$\delta_m = \begin{bmatrix} \Delta\hat{\tau} - f_\tau(x_{e,i}, y_{e,i}) \\ \Delta\hat{f} - f_f(x_{e,i}, y_{e,i}) \end{bmatrix}.$$

$$\mathbf{A} = \begin{bmatrix} f'_\tau(x_{e,i}, y_{e,i}) \\ f'_f(x_{e,i}, y_{e,i}) \end{bmatrix}$$

The gradients of TDOA and FDOA are known to be [16]:

$$\nabla\text{TDOA} = f'_\tau(x_{e,i}, y_{e,i}) = \frac{1}{c}(\mathbf{u}_2 - \mathbf{u}_1) \tag{7.10}$$

$$\nabla\text{FDOA} = f'_f(x_{e,i}, y_{e,i}) = \frac{f_0}{c}\left(\frac{(\mathbf{I} - \mathbf{u}_2\mathbf{u}_2^T)\mathbf{v}_2}{R_2} - \frac{(\mathbf{I} - \mathbf{u}_1\mathbf{u}_1^T)\mathbf{v}_1}{R_1}\right) \tag{7.11}$$

where $\mathbf{I}$ is an identity matrix.

If $\mathbf{A}$ is not square such as when multiple measurements of TDOA/FDOA are used for a combined solution then one must take the Moore-Penrose pseudoinverse in order to solve for Δp_i. Additionally the covariance matrix, $\mathbf{W} = \mathrm{E}[(\delta_m - \mathrm{E}[\delta_m])(\delta_m - \mathrm{E}[\delta_m])^T]$, can be inserted in order to properly weight the constraints using estimation statistics from the measurements [16]. Thus, the equation to solve for the change in position is now updated as:

$$\Delta p_i = (\mathbf{A}^T\mathbf{W}\mathbf{A})^{-1}\mathbf{A}^T\mathbf{W}\delta_m \tag{7.12}$$

After solving for Δp_i, we must update the previous approximated solution and repeat until convergence, thus solving for the transmitter's position. Adding the scale factor λ to limit

the step size of the change in position can help prevent divergence from the true solution:

$$p_{i+1} = p_i + \frac{1}{\lambda}\Delta p_i. \tag{7.13}$$

where λ can be adjusted during the iteration process to slow or speed up the rate of change. The stopping criteria for this iterative technique is typically based on the distance between the previous and current guess of the emitter's position. If the distance is less than or equal to some threshold (typically a value around 1×10^{-6} meters is used) then the program is ended and the result is said to have converged. A divergent result occurs if the program iterates until some large number of iterations has occurred at which point the program must be forced to stop. When a divergent result occurs it can often be detected and discarded based on the number of iterations. There are however, occasions where a solution might oscillate around the correct result but not meet the stopping criteria. Discarding solutions that appear to diverge, therefore has the associated cost of potentially discarding a good position estimate.

7.1 Geolocation Simulation and Results

In this section TDOA/FDOA data was simulated as described in Chapter 5 however a much higher resolution CAF was used in order to get the TDOA/FDOA resolution necessary for practical geolocation results. Then using the Newton-Raphson method as described in the previous section the emitter's location was estimated from the CAF simulated TDOA/FDOA. The results below show that MIMO signals cause larger errors in the estimated emitter's position, but that these errors can be detected and filtered using the method described in Chapter 6.

The position RMSE in Figure 7.5 shows that SISO has the best performance with STBC

performing much worse than SISO but better than SMUX. The SISO scatter plot in Figure 7.7 shows a nice error ellipse around the true emitter location characteristic of TDOA/FDOA positioning. It isn't until the SNR is very low for SISO, such as in Figure 7.8, that erroneous TDOA/FDOA start to cause the geolocation solution to diverge. In Figure 7.9 the scatter plots of the estimated position show clusters of position estimates that are extremely far from the correct result and are caused by divergent Newton-Raphson solutions. After a large number of iterations the geolocation program is stopped and solutions that were in the process of diverging form a crescent. If the program were to continue perhaps a solution would have converged but for our purposes we consider these results to be divergent. In general SMUX had more solutions that diverged whereas STBC position estimates more often converged into noticeable clusters due to the sidelobes as shown in Figure 7.10. Therefore because there were more divergent solutions for SMUX the RMSE leveled off much higher. It should be noted that the average error for MIMO is unacceptably high, regardless of the number of antennas or the method of transmission.

A more accurate representation of geolocation performance is shown in the probability that the position error is less than 50 meters as in Figure 7.6. This is a better metric because it essentially represents the probability of finding the CAF main lobe whereas the RMSE is heavily influenced by a small number of very large position errors (i.e. when the solution diverges). When the main lobe of the CAF is found the errors in TDOA/FDOA will be small, and result in relatively small position errors as well. This result shows that MIMO with two antennas is best, and preferably using spatial multiplexing. The reason why STBC using four antennas has such poor performance is probably once again due to the CAF sidelobes since four or more sidelobes can arise.

When filtering is used such as in Chapter 6 to detect and remove CAF TDOA/FDOA errors the overall performance for both SISO and MIMO improves. In Figures 7.11 and 7.12 the

position RMSE is shown to improve for larger CAF magnitude detection thresholds. Once again the effect of the sidelobes is noticeable when filtering, because for STBC the RMSE does not approach zero until the threshold is large enough to filter the sidelobes. Also in Figure 7.11 the STBC position RMSE appears to increase as the SNR increases for different filtering thresholds. This effect is once again due to the fact that as the SNR increases so does the sidelobe CAF magnitude which might be greater than the filtering threshold; it is less dependent on the noise power than it is the signal power. The effects of filtering on the probability of position error being less than 50 meters can be seen in Figures 7.13 and 7.14. These figures show that two antenna MIMO techniques are more likely to result in smaller position errors and require smaller filtering thresholds than four antenna MIMO techniques which require very large filtering thresholds.

Therefore the large TDOA/FDOA errors that we predicted theoretically and saw in the CAF simulations cause even larger errors in position and can cause the Newton-Raphson method to diverge. The effects of the sidelobes also cause clusters in position that increase the RMSE for STBC MIMO and can be difficult to filter. In general more antennas at the transmitter results in more and larger position errors.

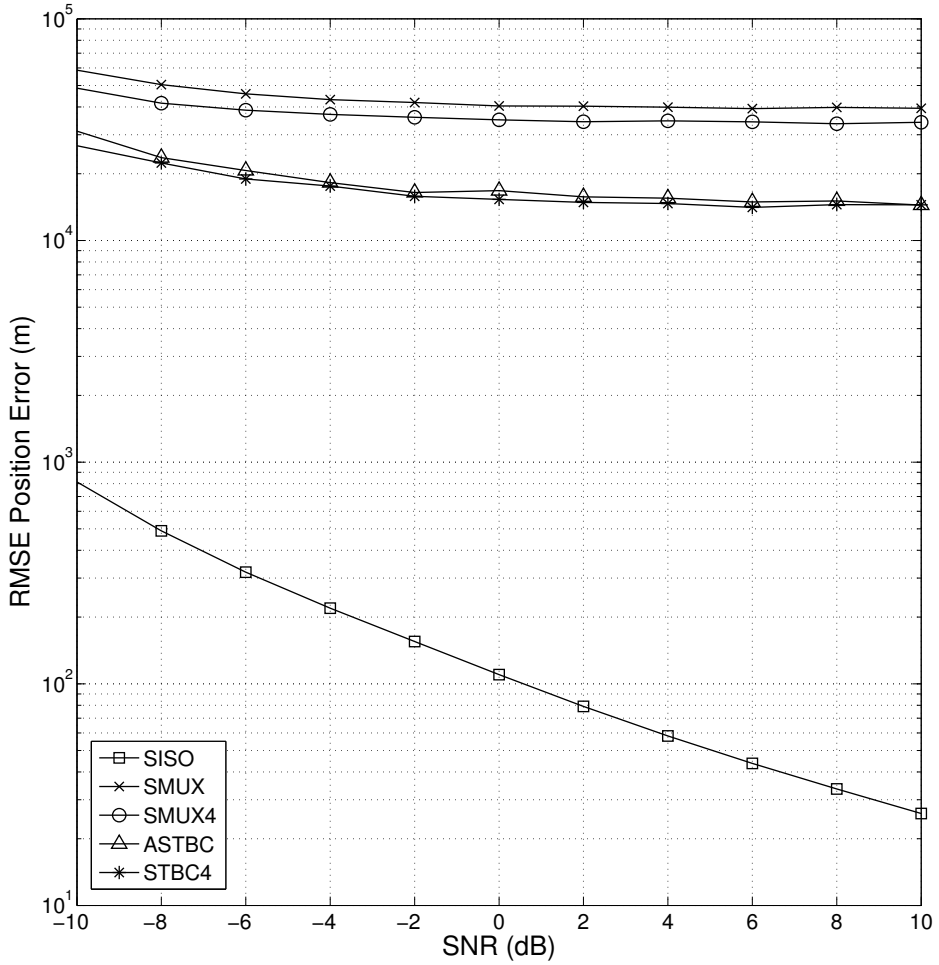

Figure 7.5: Geolocation Position RMSE. MIMO signals cause very large errors in position because they are not able to find the CAF main lobe, these large errors in TDOA/FDOA translate to position. In general SMUX shows better performance over STBC probably due to the sidelobes which cause larger errors in TDOA/FDOA on average.

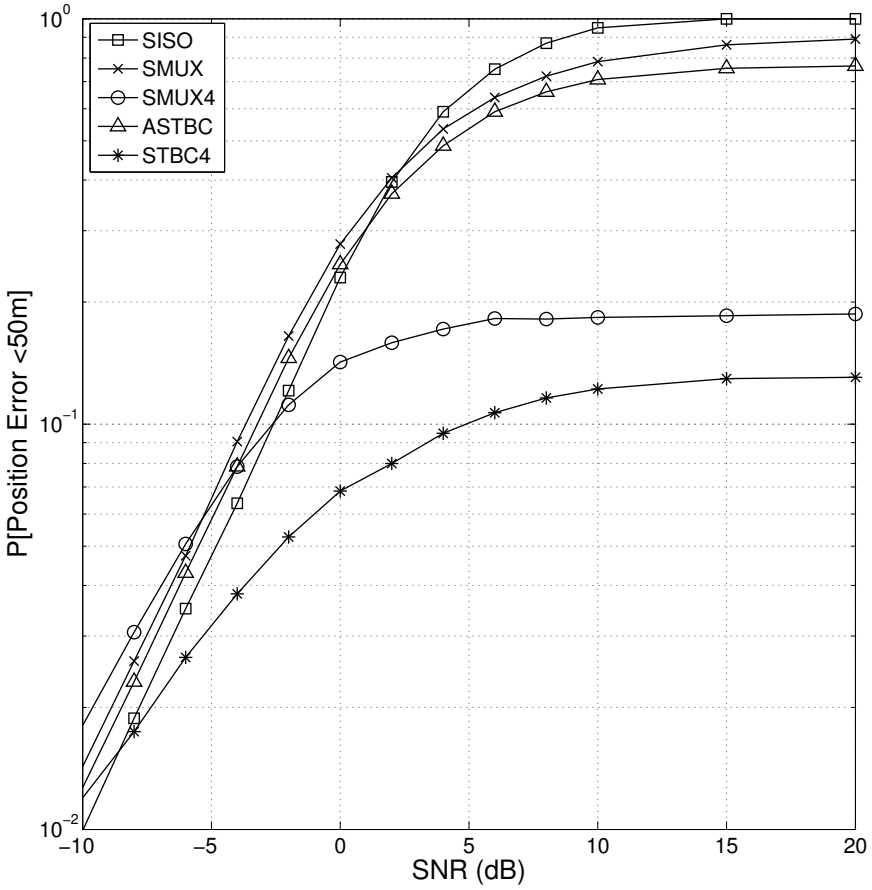

Figure 7.6: Geolocation Probability of Error. The probability that the position error is less than 50 m is plotted using CAF simulated TDOA/FDOA data. This shows better performance for MIMO signals than what would be assumed from the position RMSE. Two antenna MIMO signals provided better probability of error results than four antennas.

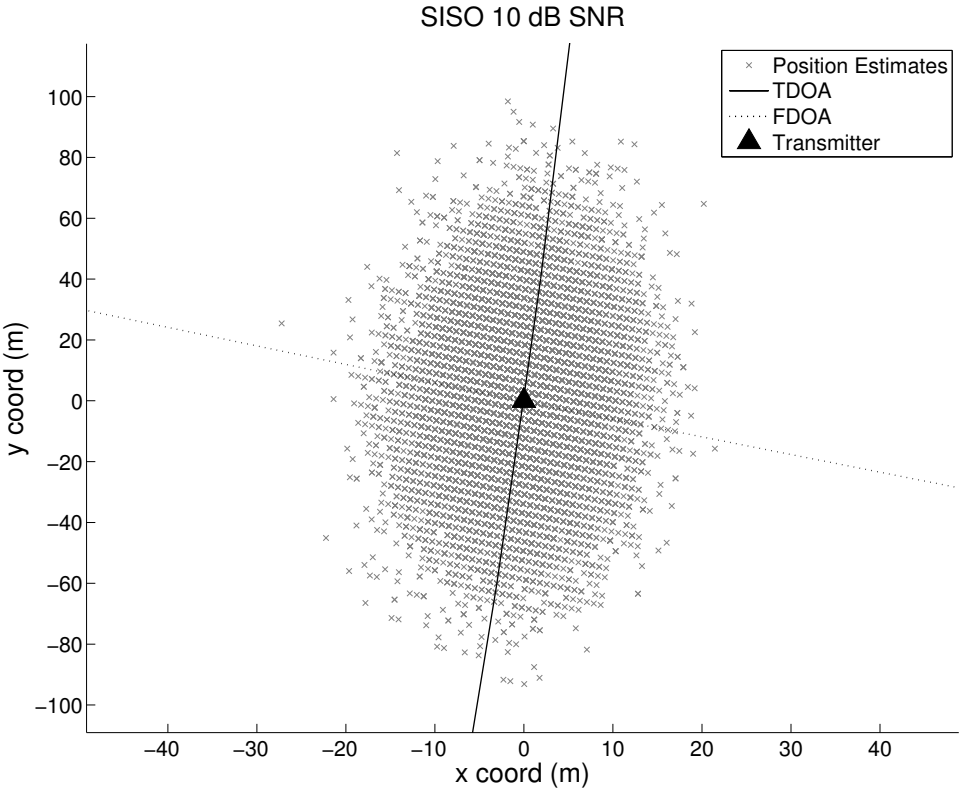

Figure 7.7: SISO Geolocation Scatter Results 10 dB SNR. A nice cluster around the true emitter position is visible with no divergent results. Due to the geometry of the emitter and collectors in this scenario TDOA mainly contributes to the x-axis where FDOA controls the y-axis.

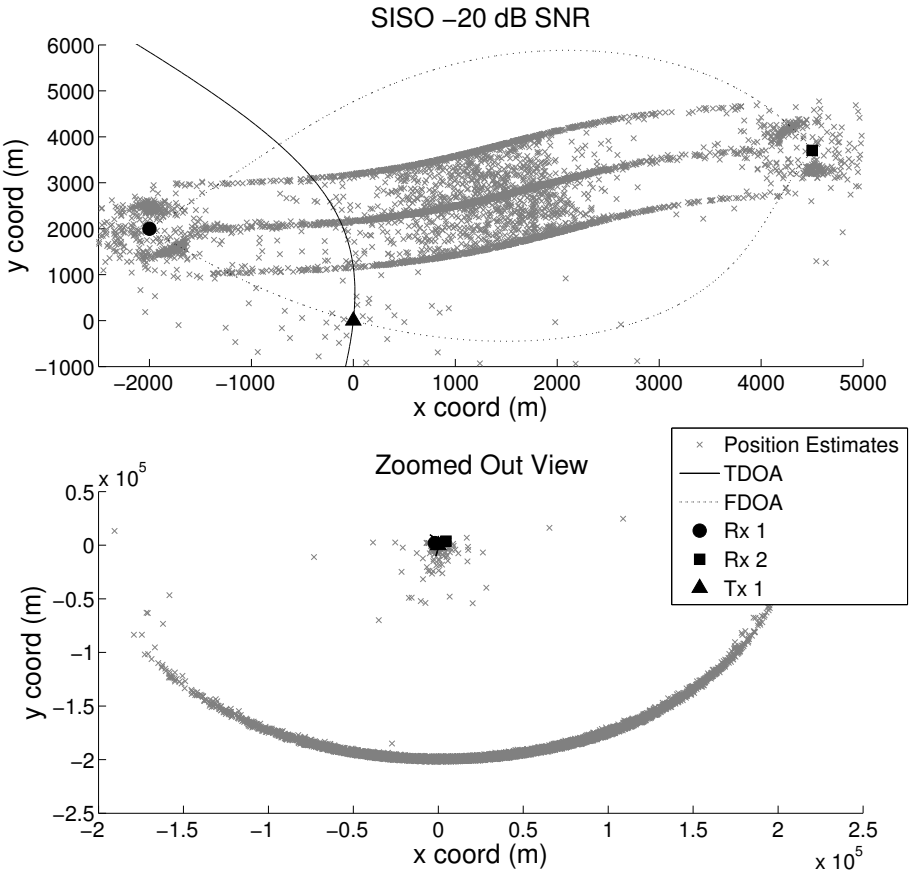

Figure 7.8: SISO Geolocation Scatter Results -20 dB SNR. At this low SNR there are solutions that diverge as shown in the zoomed out view. When we zoom in the results are interesting and there are clusters and lines of convergence that occur due to the gradients of TDOA/FDOA governed by the emitter-collector geometry.

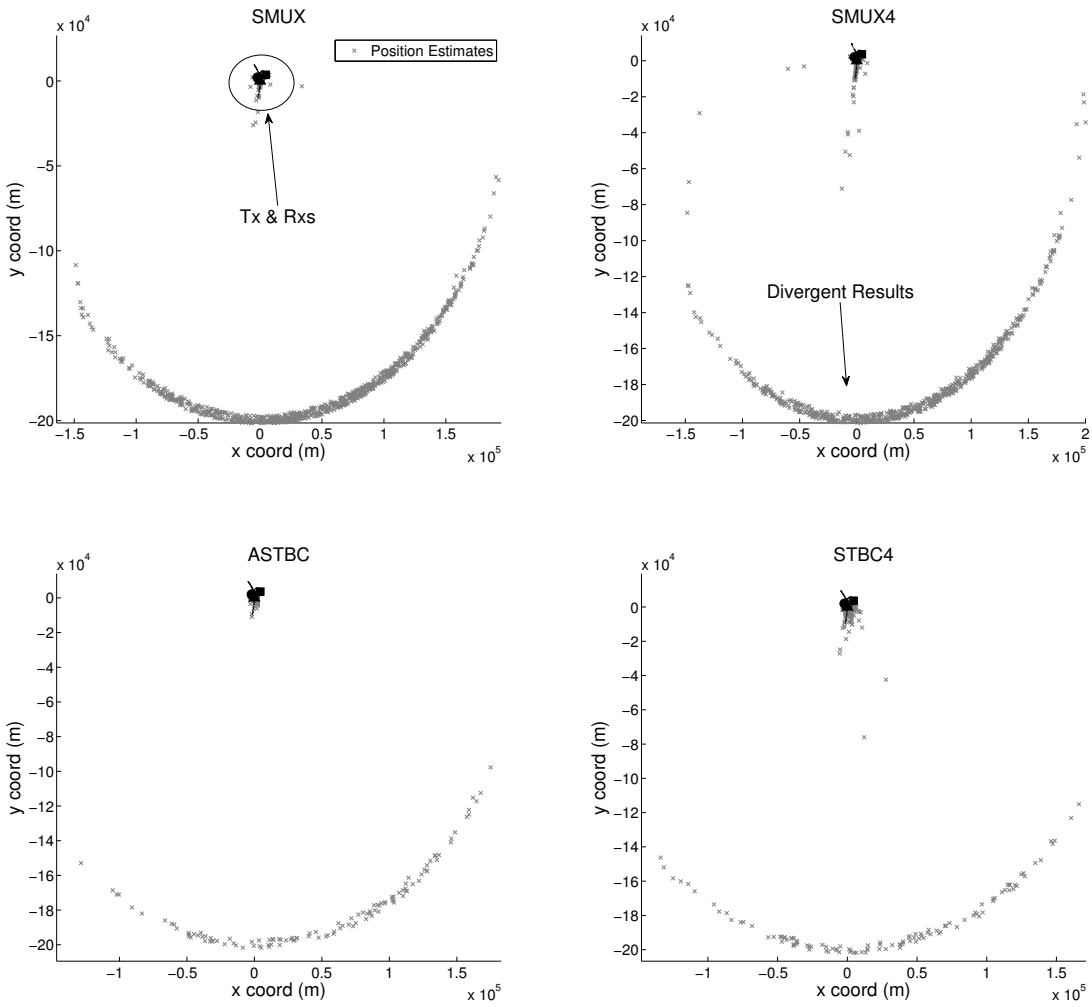

Figure 7.9: MIMO Geolocation Scatter Divergent Results 10 dB SNR. Showing the full view of the geometry of the position estimates, for a zoomed in view of the scatter results see Figure 7.10. Due to large errors in TDOA/FDOA the Newton-Raphson method diverged and after 200 iterations the program was stopped resulting in position estimates extremely far from the correct position. STBC did not diverge as often as SMUX due to the presence of the sidelobes.

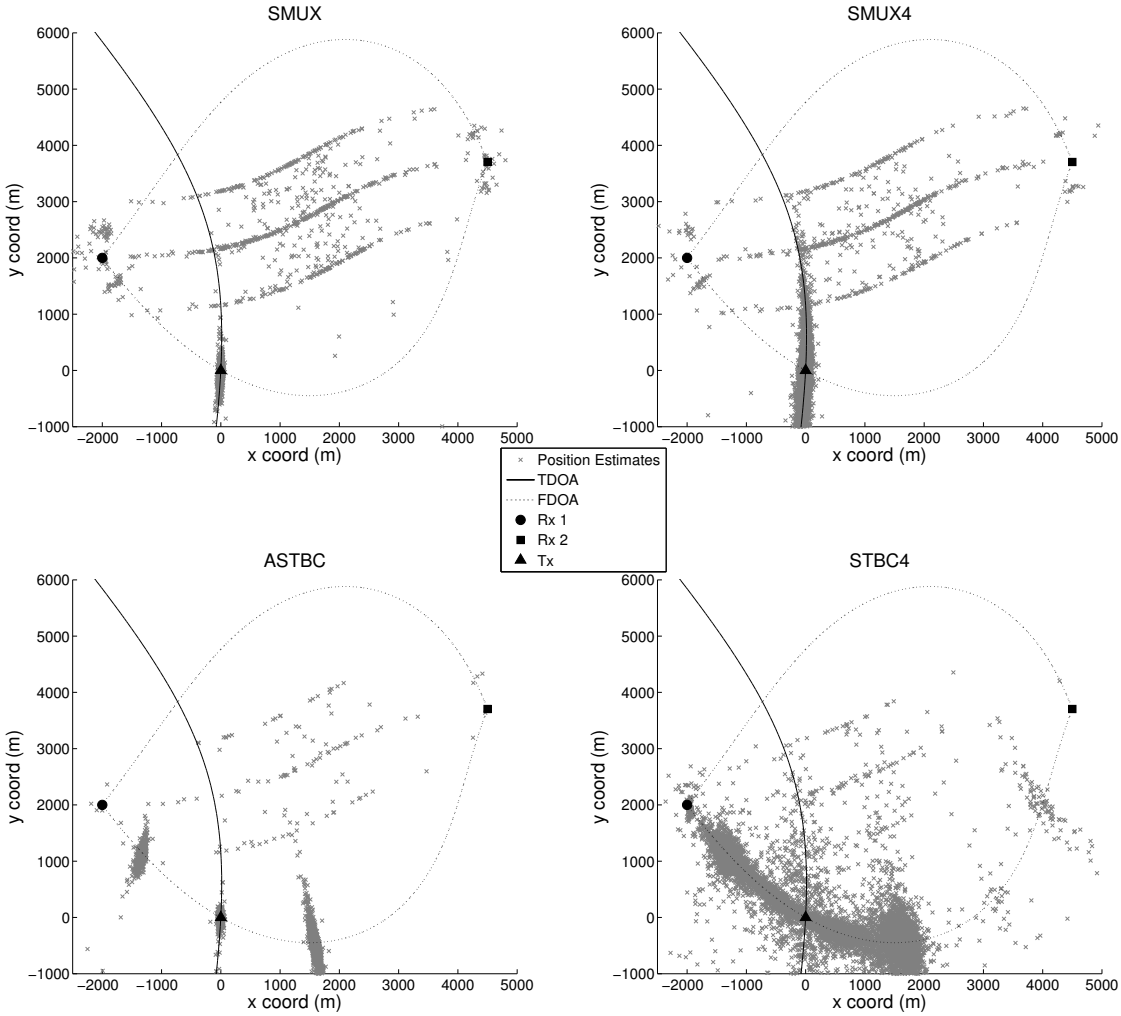

Figure 7.10: MIMO Geolocation Scatter Results 10 dB SNR. A zoomed view of the general system geometry. Similar scattering can be seen for SISO only at extremely low SNRs (-20 dB). The effects of the sidelobes can really be seen for the ASTBC results where there are two clusters on either side of the main cluster. While SMUX diverged more often than STBC due to the sidelobes the STBC position error is larger on average due to the sidelobes.

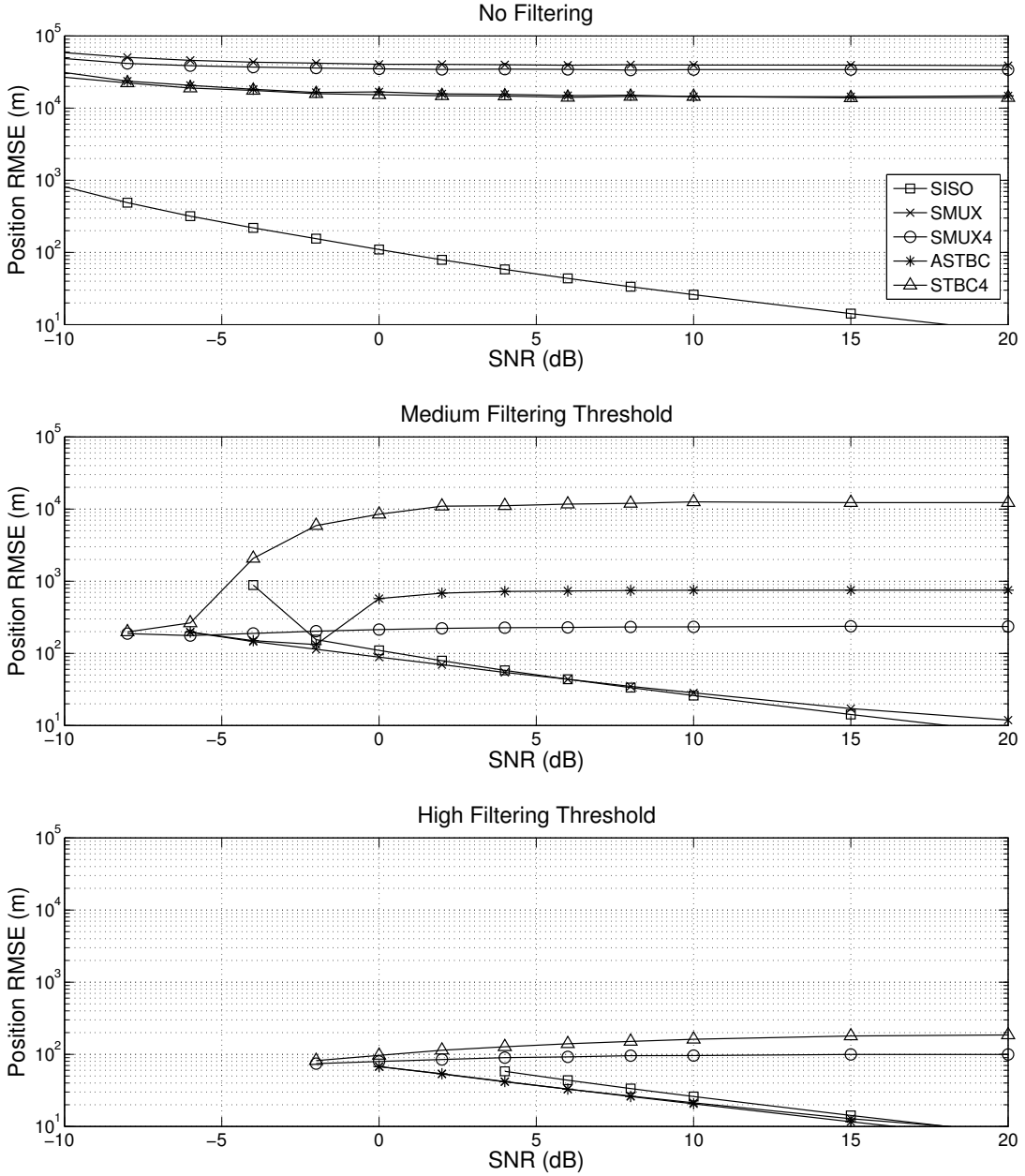

Figure 7.11: Position RMSE with Filtering. For the "Medium" filtering threshold once again the SMUX RMSE drops to that of SISO whereas the STBC RMSE curves appear to increase as SNR increases. This effect is once again due to the sidelobes present in the STBC CAF. With the "High" filtering threshold this effect is less noticeable but still not filtered out completely.

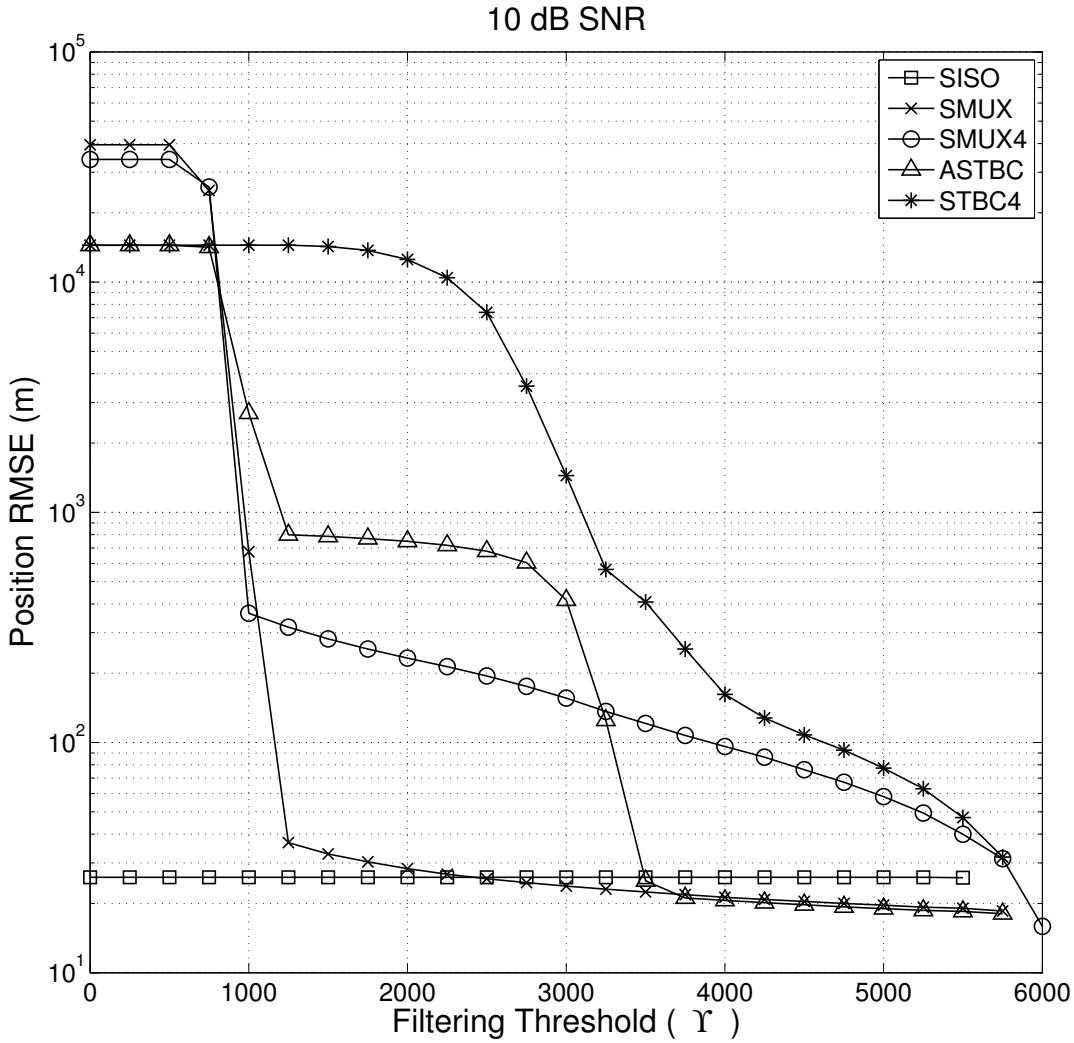

Figure 7.12: Position RMSE vs. Filtering Threshold 10 dB SNR. With SNR kept constant the position RMSE drops as a function of the filtering threshold. In particular the SMUX RMSE drops rapidly as the filtering threshold increases but the STBC RMSEs have noticeable cliffs due to the sidelobes. The SISO position RMSE remains flat because the resolution in TDOA/FDOA is limited causing small perturbations in TDOA/FDOA that cannot be filtered out.

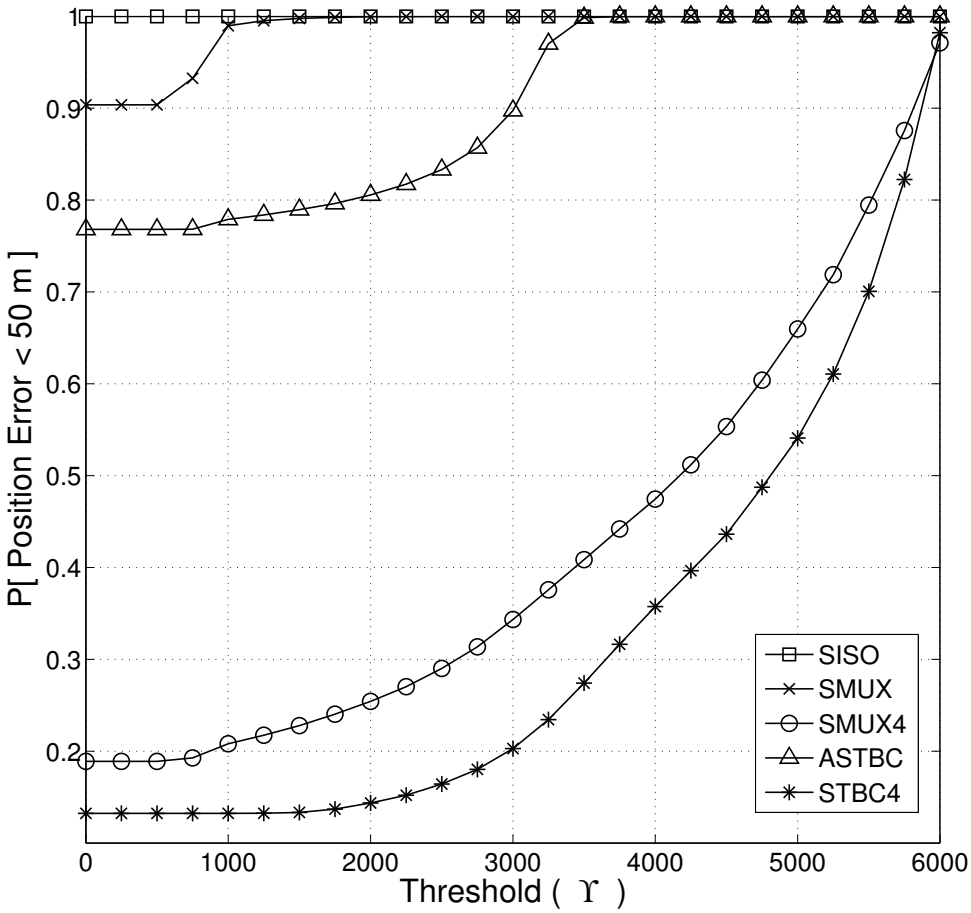

Figure 7.13: Position Probability of Error vs. Filtering Threshold 100 dB SNR. With SNR kept constant this figure shows the effects of filtering on the position estimates without the presence of AWGN. Even without noise SMUX4 and STBC4 require large filtering thresholds in order to increase the probability of error being within 50 meters. At 100 dB SNR there are no errors for SISO and so the probability curve remains flat despite the filtering threshold.

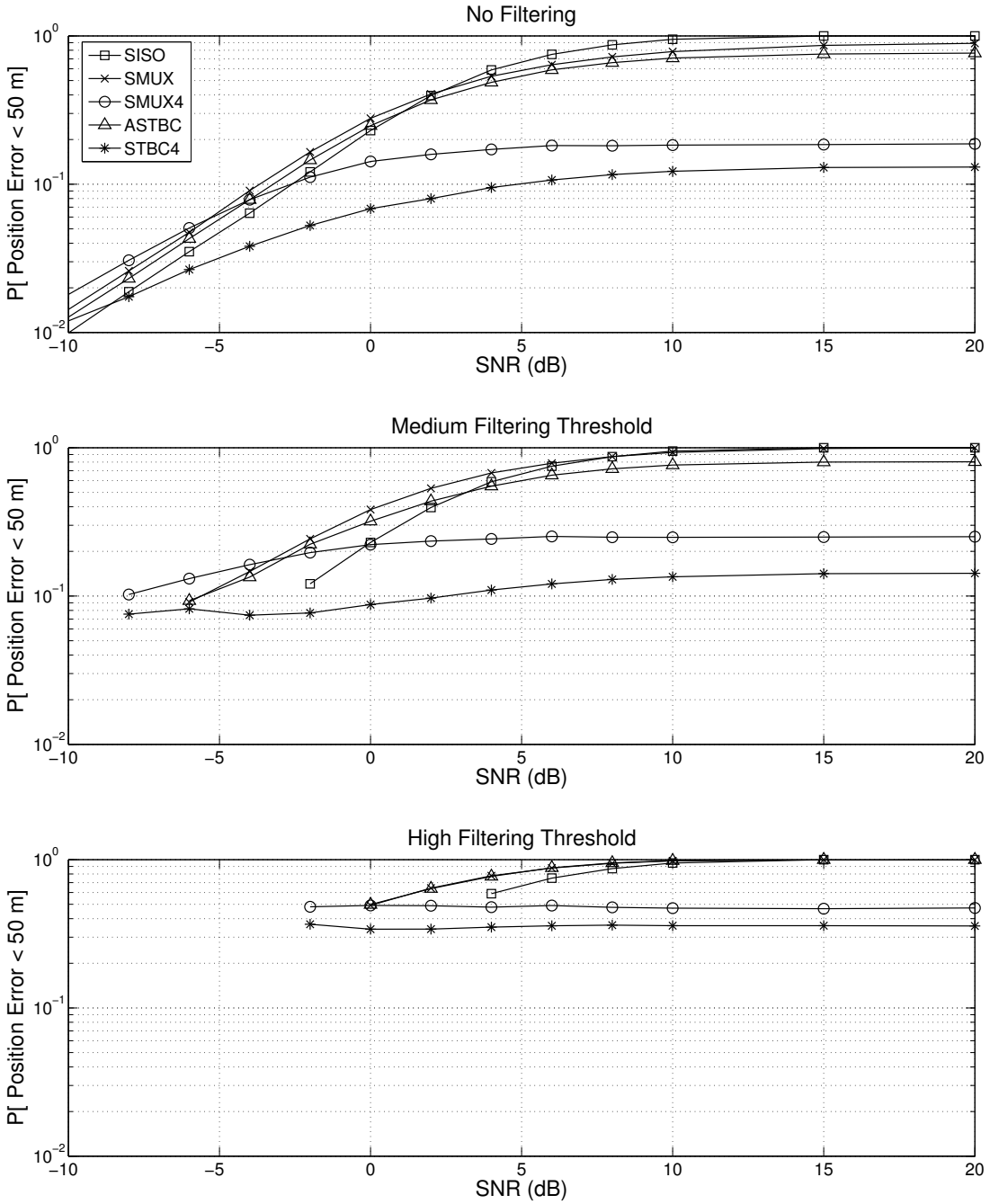

Figure 7.14: Position Probability of Error with Filtering. Probability that the position error is less than 50 meters for different filtering thresholds showing how errors are more likely to be smaller (within 50 m) with larger filtering thresholds.

Chapter 8

Conclusion

By using a detection theory framework, the CAF performance in terms of TDOA/FDOA probability of error was characterized for SISO and MIMO transmission. The probability of finding the correct TDOA/FDOA bin is analogous to finding the main lobe of the CAF surface. Once the main lobe of the CAF is found, it is assumed that further processing can increase TDOA/FDOA resolution and accuracy with the overall performance akin to SISO. In order to derive the probability of error (the probability of not finding the correct TDOA/FDOA bin, or CAF main lobe) first the distributions of the CAF magnitude were derived for both SISO and MIMO signals.

The SISO CAF magnitude main lobe was found to follow the Rice distribution while the magnitude of the noise bins was shown to be Rayleigh. The MIMO CAF magnitude distributions were much more complex. Fundamentally the MIMO distributions featured a sum of random complex vectors proportional to the number of antennas. Even in the absence of noise, the main lobe's magnitude can be diminished and the CAF surface will fail to produce any discernible peak depending on how the transmitted signals combine at the receiver. When noise is present, the main lobe can disappear below the noise floor. The probability of

error was shown to be the probability that the main lobe is less than the max of all the noise bins. See Appendix A for a summary of the CAF magnitude distributions and probabilities of error.

The theoretical and simulated results show that SISO outperforms MIMO with a better probability of finding the main lobe and thus lower RMSE. It can be generalized that when the MIMO signals add coherently at the receivers the CAF performance is at best as good as SISO. However when the signals combine incoherently, the TDOA/FDOA errors are typically very large because the CAF main lobe can not be found. By once again applying detection theory, it was shown that CAF errors for SISO and MIMO can be detected and removed. Using the CAF magnitude as a decision statistic and applying a threshold, the probability of error (also corresponding to the probability of false alarm) can be reduced. The cost of this approach is that potentially correct TDOA/FDOA data can be thrown away. Thus as the filtering threshold on the CAF magnitude increases, the probability of missed detection increases, and more potentially useful TDOA/FDOA data can be thrown out.

Finally geolocation, and how TDOA/FDOA translate to position was discussed in order to show how TDOA/FDOA errors affect position estimation. In general TDOA and FDOA yield a set of hyperbolic and complex quadratic curves, at the intersection of both lies the location of the emitter. The overall result was that MIMO signals cause large errors in position when the main lobe of the CAF cannot be found, these large errors increase the position RMSE. The probability of a position error less than 50 meters shows that MIMO signals don't perform as bad as one might expect from the probability of TDOA/FDOA error discussed previously. There is however a noticeable percentage drop in performance in this regard.

In conclusion, geolocation of a transmitter using MIMO by CAF calculation of TDOA/FDOA suffers from the effects of multiple channels, the very aspect that makes MIMO so attractive

for communication systems. In the future to solve this problem a system using multiple antennas could be used to remove the effects of the channel. Otherwise a method that involves simultaneously estimating the channel matrix and TDOA/FDOA must be determined, perhaps an iterative approach is possible. It should also be noted that most MIMO systems employ the use of pilots (some known sequence of transmitted symbols) for channel state information estimation. These pilots could be used for calculating TDOA/FDOA using a CAF or other estimation technique assuming *a priori* knowledge of the structure of pilots.

Future directions in TDOA/FDOA based research could include image processing techniques to improve CAF resolution and accuracy. Recently a new method called the Direct Position Determination (DPD) was proposed as an ML estimate of position using delay and Doppler. This method estimates the position of the emitter in one step, instead of first estimating delay and Doppler separately and then determining the position. The new method is said to meet the CRLB at lower SNR's compared to the two step approaches, but at the cost of increased computational complexity. Therefore there is potential future work studying the effects of MIMO signals on the DPD.

Bibliography

[1] A. Abdi, H. Hashemi, and A. Nader-Esfahani. On the PDF of the sum of random vectors. *IEEE Transactions on Communications*, 48(1):7–12, January 2000.

[2] S. Alamouti. A simple transmit diversity technique for wireless communications. *Selected Areas in Communications, IEEE Journal on*, 16(8):1451–1458, 1998.

[3] L. Auslander and R. Tolimieri. Computing decimated finite cross-ambiguity functions. *Acoustics, Speech and Signal Processing, IEEE Transactions on*, 36(3):359–364, 1988.

[4] M. Chen and M. Fowler. Data compression for multi-parameter estimation for emitter location. *Aerospace and Electronic Systems, IEEE Transactions on*, 46(1):308–322, 2010.

[5] P. Chestnut. Emitter location accuracy using TDOA and differential doppler. *Aerospace and Electronic Systems, IEEE Transactions on*, AES-18(2):214–218, 1982.

[6] J. Daba and M. Bell. Statistics of the scattering cross-section of a small number of random scatterers. *IEEE Transactions on Antennas and Propagation*, 43(8):773–783, August 1995.

[7] H. David and H. Nagaraja. *Order Statistics*. Wiley, 3rd edition, 2003.

[8] R. Esposito and L. Wilson. Statistical properties of two sine waves in Gaussian noise. *IEEE Transactions on Information Theory*, 19(2):176–183, 1973.

[9] M. Fowler and X. Hu. Signal models for TDOA/FDOA estimation. *IEEE Transactions on Aerospace and Electronic Systems*, 44(4), October 2008.

[10] K. Ho and Y. Chan. Geolocation of a known altitude object from TDOA and FDOA measurements. *Aerospace and Electronic Systems, IEEE Transactions on*, 33(3):770–783, 1997.

[11] M. Jankiraman. *Space-time codes and MIMO systems*. Artech House, Inc., 2004.

[12] J. Johnson. Implementing the cross ambiguity function and generating geometry-specific signals. Master's thesis, Naval Post Graduate School, 2001.

[13] S. Kay. *Fundamentals of Statistical Signal Processing: Estimation Theory*, volume 1 of *Prentice Hall Signal Processing Series*. Prentice Hall, 1993.

[14] D. Musicki and W. Koch. Geolocation using tdoa and fdoa measurements. In *Information Fusion, 2008 11th International Conference on*, pages 1–8, 2008.

[15] J. Overfield, Z. Biskaduros, and R. M. Buehrer. Geolocation of MIMO signals using the cross ambiguity function and TDOA/FDOA. In *Communications (ICC), 2012 IEEE International Conference on*, pages 3648–3653, 2012.

[16] T. Pattison and S. Chou. Sensitivity analysis of dual-satellite geolocation. *Aerospace and Electronic Systems, IEEE Transactions on*, 36(1):56–71, 2000.

[17] R. Poisel. *Introduction to Communication Electronic Warfare Systems*. Artech House, INC., 2002.

[18] R. Poisel. *Electronic Warfare Target Location Methods*. Artech House, INC., 2005.

[19] M. Pourhomayoun, M. Fowler, and N. Wu. Spatial sparsity based emitter localization. In *Information Sciences and Systems (CISS), 2012 46th Annual Conference on*, pages 1–4, 2012.

[20] J. Proakis and M. Salehi. *Digital Communications*. McGraw-Hill, 5 edition, 2008.

[21] S. Rice. Probability distributions for noise plus several sine waves–the problem of computation. *IEEE Transactions on Communications*, 22(6):851–853, 1974.

[22] M. Simon. On the probability density function of the squared envelope of a sum of random phase vectors. *IEEE Transactions on Communications*, pages 993–996, 1985.

[23] S. Stein. Algorithms for ambiguity function processing. *Acoustics, Speech and Signal Processing, IEEE Transactions on*, 29(3):588–599, 1981.

[24] S. Stein. Differential delay/doppler ml estimation with unknown signals. *Signal Processing, IEEE Transactions on*, 41(8):2717–2719, 1993.

[25] D. Torrieri. Statistical theory of passive location systems. *Aerospace and Electronic Systems, IEEE Transactions on*, AES-20(2):183–198, 1984.

[26] M. Wax. The joint estimation of differential delay, doppler, and phase (corresp.). *Information Theory, IEEE Transactions on*, 28(5):817–820, 1982.

[27] A. Weiss. Direct geolocation of wideband emitters based on delay and doppler. *Signal Processing, IEEE Transactions on*, 59(6):2513–2521, 2011.

[28] C. Yatrakis. Computing the cross-ambiguity function. Master's thesis, Binghamton University, 2005.

[29] S. Zekavat and R. M. Buehrer. *Handbook of Position Location: Theory, Practice, and Advances*. John Wiley and Sons Ltd, 2011.

Appendix A

CAF Magnitude Distributions & Probability of Error Summary

Below are several charts that summarize the CAF magnitude distributions and the probabilities of error for SISO and MIMO along with their corresponding parameters:

r =1, 2, ... Receiver index
N_t =1, 2, ... Number of transmitting antennas, number of simultaneously transmitted signals
P_r = Signal power at the rth receiver
M = Number of TDOA search bins
N = Number of FDOA search bins

Distribution of the CAF Main Lobe Magnitude	
SISO	$F_{C_p}(c) = 1 - \mathcal{Q}_1\left(\frac{v}{\sigma_c}, \frac{c}{\sigma_c}\right)$
MIMO	$F_{c_p}(c) = \int_0^\infty c\mathcal{J}_0(Pz)^{N_t}\mathcal{J}_1(cz)e^{\frac{z^2\sigma_{c_p}^2}{2}}dz$ $P = \frac{T\sqrt{P_1P_2}}{N_t}$

Distribution of the CAF Noise Bins	
SISO	$F_n(\gamma) = 1 - e^{\frac{-\gamma^2}{2\sigma^2}}$
MIMO	$\sigma^2 = \frac{T}{2}(P_1\sigma_{n,2}^2 + P_2\sigma_{n,1}^2 + \sigma_{n,1}^2\sigma_{n,2}^2) + \sigma_\beta^2$
BPSK	$\sigma_\beta^2 = \frac{T}{2}P_1P_2$
QPSK	$\sigma_\beta^2 = \frac{T}{4}P_1P_2$

Distribution of the CAF Main Lobe Magnitude	
SISO	$\int_0^\infty (MN-1)\frac{\gamma}{\sigma^2}\left(1 - e^{\frac{-\gamma^2}{2\sigma^2}}\right)^{MN-2} e^{\frac{-\gamma^2}{2\sigma^2}}\left(1 - \mathcal{Q}_1\left(\frac{v}{\sigma_c}, \frac{\gamma}{\sigma_c}\right)\right) d\gamma$
MIMO	$\int_0^\infty (MN-1)\frac{\gamma}{\sigma^2}\left(1 - e^{\frac{-\gamma^2}{2\sigma^2}}\right)^{MN-2} e^{\frac{-\gamma^2}{2\sigma^2}} \int_0^\infty \gamma\mathcal{J}_0(Pz)^{N_t}\mathcal{J}_1(\gamma z)e^{\frac{z^2\sigma_{c_p}^2}{2}} dz d\gamma$

Parameters	
SISO	$v = \frac{T\sqrt{P_1P_2}}{2}$ $\sigma_c^2 = \frac{T}{2}(P_1\sigma_{n,2}^2 + P_2\sigma_{n,1}^2 + \sigma_{n,1}^2\sigma_{n,2}^2)$
STBC	$\sigma_{c_p}^2 = \sigma_c^2$
SMUX	$\sigma_{c_p}^2 = \sigma_c^2 + \frac{TP_1P_2}{N_t^2}\left(\frac{N_t^2 - N_t}{2}\right)$